COMILLAS
UNIVERSIDAD PONTIFICIA
ICAI

GRADO EN INGENIERÍA EN TECNOLOGÍAS INDUSTRIALES

TRABAJO FIN DE GRADO

Optimization of the recline angle of the back of a restraint system for infants under two years old to maximize the security and ergonomics of the system

Autor: Rodrigo Vasserot Tolmos

Director: Francisco José López Valdés

Madrid

Junio de 2021

Declaro, bajo mi responsabilidad, que el Proyecto presentado con el título

Optimization of the recline angle of the back of a restraint system for infants under two years old to maximize the security and ergonomics of the system

en la ETS de Ingeniería - ICAI de la Universidad Pontificia Comillas en el

curso académico 2020/21 es de mi autoría, original e inédito y

no ha sido presentado con anterioridad a otros efectos.

El Proyecto no es plagio de otro, ni total ni parcialmente y la información que ha sido

tomada de otros documentos está debidamente referenciada.

Fdo.: Rodrigo Vasserot Tolmos Fecha: 20/07/2021

Autorizada la entrega del proyecto

EL DIRECTOR DEL PROYECTO

LOPEZ VALDES FRANCISCO JOSE - 09437440B

Firmado digitalmente por LOPEZ VALDES FRANCISCO JOSE - 09437440B
Fecha: 2021.07.20 17:12:38 -04'00'

Fdo.: Francisco José López Valdés Fecha: 20/07/2021

AUTHORIZATION FOR DIGITALIZATION, STORAGE AND DISSEMINATION IN THE NETWORK OF THE END-OF-DEGREE PROJECTS, MASTER PROJECTS DISSERTATIONS OR BACHILLERATO REPORTS

1. Declaration of authorship and accreditation thereof.

The author Mr. /Ms. RODRIGO VASSEROT TOLMOS

HEREBY DECLARES that he/she owns the intellectual property rights regarding the piece of work: OPTIMIZATION OF THE RECLINE ANGLE OF THE BACK OF A RESTRAINT SYSTEM FOR INFANTS UNDER TWO YEARS OLD TO MAXIMIZE THE SECURITY AND ERGONOMICS OF THE SYSTEM
that this is an original piece of work, and that he/she holds the status of author, in the sense granted by the Intellectual Property Law.

2. Subject matter and purpose of this assignment.

With the aim of disseminating the aforementioned piece of work as widely as possible using the University's Institutional Repository the author hereby **GRANTS** Comillas Pontifical University, on a royalty-free and non-exclusive basis, for the maximum legal term and with universal scope, the digitization, archiving, reproduction, distribution and public communication rights, including the right to make it electronically available, as described in the Intellectual Property Law. Transformation rights are assigned solely for the purposes described in a) of the following section.

3. Transfer and access terms

Without prejudice to the ownership of the work, which remains with its author, the transfer of rights covered by this license enables:

a) Transform it in order to adapt it to any technology suitable for sharing it online, as well as including metadata to register the piece of work and include "watermarks" or any other security or protection system.

b) Reproduce it in any digital medium in order to be included on an electronic database, including the right to reproduce and store the work on servers for the purposes of guaranteeing its security, maintaining it and preserving its format.

c) Communicate it, by default, by means of an institutional open archive, which has open and cost-free online access.

d) Any other way of access (restricted, embargoed, closed) shall be explicitly requested and requires that good cause be demonstrated.

e) Assign these pieces of work a Creative Commons license by default.

f) Assign these pieces of work a HANDLE (*persistent* URL). by default.

4. Copyright.

The author, as the owner of a piece of work, has the right to:

a) Have his/her name clearly identified by the University as the author

b) Communicate and publish the work in the version assigned and in other subsequent versions using any medium.

c) Request that the work be withdrawn from the repository for just cause.

d) Receive reliable communication of any claims third parties may make in relation to the work and, in particular, any claims relating to its intellectual property rights.

5. Duties of the author.

The author agrees to:

a) Guarantee that the commitment undertaken by means of this official document does not infringe any third party rights, regardless of whether they relate to industrial or intellectual property or any other type.

b) Guarantee that the content of the work does not infringe any third party honor, privacy or image rights.
c) Take responsibility for all claims and liability, including compensation for any damages, which may be brought against the University by third parties who believe that their rights and interests have been infringed by the assignment.
d) Take responsibility in the event that the institutions are found guilty of a rights infringement regarding the work subject to assignment.

6. Institutional Repository purposes and functioning.

The work shall be made available to the users so that they may use it in a fair and respectful way with regards to the copyright, according to the allowances given in the relevant legislation, and for study or research purposes, or any other legal use. With this aim in mind, the University undertakes the following duties and reserves the following powers:

a) The University shall inform the archive users of the permitted uses; however, it shall not guarantee or take any responsibility for any other subsequent ways the work may be used by users, which are non-compliant with the legislation in force. Any subsequent use, beyond private copying, shall require the source to be cited and authorship to be recognized, as well as the guarantee not to use it to gain commercial profit or carry out any derivative works.
b) The University shall not review the content of the works, which shall at all times fall under the exclusive responsibility of the author and it shall not be obligated to take part in lawsuits on behalf of the author in the event of any infringement of intellectual property rights deriving from storing and archiving the works. The author hereby waives any claim against the University due to any way the users may use the works that is not in keeping with the legislation in force.
c) The University shall adopt the necessary measures to safeguard the work in the future.
d) The University reserves the right to withdraw the work, after notifying the author, in sufficiently justified cases, or in the event of third party claims.

Madrid, on 17 of April , 2021

Chapter 1. HEREBY ACCEPTS

Signed RODRIGO VASSEROT 

Reasons for requesting the restricted, closed or embargoed access to the work in the Institution's Repository

GRADO EN INGENIERÍA EN TECNOLOGÍAS INDUSTRIALES

TRABAJO FIN DE GRADO

Optimization of the recline angle of the back of a restraint system for infants under two years old to maximize the security and ergonomics of the system

Autor: Rodrigo Vasserot Tolmos

Director: Francisco José López Valdés

Madrid

Junio de 2021

Acknowledgements

After the completion of this study, I would like to express my gratitude and appreciation to those whose support and help provided contributed to the culmination of my Undergraduate Thesis Project:

To Francisco López Valdés and Manuel Valdano for their permanent advice and collaboration and for all the qualifications I have acquired working under their guidance.

To Miguel Cabello Reyes for his hardworking mentality during the project and for how comfortable this journey has been working hand in hand with him.

To my family for being constantly supportive during the long hours of hard work put to this study.

To my friends for being able to put up for my unavailability during several months, while being supportive to bring the best of me.

To the Lord Almighty for giving me the chance to revel in the culmination of this project.

OPTIMIZATION OF THE RECLINE ANGLE OF THE BACK OF A RESTRAINT SYSTEM FOR INFANTS UNDER TWO YEARS OLD TO MAXIMIZE THE SECURITY AND ERGONOMICS OF THE SYSTEM

Author: Vasserot Tolmos, Rodrigo.
Supervisor: López Valdés, Francisco José.
Collaborating Entity: Karwala Sp.

ABSTRACT

Making use of simulations in MADYMO, Siemens' multibody software, this paper concludes that there is not an optimal recline angle of the back of Karwala Sp.'s rear-facing child restraint system model Pixel AV304 for under two-year-olds which maximizes security and ergonomics. The simulation model was validated using signals of accelerations and forces recorded during a frontal crash test with a Q1.5 dummy following R-129 regulation.

Keywords: Child Restraint System (CRS), frontal impact test, rear-facing, MADYMO, R129, injury biomechanics

1. Introduction

There has recently been an increasing concern on road accidents and injuries passengers suffer from these incidents. More specifically and due to their vulnerability and YPLL [1], children are one of the main characters on which researchers have focused improvements of restraint systems and protection elements which ensure safer trips for infants in automobiles. An increase of 247% of vehicle usage worldwide from 2000 to 2016 [2] followed by a reduction of 27% of infant casualties in road accidents in the USA from 2007 to 2014 denotes the importance of the matter.

This project aims to optimize a specific child restraint system using software simulations in MADYMO analysing physical variables such as acceleration and loads measured in head, thorax, upper neck and lumbar area, which can be translated to possible injury risk. The recline angles that have been analysed in this project range from 34 to 54º from vertical, as the original Pixel AV304's recline angle has been estimated at 44º, with intervals of 2.5º.

The correct completion of this project may have a direct beneficial effect on today's society due to the analysis of a present child restraint system and its improvement to increase children's safety on the road, which sometimes is taken for granted. Suffice it to say, the study will also shed light on road safety for future investigation on infant restraint system and, in particular, on the effect of the recline angle of the back of these. Furthermore, the publication of this project will provide a properly validated model of R-129 regulation components for future MADYMO simulations and other motor vehicle crash simulators.

2. State of the Art

2.1 Motor vehicle related pediatric injuries

Since the automotive industry started to develop in 1886, road safety has always been a main concern, especially following the development of the three-point-seat-belt by Volvo in 1959, which impulse the development of child restraint systems. [3]

The number of fatalities registered between 2000 and 2009 in motor vehicle accidents in the USA suffered by people aged 0-19 experienced a reduction of 41% and ceased to be the leading cause of unintentional death between children aged 1-4 years old in 2007.[4] Furthermore, in Europe, child fatalities descended from 1300 to 654 in 2015, which represents a 50% reduction, whereas total road deaths experienced a reduction of only 39% [5]. This reduction can be largely attributed to the use of child restraint systems.

In addition, even when the CRS is not 100% perfectly used, in comparison to unrestrained children, the risk of death or serious injury when using a rearward-facing child restraint system is a 71% lower and a 54% lower when it comes to forward-facing restraint systems.[6] More specifically for younger children from 0 to 2 years old, rearward-facing restraint systems have an injury rate registered which is 0.57 times the injury rate registered for that of forward-facing systems. In addition, rear-facing restraints are 5.57 times safer in side impacts and 1.23 times safer in frontal impacts compared to front-facing restraints.[7] The National Highway Traffic Safety Administration (NHTSA) recommends that rear-facing systems with incorporated harness should be used for children aged 3 or below.[8] This way, children up to 4 years old in Sweden experienced a reduction of 90% risk for AIS 2+ injuries when using rear-facing CRSs in comparison to those unrestrained.[9]

2.2 Importance of seatback angle in rear-facing CRS

According to N. Yoganandan et al [7], child restraint systems' ability to properly restrain the occupant to the vehicle diminishes if the recline angle exceeds 45º to the vertical axis, as a result of the force exerted by the seat projecting the infant upwards becoming greater than resulting force exerted by the back of the restraint system. This means that a smaller recline angle of the back of the CRS increases the security and protection provided. On the other hand, newborns' head must be prevented from hanging forward, given that this could result in airway obstruction, as children are not able to hold their heads erect and steady enabling postural control in a seating position until 2-3 months old.[10] This way, N. Yoganandan et al [11] conclude that a recline angle of 45º from vertical provides the best compromise between both aspects, not recommending an angle smaller than 30º [12]

Sherwood et al [13,14] concluded once again in experimental tests performed with CRABI 12-month-old dummy and Q1.5 dummies that rearward-facing child restraint systems offer a greater protection than forward-facing. However, no conclusions were drawn on the most convenient recline angles which optimizes the occupants' safety.

2.3 Pediatric Injury Biomechanics and Assessment

Pediatric biomechanical studies help develop the child restraint system industry, thus contribute to the improvement of infant protection during motor vehicle crash accidents. The injury criteria to which injury risk graphs and Injury Assessment Reference Values (IARVs) are translated for Q-dummies are the only ones used in pediatric injury analysis. However, injury criteria are usually calculated and developed based on evaluations performed to just one dummy and they are later translated to other dummies via scaling. This has led to the inclusion of specific injury criteria calculation for each dummy, improving the reliability of these criteria. [15] This has been impulse by the two most important projects carried out by the EU so far on the matter: CHILD and CASPER projects. [16-18]

2.4 The Q-family of pediatric crash test dummies. Experimental crash testing and computer simulated tests

The R129 regulation states that Q-dummies are preferable when it comes to child injury risk assessment. [19] The dummy which corresponds to an 18-month-old with 11.1 kg of mass is the Q1.5, which is used in PIXEL AV304's impact test.

Similarly to this project, various studies require the design of a computational model which represents a real-life road accident or impact test. In order to confirm the reliability of the computational model and its results, the CORA rating is widely used as an objective metric of time-history similarity used to verify the computational model's validity. [20,21]

Furthermore, the MADYMO (MAthematical DYnamic MOdel) software is widely used in the automotive industry and allows to build a computational model of a motor vehicle crash using multibody three-dimensional technology combined with FE models. Many studies carried out in the recent years used MADYMO as the ideal impact simulator software to perform the experiment. [22-25]

Lastly, a general review of similar studies carried out on the field is beneficial to understand the method followed during the project or its justification. Wismans et al [24] performed MADYMO 3D simulations of Hybrid III dummy sled tests to recommend dummy model improvements. They did this by comparing model and experimental test acceleration-time histories, which can help determine the similarity between reality and simulations. Yuanzhi Hu et al [25] modelled the effects of seat belts on occupant kinematics and injury risk. Unfortunately, occupants were adults and the impact analysed was a rollover. Nonetheless, injury evaluation was performed using HIC, N_{ij} and CTI. On the other hand, Menon et al [23] carried out a similar project to the present although analysing seating angles of high back booster seats following FMVSS 213, which does not cover children under 2 years old in the EU. Despite the mentioned dissimilarities, MADYMO was the mathematical model used and a multibody bench seat was used, instead of an FE model with foam behaviour.

3. Methodology

Firstly, Karwala-Avionaut performed an homologation test on the Pixel AV304 child restraint system. This test was performed following the R-129 regulation, which dictates the necessary conditions that must be met for the homologation test to be considered valid. The CAD model of the original Pixel AV304 was pre-processed using LS-Post and materials were assigned to obtain its physical properties. Secondly, a validation model was created in MADYMO, which is the main tool used during the project. This model fulfils the R-129 regulation and aims to resemble as much as possible the real-life homologation test. The tool used to calculate the level of resemblance between the simulation model and the frontal impact test performed by Karwala-Avionaut was the CORA rating. After this validation process, the alternative models with different recline angles were obtained using LS-PrePost and imported in MADYMO to replace the original model. After the completion of the alternative models' simulations, data on accelerations, forces, torques and biomechanical metrics were gathered and analysed using MADYMO's post-processor and Excel. Finally, with all this information, the relevant injury criteria were analysed and conclusions on the effect of recline angle on occupant safety were drawn. A summary of this information is presented in Figure 1.

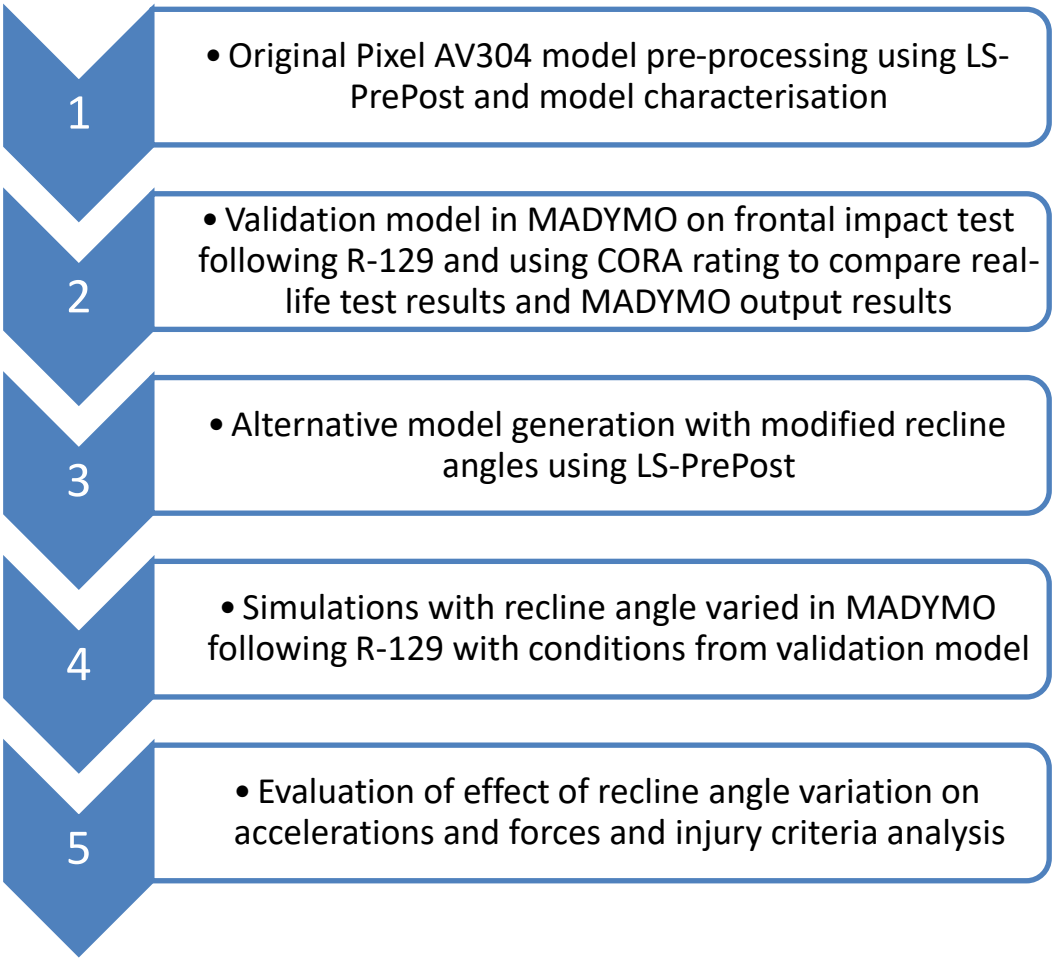

Figure 1 – Summary of methodology followed in this project

4. Results

4.1 Final validation model CORA rating

The final validation model election came down to three possible options. The model that was chosen as the final validation model, which would be replaced by the alternative models with different recline angles was that with the highest CORA rating for the neck axial force. The final CORA rating obtained was 0.713, calculated with the signals presented in Table 1, which are those commonly used for frontal impact tests. Nevertheless, the neck axial force was not considered in the CORA rating calculation as the values registered were substantially low and the signal was very noisy, which made it very complicated to model. A comparison between real-life impact test and the MADYMO model is presented in Figure 2.

Table 1 - CORA ratings for dummy's output signals and weights of final validation MADYMO model

Variable	*Axis*	*Cora Signal Identifier*	*CORA rating weight*	*CORA rating*
Head Acceleration	X	**11HEAD0000Q2ACXA**	0.2	0.790
	Z	**11HEAD0000Q2ACZA**	0.2	0.587
Neck Force	X	11NECKUP00Q2FOZB	0	0.345
Neck Torque	Y	**11NECKUP00Q2MOYB**	0.2	0.602
Thorax Acceleration	X	**11THSP0000Q2ACXA**	0.2	0.768
	Z	**11THSP0000Q2ACZA**	0.2	0.817

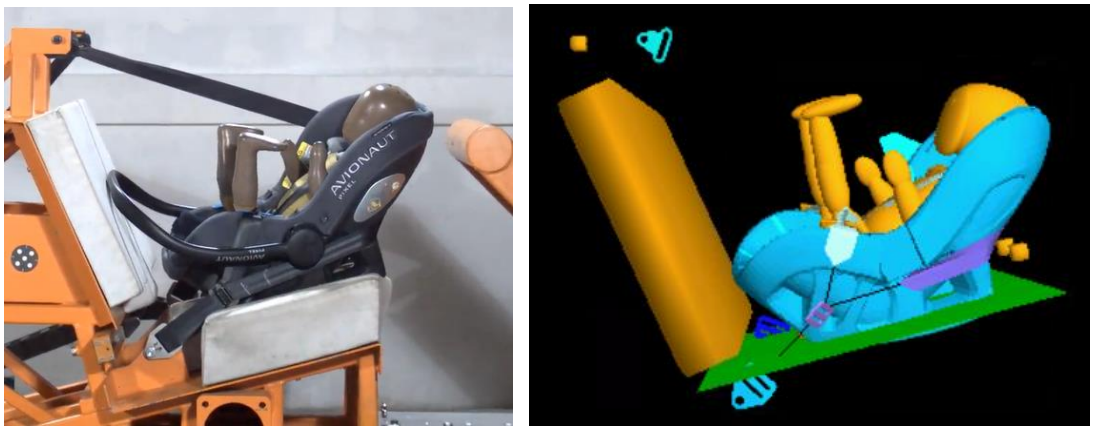

Figure 2 - a) CRS maximum seat penetration in real-life frontal impact test (t=89ms)
b) CRS maximum seat penetration in MADYMO simulation (t=90ms)

4.2 Recline angle variation

After the validation model was completed, the original Pixel AV304 CRS was replaced by the alternative models with different recline angles. The most relevant results are presented in Table 2, which help analyse the most convenient recline angle possible.

Table 2 – Relevant results obtained depending on recline angle variation

Position	MODEL	HIC15	UPPER NECK COMPRESSION (N)	UPPERNECK TENSION	UPPER NECK Y MOMENT	LUMBAR MY (Nm)
Unit	-	-	N	N	Nm	Nm
Vert	-10	59,262	-174,11	66,78	-16,22	40,09
	-7,5	65,682	-157,66	85,71	-16,68	41,88
	-5	68,889	-179,84	50,05	-18,46	40,15
	-2,5	66,306	-249,19	85,19	-20,09	21,73
Original	0	82,191	-113,34	60,54	-20,78	11,11
Horiz	2,5	76,636	-106,91	81,37	-23,11	10,66
	5	94,546	-106,96	216,88	-20,69	11,38
	7,5	91,905	-107,42	207,74	-19,65	12,02
	10	92,088	-103,98	315,04	-17,74	13,27

Higher thorax and head accelerations in the Z axis were recorded for more reclined configuration, given the reduction of head restraining. This also results in an increase of peak upper neck tension recorded during the simulation, which can be caused by excessive head acceleration, thus stretching all the spine's vertebrae. Furthermore, the peak upper neck moment recorded in the Y axis is maximum for configurations near 45º of recline angle. Lastly, the greatest drawback of more vertical configurations results in lumbar loading, where higher forces and moments are recorded due to a possible excessive upright position of the dummy. However, the lumbar region could not be validated prior to the analysis, which diminishes the reliability of these results.

5. Conclusions

A valid simulation model of the CRS under study in a frontal impact test following R129 in MADYMO was achieved with a final CORA rating of 0.713. This objective was fully accomplished thanks to the complete modelling of the R129 test bench including all belts and seat and back cushion, as well as dummy and CRS inclusion in MADYMO. Consequently, a satisfactory model was obtained for frontal impact test modelling.

Regarding the analysis of results, alternative models for the Pixel AV304 with different recline angles were successfully generated and the injury criteria were applied to all models simulated. A clear increase in head and thorax acceleration in the Z axis were observed for more reclined configurations, which resulted in higher HIC values, whereas X axis accelerations remained very similar. Secondly, regarding upper neck loading, more upright configurations produced higher compression loading, whereas more reclined configurations produced higher tension loading as a result of an increase in the head's acceleration in the Z axis. Lastly, lumbar loading was classified as the greatest drawback for more vertical configurations, as forces and moments registered in this region acquired worrying values and should be taken into consideration.

Unfortunately, it was not possible to obtain an optimal recline angle for the back of the Pixel AV304. A more upright configuration results in safer occupant positioning in all aspects except for that corresponding to lumbar region protection. Furthermore, analysis

on airway obstruction and head hanging problems typical for these configurations could be beneficial. Furthermore, the development of proper neck injury criteria for the Q1.5 dummy would also be beneficial, as these values have been estimated in this project.

Further investigation on the effect of recline angle variation on child safety can still be performed. This analysis could be performed using a human body model (HBM) substituting the Q1.5 dummy and evaluating the similarity between both models. Furthermore, in case of official upper neck injury criteria development for Q1.5 dummy, results could be evaluated again taking into considerations these hypothetic modifications. In addition, more reliable results could be obtained in case of including information on lumbar acceleration and forces for the validation model. Lastly, an optimal recline angle could be obtained by elaborating an optimization model with the weights desired for the variables that are considered more relevant.

6. Referencias

[1] J. W. Gardner and J. S. Sanborn, "Years of Potential Life Lost (YPLL) - What Does it Measure?" 1990.

[2] W. H. Organization, Global Status on Road Safety 2018. 2018.

[3] Y. Haland, "The Evolution of the Three Point Seat Belt From Yesterday to Tomorrow," *Ircobi*, no. September, pp. 3–15, 2006.

[4] J. Gilchrist, M. Ballesteros, and E. Parker, "Vital Signs: Unintentional Injury Deaths Among Persons Aged 0–19 Years — United States," *Mortal. Wkly. Rep.*, vol. 61, 2012.

[5] European Road Safety Observatory, "Traffic safety basic facts 2017: Children," p. 25, 2017, [Online]. Available: https://ec.europa.eu/transport/road_safety/sites/roadsafety/files/pdf/statistics/dacota/bfs2017_children.pdf.

[6] K. CJ, "An evaluation of child passenger safety: The effectiveness and benefits of safety seats," vol. DOT HS 806, no. February, pp. 1–482, 1986.

[7] B. Henary *et al.*, "Car safety seats for children: Rear facing for best protection," *Inj. Prev.*, vol. 13, no. 6, pp. 398–402, 2007, doi: 10.1136/ip.2006.015115.

[8] "Car Seats and Booster Seats | NHTSA." https://www.nhtsa.gov/equipment/car-seats-and-booster-seats (accessed Jun. 20, 2021).

[9] L. Jakobsson, I. Isaksson-Hellman, and B. Lundell, "Safety for the Growing Child - Experiences From Swedish Accident Data," *Proc. 19th Int. Tech. Conf. Enhanc. Saf. Veh.*, 2005.

[10] C. D. De Lima-Alvarez, E. Tudella, J. Van Der Kamp, and G. J. P. Savelsbergh, "Early development of head movements between birth and 4 months of age: A longitudinal study," *J. Mot. Behav.*, vol. 46, no. 6, pp. 415–422, 2014, doi: 10.1080/00222895.2014.929562.

[11] N. Yoganandan, A. Nahum, and J. Melvin, “Chapter 23: Best Practice Recommendations for Protecting Child Occupants,” in *Accidental injury. Biomechanics and Prevention. Vol 9*, 2015, pp. 697–715.

[12] G. R. Whitman, A. V Hart, L. Sicher, B. Benda, and L. A. D. Aulerio, “Rear-Facing Child Safety Seat Performance in Frontal NCAP Level Crashes,” no. 13, pp. 1–14, 2013.

[13] C. P. Sherwood and J. R. Crandall, “Frontal sled tests comparing rear and forward facing child restraints with 1-3 year old dummies,” *Annu. Proc. - Assoc. Adv. Automot. Med.*, pp. 169–180, 2007.

[14] C. P. Sherwood, Y. Abdelilah, J. R. Crandall, S. L. Stevens, J. M. Saggese, and M. R. Eichelberger, “The performance of various rear facing child restraint systems in a frontal crash,” *Annu. Proc. - Assoc. Adv. Automot. Med.*, pp. 303–321, 2004.

[15] R. Eppinger *et al.*, “Development of Improved Injury Criteria for the Assessment of Advanced Automotive Restraint Systems - II,” *Nthsa*, no. November, 1999.

[16] National Center for Health Statistics (NCHS), *The international classification of diseases*. 2008.

[17] J. R. Crandall, B. S. Myers, D. F. Meaney, and S. Z. Schmidtke, “Chapter 2: Epidemiology of Child Motor Vehicle Crash Injuries and Fatalities,” in *Pediatric Injury Biomechanics*, 2013, pp. 33–86.

[18] A. Palisson, F. Cassan, X. Trosseille, P. Lesire, and F. Alonzo, “Estimating Q3 dummy injury criteria for frontal impacts using the child project results and scaling reference values,” *Int. Res. Counc. Biomech. Inj. - 2007 Int. IRCOBI Conf. Biomech. Inj. Proc.*, no. September, pp. 263–276, 2007.

[19] K. de Jager *et al.*, “Assessing new child dummies and criteria for assessment of child occupant,” *19th Int. Tech. Conf. Enhanc. Saf. Veh.*, no. June, 2005.

[20] M. Seshadri, “CORrelation and Analysis (CORA) in Visual-Environment,” pp. 1–2, 2016.

[21] D. L. Albert, “Variations in User Implementation of the CORA Rating Metric,” *Stapp Car Crash J.*, vol. 64, no. November, pp. 1–30, 2020, doi: 10.4271/2020-22-0001.

[22] T. Ueda, Y. Tatenoi, and T. Nakanishi, “Applications of Occupant Safety Simulation using MADYMO,” vol. 58, no. 165, pp. 1–8, 2012.

[23] R. Menon, Y. Ghati, and P. Jain, “MADYMO simulation study to optimize the seating angles and belt positioning of high back booster seat,” pp. 1–12.

[24] J. Wismans and J. H. A. Hermans, “MADYMO 3D Simulations of Hybrid III Dummy Sled Tests,” 1988.

[25] Y. Hu, C. E. Neal-Sturgess, A. M. Hassan, and R. Guo, “Modelling the effects of seat belts on occupant kinematics and injury risk in the rollover of a sports utility vehicle (SUV),” *SAE Tech. Pap.*, no. 724, pp. 776–790, 2007, doi: 10.4271/2007-01-1502.

OPTIMIZACIÓN DEL GRADO DE INCLINACIÓN DEL RESPALDO DE UN SISTEMA DE RETENCIÓN INFANTIL PARA MENORES DE DOS AÑOS MAXIMIZANDO LA SEGURIDAD Y ERGONOMÍA

Autor: Vasserot Tolmos, Rodrigo.
Director: López Valdés, Francisco José.
Entidad Colaboradora: Karwala Sp.

RESUMEN DEL PROYECTO

Haciendo uso de simulaciones en MADYMO, el software multicuerpo de Siemens, este trabajo concluye que no existe un ángulo óptimo de reclinación del respaldo del sistema de retención infantil Pixel AV304 de Karwala Sp. para menores de dos años que maximice la seguridad y la ergonomía. El modelo de simulación se validó utilizando señales de aceleraciones y fuerzas registradas durante un ensayo de choque frontal con un dummy Q1.5 siguiendo la normativa R-129.

Palabras clave: Sistema de retención infantil (SRI), ensayo de impacto frontal, contramarcha, MADYMO, R129, biomecánica de lesiones

1. Introducción

En los últimos tiempos ha aumentado la preocupación por los accidentes de tráfico y las lesiones que sufren los pasajeros a causa de estos incidentes. En concreto, y debido a su vulnerabilidad y a la gravedad de los mismos [1], los niños son uno de los principales protagonistas en los que los investigadores han centrado las mejoras de los sistemas de retención y los elementos de protección que garantizan viajes más seguros para los bebés en los automóviles. El aumento del 247% del uso de vehículos en todo el mundo entre 2000 y 2016 [2], seguido de la reducción del 27% de las víctimas infantiles en accidentes de tráfico en EE.UU. entre 2007 y 2016 denota la importancia del asunto.

Este proyecto pretende optimizar un sistema de retención infantil específico mediante simulaciones de software en MADYMO analizando variables físicas como la aceleración y las cargas medidas en la cabeza, el tórax, la parte superior del cuello y la zona lumbar, que pueden traducirse en un posible riesgo de lesiones. Los ángulos de reclinación que se han analizado en este proyecto oscilan entre 34 y 54º respecto a la vertical, ya que el ángulo de reclinación original del Pixel AV304 se ha estimado en 44º, con intervalos de 2,5º.

La correcta realización de este proyecto puede tener un efecto beneficioso directo en la sociedad actual debido al análisis de un sistema de retención infantil actual y su mejora para aumentar la seguridad de los niños en la carretera, que a veces se da por supuesta. Basta decir que el estudio también arrojará luz sobre la seguridad vial para futuras investigaciones sobre el sistema de retención infantil y, en particular, sobre el efecto del ángulo de reclinación del respaldo de éstos. Además, la publicación de este proyecto proporcionará un modelo debidamente validado de los componentes de la normativa R-129 para futuras simulaciones del MADYMO y otros simuladores de choque de vehículos de motor.

2. Estado de la técnica

2.1 Lesiones pediátricas relacionadas con los vehículos de motor

Desde que la industria del automóvil comenzó a desarrollarse en 1886, la seguridad vial ha sido siempre una de las principales preocupaciones, especialmente tras el desarrollo del cinturón de seguridad de tres puntos por parte de Volvo en 1959, que impulsó el desarrollo de los sistemas de retención infantil. [3]

El número de víctimas mortales registradas entre 2000 y 2009 en accidentes de vehículos de motor en EE.UU. sufridos por personas de 0 a 19 años experimentó una reducción del 41% y dejó de ser la principal causa de muerte no intencionada entre los niños de 1 a 4 años en 2007 [4] Además, en Europa, las víctimas mortales infantiles descendieron de 1.300 a 654 en 2015, lo que representa una reducción del 50%, mientras que el total de muertes en carretera experimentó una reducción de sólo el 39% [5]. Esta reducción puede atribuirse en gran medida al uso de sistemas de retención infantil.

Además, incluso cuando el SRI no se utiliza perfectamente al 100%, en comparación con los niños sin cinturón de seguridad, el riesgo de muerte o de lesiones graves cuando se utiliza un sistema de retención infantil orientado hacia atrás es un 71% menor y un 54% menor cuando se trata de sistemas de retención orientados hacia delante[6] Más concretamente, en el caso de los niños más pequeños, de 0 a 2 años, los sistemas de retención a contramarcha registran una tasa de lesiones 0,57 veces superior a la de los sistemas orientados a favor de la marcha. Además, los sistemas de retención a contramarcha son 5,57 veces más seguros en los impactos laterales y 1,23 veces más seguros en los impactos frontales en comparación con los sistemas orientados a favor de la marcha.[7] La Administración Nacional de Seguridad del Tráfico en Carreteras (NHTSA) recomienda que los sistemas a contramarcha con arnés incorporado se utilicen para niños de 3 años o menos.[8] De este modo, los niños de hasta 4 años en Suecia experimentaron una reducción del 90% del riesgo de lesiones AIS 2+ al utilizar los SRI a contramarcha en comparación con los que no estaban sujetos.[9]

2.2 Importancia del ángulo del respaldo en los SRI orientados a contramarcha

Según N. Yoganandan et al [7], la capacidad de los sistemas de retención infantil para sujetar adecuadamente al ocupante al vehículo disminuye si el ángulo de reclinación supera los 45º con respecto al eje vertical, como resultado de que la fuerza ejercida por el asiento que proyecta al bebé hacia arriba es mayor que la fuerza resultante ejercida por el respaldo del sistema de retención. Esto significa que un menor ángulo de reclinación del respaldo del SRI aumenta la seguridad y la protección proporcionadas. Por otro lado, hay que evitar que la cabeza de los recién nacidos cuelgue hacia delante, ya que esto podría provocar una obstrucción de las vías respiratorias, al ser los niños incapaces de mantener la cabeza erguida y estable permitiendo el control postural en posición sentada hasta los 2-3 meses de edad[10] Así, N. Yoganandan et al [11] concluyen que un ángulo de reclinación de 45º con respecto a la vertical proporciona el mejor compromiso entre ambos aspectos, no recomendando un ángulo inferior a 30º[12].

Sherwood et al [13,14] concluyeron, una vez más, en las pruebas experimentales realizadas con el dummy CRABI 12-month-old y el Q1.5, que los sistemas de retención infantil orientados a contramarche ofrecen una mayor protección que los a favor de la marcha. Sin embargo, no se extrajeron conclusiones sobre los ángulos de reclinación más convenientes que optimizan la seguridad de los ocupantes.

2.3 Biomecánica y evaluación de lesiones pediátricas

Los estudios biomecánicos pediátricos ayudan a desarrollar la industria de los sistemas de retención infantil, contribuyendo así a la mejora de la protección de los bebés durante los accidentes de tráfico. Los criterios de lesión a los que se traducen los gráficos de riesgo de lesión y los valores de referencia de evaluación de lesiones (IARV) para los dummies Q son los únicos que se utilizan en el análisis de las lesiones pediátricas. Sin embargo, los criterios de lesión suelen calcularse y desarrollarse a partir de evaluaciones realizadas a un solo dummy y, posteriormente, se trasladan a otros dummies mediante un escalado. Esto ha llevado a incluir el cálculo de criterios de lesión específicos para cada dummy, mejorando la fiabilidad de estos criterios. [15] Esto ha sido impulsado por los dos proyectos más importantes llevados a cabo por la UE hasta el momento en esta materia: Los proyectos CHILD y CASPER. [16-18]

2.4 La familia Q de maniquíes pediátricos para ensayos de impacto. Ensayos de impacto experimentales y pruebas simuladas por ordenador

El reglamento R129 establece que los dummies Q son preferibles cuando se trata de evaluar el riesgo de lesiones en los niños. [19] El dummy que corresponde a un niño de 18 meses con 11,1 kg de masa es el Q1.5, que se utiliza en el ensayo de impacto de PIXEL AV304.

Al igual que en este proyecto, varios estudios requieren el diseño de un modelo computacional que represente un accidente de tráfico o un ensayo de impacto real. Para confirmar la fiabilidad del modelo computacional y sus resultados, se utiliza la clasificación CORA como métrica objetiva de la similitud entre señales temporales utilizada para verificar la validez del modelo computacional. [20,21]

Además, el software MADYMO (MAthematical DYnamic MOdel) se utiliza ampliamente en la industria del automóvil y permite construir un modelo computacional de un choque de vehículos utilizando tecnología multicuerpo combinada con modelos de elementos finitos. Muchos estudios realizados en los últimos años han utilizado MADYMO como software simulador de impactos ideal para realizar el experimento. [22-25]

Por último, una revisión general de estudios similares realizados sobre el terreno es beneficiosa para comprender el método seguido durante el proyecto o su justificación. Wismans et al [24] realizaron simulaciones en MADYMO 3D de las pruebas del trineo del maniquí Hybrid III para recomendar mejoras en el modelo del dummy. Para ello, compararon las señales de aceleración-tiempo del modelo y de las pruebas experimentales, lo que puede ayudar a determinar la similitud entre la realidad y las

simulaciones. Yuanzhi Hu et al [25] modelaron los efectos de los cinturones de seguridad en la cinemática de los ocupantes y el riesgo de lesiones. Lamentablemente, los ocupantes eran adultos y el impacto analizado fue un vuelco. No obstante, la evaluación de las lesiones se realizó mediante HIC, Nij y CTI. Por otro lado, Menon et al [23] llevaron a cabo un proyecto similar al presente, aunque analizando los ángulos de asiento de los asientos elevados de respaldo según la norma FMVSS 213, que no cubre a los niños menores de 2 años en la UE. A pesar de las mencionadas disimilitudes, el modelo matemático utilizado fue MADYMO y se utilizó un asiento de banco multicuerpo, en lugar de un modelo de elementos finitos con comportamiento de espuma.

3. Metodología

En primer lugar, Karwala-Avionaut realizó una prueba de homologación del sistema de retención infantil Pixel AV304. Esta prueba se realizó siguiendo la normativa R-129, que dicta las condiciones necesarias que deben cumplirse para que la prueba de homologación se considere válida. El modelo CAD del Pixel AV304 original se preprocesó con LS-Post y se asignaron los materiales para obtener sus propiedades físicas. En segundo lugar, se creó un modelo de validación en MADYMO, que es la principal herramienta utilizada durante el proyecto. Este modelo cumple con la normativa R-129 y pretende asemejarse lo máximo posible a la prueba de homologación real. La herramienta utilizada para calcular el nivel de parecido entre el modelo de simulación y la prueba de impacto frontal realizada por Karwala-Avionaut fue la calificación CORA. Tras este proceso de validación, se obtuvieron los modelos alternativos con diferentes ángulos de reclinación mediante LS-PrePost y se importaron en MADYMO para sustituir al modelo original. Tras la finalización de las simulaciones de los modelos alternativos, se recopilaron y analizaron los datos de aceleraciones, fuerzas, momentos y variables biomecánicas mediante el postprocesador de MADYMO y Excel. Finalmente, con toda esta información, se analizaron los criterios de lesión pertinentes y se extrajeron conclusiones sobre el efecto del ángulo de reclinación en la seguridad de los ocupantes.

4. Resultados

4.1 Clasificación CORA del modelo de validación final

La elección del modelo de validación final se redujo a tres opciones posibles. El modelo que se eligió como modelo de validación final, que sería sustituido por los modelos alternativos con diferentes ángulos de reclinación, fue el que obtuvo la mayor calificación CORA para la fuerza axial del cuello. El índice CORA final obtenido fue de 0,713, calculado con las señales presentadas en la Tabla 1, que son las que se utilizan habitualmente en los ensayos de impacto frontal. No obstante, la fuerza axial del cuello no se tuvo en cuenta en el cálculo de la calificación CORA, ya que los valores registrados eran sustancialmente bajos y la señal tenía mucho ruido, lo que hacía muy complicado su modelado. En la Figura 1 se muestra una comparativa del modelo real y el modelo de MADYMO.

Tabla 1 -Puntuación CORA para señales del dummy y pesos del modelo final de validación de MADYMOl

Variable	*Axis*	*Cora Signal Identifier*	*CORA rating weight*	*CORA rating*
Head Acceleration	X	**11HEAD0000Q2ACXA**	0.2	0.790
	Z	**11HEAD0000Q2ACZA**	0.2	0.587
Neck Force	X	11NECKUP00Q2FOZB	0	0.345
Neck Torque	Y	**11NECKUP00Q2MOYB**	0.2	0.602
Thorax Acceleration	X	**11THSP0000Q2ACXA**	0.2	0.768
	Z	**11THSP0000Q2ACZA**	0.2	0.817

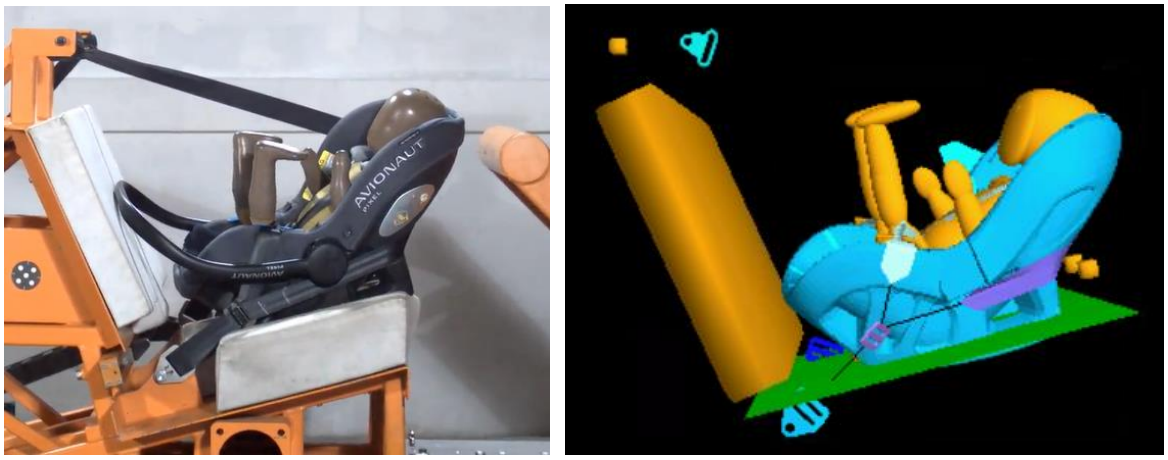

Figura 1 - a) CRS maximum seat penetration in real-life frontal impact test (t=89ms)
b) CRS maximum seat penetration in MADYMO simulation (t=90ms)

4.2 Variación del ángulo de reclinación

Una vez completado el modelo de validación, se sustituyó el SRI original Pixel AV304 por los modelos alternativos con diferentes ángulos de reclinación. Los resultados más relevantes se presentan en la Tabla 2, que ayudan a analizar el ángulo de reclinación más conveniente posible.

Table 2 – Relevant results obtained depending on recline angle variation

Position	MODEL	HIC15	UPPER NECK COMPRESSION (N)	UPPERNECK TENSION	UPPER NECK Y MOMENT	LUMBAR MY (Nm)
Unit	-	-	N	N	Nm	Nm
Vert	-10	59,262	-174,11	66,78	-16,22	40,09
	-7,5	65,682	-157,66	85,71	-16,68	41,88
	-5	68,889	-179,84	50,05	-18,46	40,15
	-2,5	66,306	-249,19	85,19	-20,09	21,73
Original	0	82,191	-113,34	60,54	-20,78	11,11
Horiz	2,5	76,636	-106,91	81,37	-23,11	10,66
	5	94,546	-106,96	216,88	-20,69	11,38
	7,5	91,905	-107,42	207,74	-19,65	12,02
	10	92,088	-103,98	315,04	-17,74	13,27

Se registraron mayores aceleraciones del tórax y de la cabeza en el eje Z para una configuración más reclinada, dada la reducción de la sujeción de la cabeza. Esto también se traduce en un aumento de la tensión máxima de la parte superior del cuello registrada durante la simulación, lo que puede deberse a una aceleración excesiva de la cabeza, que estira todas las vértebras de la columna vertebral. Además, el momento máximo de la parte superior del cuello registrado en el eje Y es máximo para las configuraciones cercanas a los 45º de ángulo de reclinación. Por último, el mayor inconveniente de las configuraciones más verticales se produce en la carga lumbar, donde se registran fuerzas y momentos más elevados debido a una posible posición excesivamente erguida del maniquí. Sin embargo, la región lumbar no pudo ser validada antes del análisis, lo que disminuye la fiabilidad de estos resultados.

5. Conclusiones

Se logró un modelo de simulación válido del SRI en estudio en una prueba de impacto frontal siguiendo el R129 en MADYMO, con una calificación final de CORA de 0,713. Este objetivo se cumplió plenamente gracias a la modelización completa del banco de pruebas R129, incluidos todos los cinturones y el cojín del asiento y el respaldo, así como la inclusión del dummy y el SRI en MADYMO. En consecuencia, se obtuvo un modelo satisfactorio para la modelización de las pruebas de impacto frontal.

En cuanto al análisis de los resultados, se generaron con éxito modelos alternativos para el Pixel AV304 con diferentes ángulos de reclinación y se aplicaron los criterios de lesión a todos los modelos simulados. Se observó un claro aumento de la aceleración de la cabeza y el tórax en el eje Z para las configuraciones más reclinadas, lo que dio lugar a valores de HIC más elevados, mientras que las aceleraciones del eje X se mantuvieron muy similares. En segundo lugar, en lo que respecta a la carga de la parte superior del cuello, las configuraciones más erguidas produjeron una mayor carga de compresión,

mientras que las configuraciones más reclinadas produjeron una mayor carga de tracción como resultado de un aumento de la aceleración de la cabeza en el eje Z. Por último, la carga lumbar se clasificó como el mayor inconveniente para las configuraciones más verticales, ya que las fuerzas y los momentos registrados en esta región adquirieron valores preocupantes y deben tenerse en cuenta.

Lamentablemente, no fue posible obtener un ángulo de reclinación óptimo para la espalda del Pixel AV304. Una configuración más erguida da lugar a una posición más segura del ocupante en todos los aspectos, excepto en el correspondiente a la protección de la región lumbar. Además, el análisis sobre la obstrucción de las vías respiratorias y los problemas de sujeción de la cabeza típicos de estas configuraciones podría ser beneficioso. Además, también sería beneficioso el desarrollo de criterios adecuados de lesión cervical para el dummy Q1.5, cuyos valores se han estimado en este proyecto.

Se puede seguir investigando el efecto de la variación del ángulo de reclinación en la seguridad de los niños. Este análisis podría realizarse utilizando un modelo de cuerpo humano (HBM) en sustitución del dummy Q1.5 y evaluando la similitud entre ambos modelos. Además, en caso de que se desarrollen criterios oficiales de lesión en la parte superior del cuello para el dummy Q1.5, los resultados podrían evaluarse de nuevo teniendo en cuenta estas hipotéticas modificaciones. Además, se podrían obtener resultados más fiables en caso de incluir información sobre la aceleración y las fuerzas lumbares para el modelo de validación. Por último, se podría obtener un ángulo de reclinación óptimo elaborando un modelo de optimización con los pesos deseados para las variables que se consideren más relevantes.

6. Referencias

[1] J. W. Gardner and J. S. Sanborn, “Years of Potential Life Lost (YPLL) - What Does it Measure?” 1990.

[2] W. H. Organization, Global Status on Road Safety 2018. 2018.

[3] Y. Haland, “The Evolution of the Three Point Seat Belt From Yesterday to Tomorrow,” *Ircobi*, no. September, pp. 3–15, 2006.

[4] J. Gilchrist, M. Ballesteros, and E. Parker, “Vital Signs: Unintentional Injury Deaths Among Persons Aged 0–19 Years — United States,” *Mortal. Wkly. Rep.*, vol. 61, 2012.

[5] European Road Safety Observatory, “Traffic safety basic facts 2017: Children,” p. 25, 2017, [Online]. Available: https://ec.europa.eu/transport/road_safety/sites/roadsafety/files/pdf/statistics/dacota/bfs2017_children.pdf.

[6] K. CJ, “An evaluation of child passenger safety: The effectiveness and benefits of safety seats,” vol. DOT HS 806, no. February, pp. 1–482, 1986.

[7] B. Henary *et al.*, “Car safety seats for children: Rear facing for best protection,” *Inj. Prev.*, vol. 13, no. 6, pp. 398–402, 2007, doi: 10.1136/ip.2006.015115.

[8] “Car Seats and Booster Seats | NHTSA.” https://www.nhtsa.gov/equipment/car-seats-and-booster-seats (accessed Jun. 20, 2021).

[9] L. Jakobsson, I. Isaksson-Hellman, and B. Lundell, “Safety for the Growing Child - Experiences From Swedish Accident Data,” *Proc. 19th Int. Tech. Conf. Enhanc. Saf. Veh.*, 2005.

[10] C. D. De Lima-Alvarez, E. Tudella, J. Van Der Kamp, and G. J. P. Savelsbergh, “Early development of head movements between birth and 4 months of age: A longitudinal study,” *J. Mot. Behav.*, vol. 46, no. 6, pp. 415–422, 2014, doi: 10.1080/00222895.2014.929562.

[11] N. Yoganandan, A. Nahum, and J. Melvin, “Chapter 23: Best Practice Recommendations for Protecting Child Occupants,” in *Accidental injury. Biomechanics and Prevention. Vol 9*, 2015, pp. 697–715.

[12] G. R. Whitman, A. V Hart, L. Sicher, B. Benda, and L. A. D. Aulerio, “Rear-Facing Child Safety Seat Performance in Frontal NCAP Level Crashes,” no. 13, pp. 1–14, 2013.

[13] C. P. Sherwood and J. R. Crandall, “Frontal sled tests comparing rear and forward facing child restraints with 1-3 year old dummies,” *Annu. Proc. - Assoc. Adv. Automot. Med.*, pp. 169–180, 2007.

[14] C. P. Sherwood, Y. Abdelilah, J. R. Crandall, S. L. Stevens, J. M. Saggese, and M. R. Eichelberger, “The performance of various rear facing child restraint systems in a frontal crash,” *Annu. Proc. - Assoc. Adv. Automot. Med.*, pp. 303–321, 2004.

[15] R. Eppinger *et al.*, “Development of Improved Injury Criteria for the Assessment of Advanced Automotive Restraint Systems - II,” *Nthsa*, no. November, 1999.

[16] National Center for Health Statistics (NCHS), *The international classification of diseases*. 2008.

[17] J. R. Crandall, B. S. Myers, D. F. Meaney, and S. Z. Schmidtke, “Chapter 2: Epidemiology of Child Motor Vehicle Crash Injuries and Fatalities,” in *Pediatric Injury Biomechanics*, 2013, pp. 33–86.

[18] A. Palisson, F. Cassan, X. Trosseille, P. Lesire, and F. Alonzo, “Estimating Q3 dummy injury criteria for frontal impacts using the child project results and scaling reference values,” *Int. Res. Counc. Biomech. Inj. - 2007 Int. IRCOBI Conf. Biomech. Inj. Proc.*, no. September, pp. 263–276, 2007.

[19] K. de Jager *et al.*, “Assessing new child dummies and criteria for assessment of child occupant,” *19th Int. Tech. Conf. Enhanc. Saf. Veh.*, no. June, 2005.

[20] M. Seshadri, “CORrelation and Analysis (CORA) in Visual-Environment,” pp. 1–2, 2016.

[21] D. L. Albert, “Variations in User Implementation of the CORA Rating Metric,” *Stapp Car Crash J.*, vol. 64, no. November, pp. 1–30, 2020, doi: 10.4271/2020-22-0001.

[22] T. Ueda, Y. Tatenoi, and T. Nakanishi, “Applications of Occupant Safety Simulation using MADYMO,” vol. 58, no. 165, pp. 1–8, 2012.

[23] R. Menon, Y. Ghati, and P. Jain, “MADYMO simulation study to optimize the seating angles and belt positioning of high back booster seat,” pp. 1–12.

[24] J. Wismans and J. H. A. Hermans, “MADYMO 3D Simulations of Hybrid III Dummy Sled Tests,” 1988.

[25] Y. Hu, C. E. Neal-Sturgess, A. M. Hassan, and R. Guo, “Modelling the effects of seat belts on occupant kinematics and injury risk in the rollover of a sports utility vehicle (SUV),” *SAE Tech. Pap.*, no. 724, pp. 776–790, 2007, doi: 10.4271/2007-01-1502.

Contents

List of Figures

List of Tables

Chapter 1. INTRODUCTION

There has recently been an increasing concern on road accidents and injuries passengers suffer from these incidents. More specifically and due to their vulnerability, children are one of the main characters on which researchers have focused improvements of restraint systems and protection elements which ensure safer trips for infants in automobiles.

This project aims to optimize a specific child restraint system using software simulations in MADYMO analysing physical variables such as acceleration and force, which can be translated to possible injury risk.

The correct completion of this project may have a direct beneficial effect on today's society due to the analysis of a present child restraint system and its improvement to increase children's safety on the road, which sometimes is taken for granted. Suffice it to say, the study will also shed light on road safety for future investigation on infant restraint system and, in particular, on the effect of the recline angle of the back of these. Furthermore, the publication of this project will provide a properly validated model of R-129 regulation components for future MADYMO simulations and other motor vehicle crash simulators.

1.1 MOTIVATION

Due to the number of casualties and injured passengers happening in motor vehicle crashes and an increase of the number of motor vehicle users globally, a general concern has raised among scientists to study the technologies used to prevent injuries and deaths in road accidents, leading to the improvement and optimization of all systems with the mentioned goal.

Although the number of motor vehicle used has been rising for the past years up to a 247% from 2000 to 2016, the rate of casualties per 100,000 vehicles has experienced a reduction

of 53% as shown on Figure 1.1, mainly as a result of the improvement of restraint systems, belts, vehicles, roads, etc… [1]

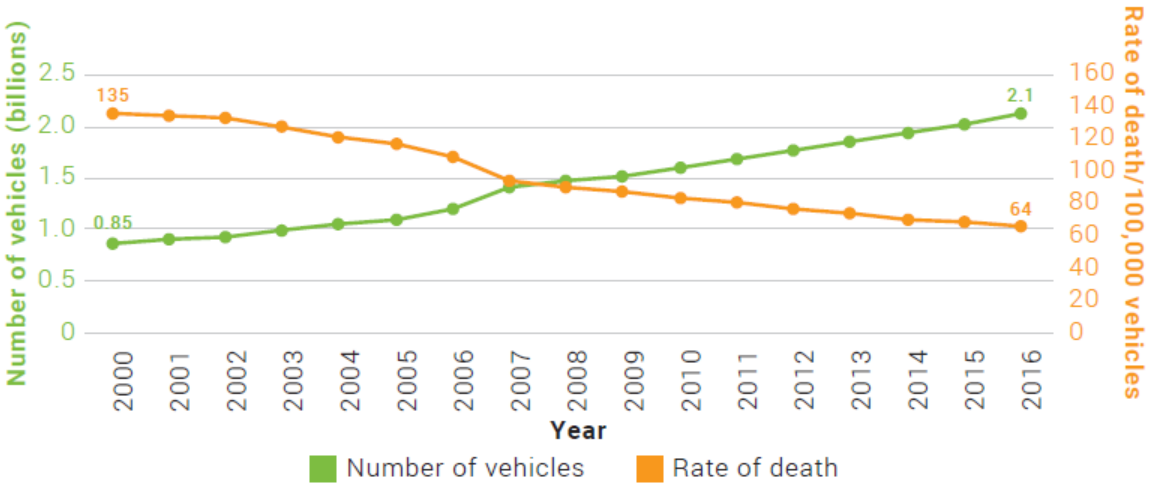

Figure 1.1 - Number of motor vehicles and road death incidence per 100,000 vehicles worldwide. (Source: W. H. Organization, 2018)

Nonetheless, this piece of information could result misleading as the rate of death has been measured per 100,000 vehicles. This number is calculated dividing the total number of casualties over the size of the population measured and multiplied times 10^n to express the death rate per 10^n individuals. In this case, given a substantial increase in number of vehicles (247% in 16 years), the reduction in rate of death per 100,000 vehicles can be justified by the increase of vehicles used, instead of by a reduction of deaths in the population. For this reason, the rate of death per individuals may offer a more objective insight on the matter. As shown in Figure 1.2, the rate of death per 100,000 inhabitants shows a reduction of a 3%, which still implicates saving thousands of lives worldwide, but denotes the existence of room for improvement. This also shows a diminution in the mean number of passengers per vehicle, as the effect noted in one graph differs from that shown in the other. [1]

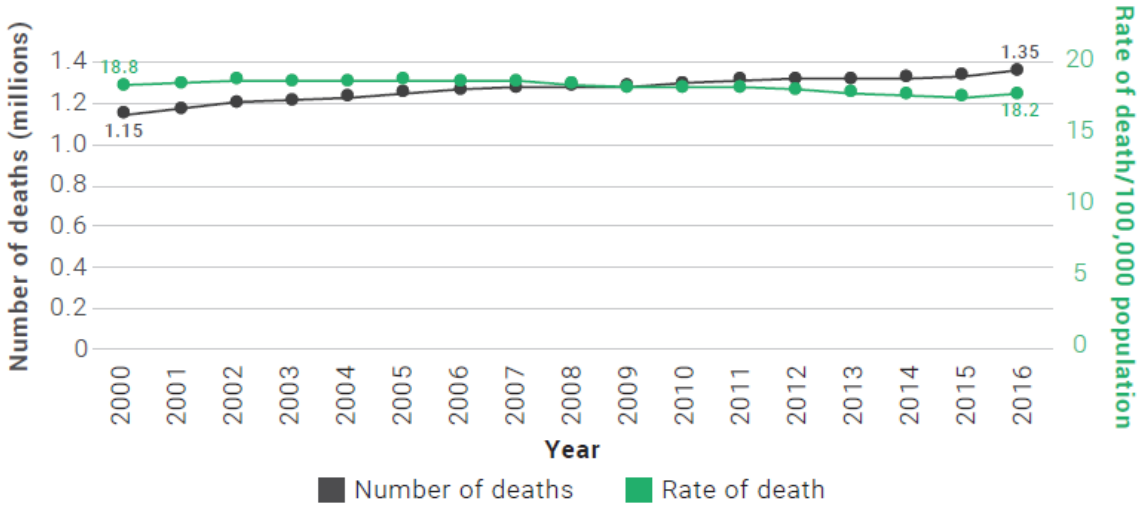

Figure 1.2 – Number and rate of road traffic death per 100,000 population worldwide. (Source: NHTSA, 2018)

More specifically, infants have been identified as one of the most vulnerable age groups when it comes to vehicle accidents. This is due to the consequences a severe injury may have on a child, as children have their whole lives ahead of them and, in case of a severe injury, they would have to carry that injury's load for the rest of their lives. Moreover, given their young age, in case of suffering a mortal road accident, the years of potential life lost (YPLL) is a metric which helps measure the years an individual would have lived if they had not died prematurely. This metric emphasises the burden premature infant casualties have on society and justifies the vulnerability of children in road safety. [2] In 2016, three children were killed each day in road traffic accidents in the USA following the distribution presented in Figure 1.3, which sets a total of 908 infant casualties as occupants in road traffic accidents. [3] This proves a higher casualty incidence for children in road traffic accidents as motor vehicles' occupants than for infant pedestrians, cyclists and other means of transport.

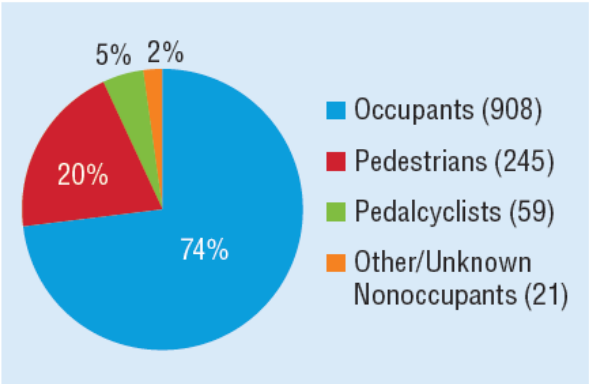

Figure 1.3 - Child casualty distribution in road traffic accidents in USA in 2016. (Source: NHTSA, 2018)

Nevertheless, an improvement on casualty and injury data on motor vehicle crashes can be easily identified throughout past recent years, as a result of all the investigation and effort scientists are placing on the matter. Figure 1.4 shows the slight reduction on infant fatalities on road accidents in USA since 2007, considering children anybody under 14 years old [3]. In a total of 10 years, the number of infant casualties in motor vehicle incidents experienced a reduction of 27%, which happened to be even greater at some points, such as 2014, year in which this statistic reaches its minimum at 1073 infant deaths. Furthermore, Figure 1.5 shows the number of fatalities in child motor accidents classified by age group in USA, all experiencing a reduction in the number of dead passengers from 2007 to 2016. [3]

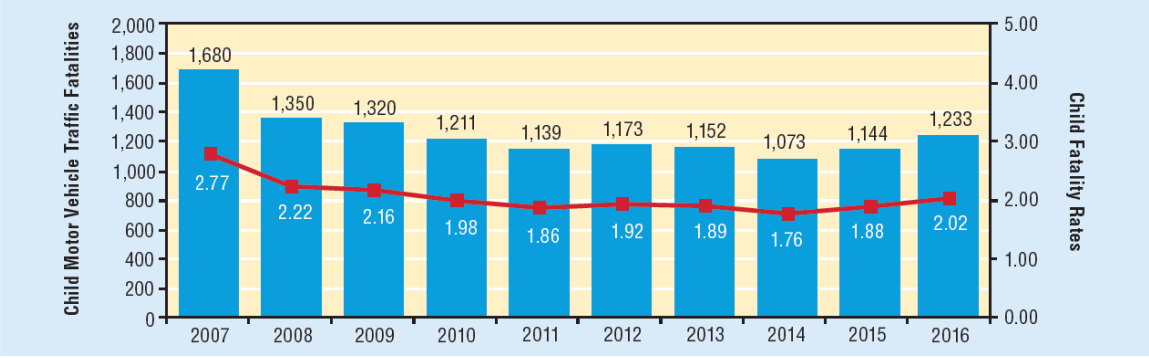

Figure 1.4 - Infant motor vehicle traffic deaths and fatality rates per 100,000 children in USA. (Source: NHTSA, 2018)

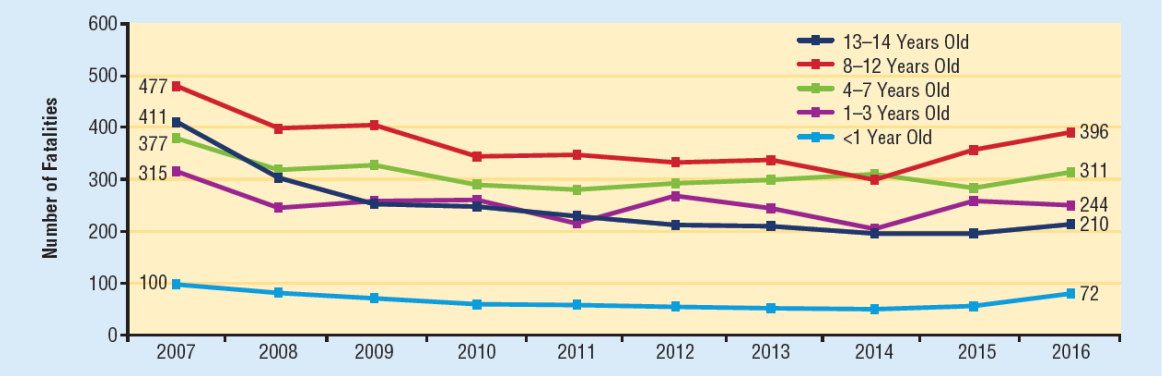

Figure 1.5 - Infant motor vehicle traffic deaths per 100,000 children by age group in USA. (Source: NHTSA, 2018)

One of the main contributions which have helped during the past years to enhance child road safety are child restraint systems (CRS). These elements have accomplished a notable reduction in the number of infant casualties and severe injuries suffered by younger passengers in motor vehicle crashes. It is believed that child restraint usage can lead to a reduction of at least 60% in child casualties [4] and child restraint systems have been identified to be most effective for children under the age of 4 years old.[5]

However, these systems undergo a constant review and different alternative models are being designed aiming to improve child protection. This design process is performed based on different regulations which help compare results obtained by different entities. In Europe, the present regulation responsible for the homologation process of CRSs is the R-129, which dictates all the necessary conditions under which tests must be performed to evaluate the convenience of certain model modifications or industrial innovation.

1.2 PROJECT'S OBJECTIVE

Taking into consideration the current situation on road safety previously presented, this study aims to improve infant protection during motor vehicle crashes enhancing investigation on child restraint systems and their configurations. For this reason, this project's goal is to improve the existing child restraint system Avionaut Pixel AV304 in order to contribute to the still constant reduction of pediatric injuries and deaths in road accidents. The restraint system used has been provided by Karwala-Avionaut, a polish child restraint manufacturer focused on the improvement of road safety, especially for infants. The aspect to optimize in the model provided will be the recline angle of the back of the Pixel AV304 which maximizes security and ergonomics for infants under two years old. This will be done by analysing the effect that a variation in the recline angle of the back of the CRS has on head and thorax acceleration, as well as neck forces and torques.

1.3 SUMMARY OF METHODOLOGY

This study will be carried out using a computational model of the restraint system, having Karwala-Avionaut provided a confidential CAD version of the Pixel model AV304 which had to be preprocessed using LS-PrePost to create a mesh and generate its respective nodes and elements with their respective materials assigned. The project's attainment is to be reached performing simulations on multielement software. The software used to evaluate the effect a variation on the recline angle of the back of the restraint system has on the vertebral health of the infant is MADYMO. This software developed by Tass International and currently owned by Siemens is widely used to perform simulations on motor vehicle crashes due to the dummy models available on the system and the flexibility it offers on elements and configurations. [6]

Prior to the analysis of the effect of the recline angle of the back on the cervical vertebrae, it is compulsory to validate the model created on MADYMO. Using accelerations measured on a real car crash test with a dummy and the restraint system model, the model is to be

modified until values of variables measured during test match those obtained with the simulation. More specifically, the validation of the model will be carried out using the signal registered for displacement and acceleration of chest, neck and head of the dummy and comparing results to the signals measured in the real crash test performed by Karwala-Avionaut using CORA, a correlation and analysis software common in the field. The method followed by CORA to calculate similarity between time-history data will be thoroughly explained in Chapter 2.3. The CORA rating aimed to categorise the model as successful is a minimum value of 0.6. Car crash tests follow certain rules so that results can be compared to one another and the simulations performed must also meet the requirements set by these rules. Both the real and the computational test were performed following the regulation R-129, which sets the conditions under which the test is completed, such as the acceleration pulse suffered by the passenger or the dimensions of the test bench. This document will provide the necessary information on the R-129 regulation to comprehend the physical context in which the simulation and the real crash test were performed, as well as the dynamic conditions to which models have to be put through.

Nonetheless, it is necessary to create a suitable computational model of the test bench cushions which emulates the behaviour of the element in real life crash tests. In order to obtain the suitable model, an impact test is performed on the cushions following certain specific rules stated in R129 regulation. Data extracted from a real-life impact test performed on a cushion enables the characterisation of the foam material used by changing foam material parameters in a model obtained from LS-PrePost.

A successful validation of the model will allow to perform the desired modifications in the recline angle of the back of the restraint system and these alternative models will be simulated under the exact same conditions as those from the validation model. The bench used for these simulations will not be modified in any aspect (positions or angles) and only the CAD file of the model will experience modifications. These modifications are to be performed using LS-PrePost varying the model's nodes and elements to reshape the restraint system and obtain a new recline angle. Should it be mentioned that both lap and shoulder

belt must be refitted for each simulation to ensure a correct placement and accommodation of both dummy and restraint system to the test bench.

After the completion of all necessary simulations, information on neck acceleration will be translated to possible injury risk, reaching a conclusion on the recline angle which best ensures the security of the infant. The possible cervical harm experienced by the passenger will be evaluated using the Head Injury Criterion (HIC), which measures the likelihood of a cervical injury following an impact, considering both the duration of the impact and the accelerations suffered by the centre of mass of the dummy's head. HIC values can be obtained for different intervals of time, standing HIC15 (15ms) and HIC36 (36ms) out as the most representative HIC values for injury detection and analysis.[7]–[9]

Another injury risk which will be analysed when evaluating new recline angle configurations is the neck injury risk. When assessing possible damage suffered in the cervical region, many variables can be considered. In this project, time-history values of neck acceleration and displacement will be used to perform a more subjective appraisal of cervical wellness and, on the other hand, a more objective insight will be provided by the neck injury criterion, N_{ij}, which is obtained by the total value of flexion bending moment and axial load after a normalization of values which depends on the passenger's age and the type of dummy used. [10]

Furthermore, it is also possible to assess thoracic injury risk, which can also help ensure the occupant's safety, by calculating the Combined Thoracic Index (CTI), formulated to summarise chest deflection and acceleration in the same criterion. For this reason, the CTI is calculated by adding up both peak chest acceleration and maximum chest deflection after normalising each value in the same way it is done when applying the neck injury criterion. The values over which data is normalised are the corresponding maximum allowable intercept values and are stipulated depending on the passenger's age and the type of dummy which is being used in the impact test. [10]

The criteria previously presented are objective indicators on the severity of a cervical and thoracic injury which can be calculated in case of measuring the occupant's head acceleration, peak moments and axial cervical forces or peak thoracic acceleration and displacement. On the other hand, due to the impossibility in real-life accidents to gather the previously mentioned data, it is necessary to resort to an injury criterion which can be executed when evaluating an injured patient: Injury Severity Score (ISS) and Abbreviated Injury Scale (AIS). These are both metrics which help turn subjective information and a diagnosis on an injured individual to more objective information which can be measured, compared and classified using numbers.[8] The AIS grades an injury from 0 to 6 depending on the level of severity of an injury being 6 the worst case scenario as shown in Table 1.1.[11] The ISS is a score between 0 and 75 obtained from adding certain AIS values from three different body components (head, neck, thorax, abdomen, etc…) as presented in equation *E. 1.1*, which helps determine the existence of multiple injuries. [12]

Table 1.1 - Abbreviated Injury Scale (AIS) vs injury severity. Source: Yoganandan et al, 2015

AIS Score	*Injury severity*
1	Minor
2	Moderate
3	Serious
4	Severe
5	Critical
6	Maximal (currently untreatable)

$$ISS = \left(MaxAIS_{bodyregion1}\right)^2 + \left(MaxAIS_{bodyregion2}\right)^2 + \left(MaxAIS_{bodyregion3}\right)^2 \quad E.\ 1.1$$

These scores can be used combined with the other criteria previously stated (head, neck and thorax) to evaluate the severity of injuries experienced by the vehicle's occupant in the project, therefore affecting the decision on the optimal recline angle of the back of Karwala-

Avionaut's child restraint system which maximizes the passenger's safety. However, it has been decided not to make use of these criteria as no medical injury examination has been performed in the project. The AIS and ISS may be used in case of working with injury data or in case of performing an analysis on injury risk and severity.

To facilitate the comprehension of the methodology followed throughout the project, it has been decided to add the following flowchart with all the main steps followed till the completion of the project. It may be useful to have a general overview of the course of the study and the tools used in each phase.

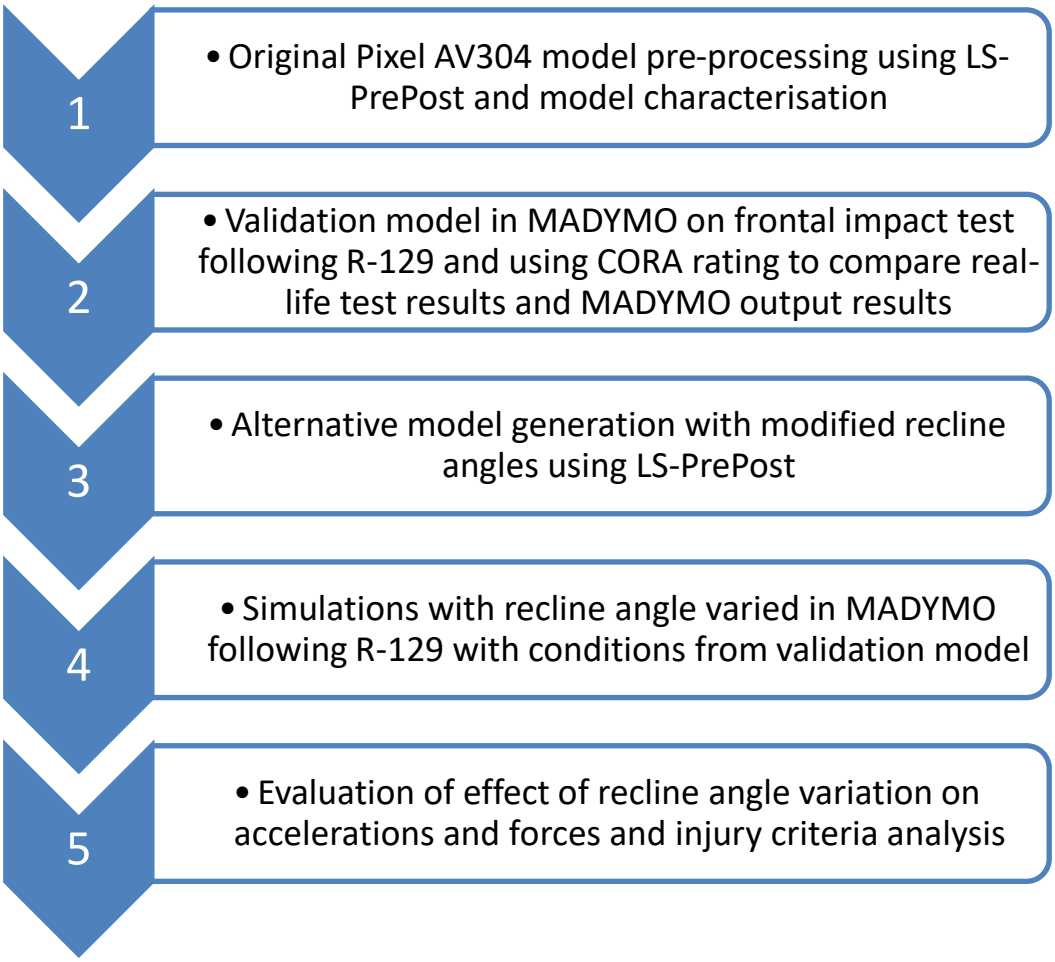

Figure 1.6 - Summary flowchart of methodology followed during project

Chapter 2. DESCRIPTION OF TECHNOLOGIES

To fully comprehend the methodology followed to the completion of the project, it is thoroughly recommended to know in advance the technologies used throughout the project. As it has been previously explained in Chapter 1.3, this project is divided into different stages, during which different tools have been used. Firstly, Karwala-Avionaut performed an homologation test on the Pixel AV304 child restraint system. This test was performed following the R-129 regulation, which dictates the necessary conditions that must be met for the homologation test to be considered valid. Secondly, the CAD model of the original Pixel AV304 was pre-processed using LS-Post and materials were assigned to obtain its physical properties. Followingly, a validation model was created in MADYMO, which is the main tool used during the project. This model fulfils the R-129 regulation and aims to resemble as much as possible the real-life homologation test. The tool used to calculate the level of resemblance between the simulation model and the frontal impact test performed by Karwala-Avionaut was the CORA rating. After this validation process, the alternative models with different recline angles were obtained using LS-PrePost and imported in MADYMO to replace the original model. After the completion of the alternative models' simulations, data on accelerations, forces, torques and biomechanical metrics were gathered and analysed using MADYMO's post-processor and Excel. Finally, with all this information, the relevant injury criteria were analysed and conclusions on the effect of recline angle on occupant safety were drawn.

The key and vital resource used in the project is Simcenter MADYMO, a software developed by Tass International and currently owned by Siemens which allows the user to create an environment suitable to perform simulations on road traffic crash tests. Should this software be unknown to the reader, the present section has been added to explain its fundamentals and basic concepts, which may enable an optimal understanding of the steps followed throughout the project and stated on Chapter 2.1.

Furthermore, it is also beneficial to describe the R-129 regulation which is the set of conditions all European road traffic accident tests must meet to allow the comparability of results to be satisfactory. This regulation sets some mandatory parameters and elements to be met when performing homologation testing on motor vehicle impacts, which helps ensure context similarity between tests, enabling an unbiased comparison between results from experiments performed by different subjects. Nonetheless, some conditions may vary in certain tests in case of almost insignificant effects on the outcome of the experiment.

In addition, Karwala-Avionaut has provided data on the test performed to homologate the Pixel AV304, having registered several physical variables throughout the impact, and this data is used for the validation of the computational model built in MADYMO in this project. In order to compare information obtained in Karwala's real-life impact and MADYMO simulations on Pixel AV304, the technique that has been decided to operate with is the CORA rating. It stands for Correlation and Analysis and is a curve comparison technique implemented to assess time-history signals taking into consideration as many aspects as possible which could enable the identification of presence or lack of similarity between two signals.[13] The CORA rating obtained from each simulation to validate the MADYMO model has been crucial to determine which configuration for certain elements in these simulations contributed to the increase in the degree of similarity between reality and simulation. For this, it is considered beneficial to explain more thoroughly in this section the fundamentals of CORA and its convenience of use in the project.

Lastly, the resting technologies used have been presented in a separate section where its mission in the project has been briefly explained. A thorough description of these technologies has been considered unnecessary due to its small use in the project and due to them being widely known. These tools are LS-PrePost, Matlab, Python and Excel.

2.1 SIMCENTER MADYMO

2.1.1 MADYMO FUNDAMENTALS

Simcenter MADYMO, which stands for MAthematical DYnamic MOdels, is a software developed by Tass International in The Netherlands.[6] It is a whole-body kinematics simulator as it enables the user to perform motor vehicle accident simulations formulating a mathematical model to describe the environment in 3D.[14]

MADYMO is one of the main software used in the road safety sector due to the complex calculations that can be executed. Not only does MADYMO offer a capacity to perform multiple labyrinthine operations simultaneously, but also offers a considerable supply of elements which commonly appear on car crash computerised reproduction, such as human dummies, common variables used in the automobile safety sector, seat belts, airbags, or even human models. All necessary calculations are executed using Langrangian methods, allowing the convergence of solutions and obtention of results.[15]

Furthermore, MADYMO permits the user to introduce a 3D element which is not present in the existing libraries created, enabling the possibility to experiment and simulate a restraint system or safety element which has been externally developed in other CAD or preprocessing programs, such as LS-PrePost or SolidWorks.

Lastly, MADYMO models are designed in a *.xml* file extension, which can be opened and modified using the Notepad. However, it is suggested to execute *.xml* files using XMADgic pre-processor, which offers a more appealing display of data and grants a simpler modification of information. After the execution of a simulation, MADYMO generates multiple files with different pieces of information. The most relevant files are a simulation run analysis as a *.log* file, a multimedia simulation output as a *.kn3*, with which the user can perform a visual analysis of the simulation, an injury risk analysis as a *.peak* file and a folder with output channels generated by the specified sensors in the dummy or human model, registering physical variables' values versus simulation time.[16] The most relevant file

extensions generated after a simulation are presented in Table 2.1 with the standard output files and in Table 2.2 with the time history output files.

Table 2.1 - Standard output files from MADYMO. Source: Siemens AG, 2020

Output type	Simcenter Madymo Ext.	Description
LOG	*.log	Overview of the progress of the simulation and errors/aborts
REPRINT	*.rep	Reprint of the input data, error messages and warnings
PEAK	*.peak & *.pkx	Scalar Injury criteria values and peak values of time history output signals (*.pkx file in xml format – mainly for Workspace Protocol Rating import)
DEBUG	*.dbg	Debug file for multi-body systems
ELMDAT	*.eld	Output file for element data
FEMOUT	*.fou	Output file for finite element models
FEMESH	*.fms	Output file for finite element models (nodal coordinates)
PREPROC	*.pre	File that contains information from the parser and/or preprocessor (information on DEFINE's)

Table 2.2 - Time history output files from MADYMO. Source: Siemens AG, 2020

Signal type	Simcenter Madymo Ext.	HDF5 Ext.	ABF Ext.	CSV Ext.	Description
ANGACC	*.acc	*.h5	*.abf	_acc.csv	Angular accelerations
ANGDIS	*.ads	*.h5	*.abf	_ads.csv	Angular displacements
ANGPOS	*.aps	*.h5	*.abf	_aps.csv	Angular positions
ANGVEL	*.avl	*.h5	*.abf	_avl.csv	Angular velocities
BODSTS	*.bds	*.h5	*.abf	_bds.csv	Body state
CARANG	*.can	*.h5	*.abf	_can.csv	Cardan restraint angles
CNTFRC	*.cntfrc	*.h5	*.abf	_cntfrc.csv	Contact loads
COGOUT	*.cogout	*.h5	*.abf	_cogout.csv	Center of gravity output file
CONTROL	*.control	*.h5	*.abf	_control.csv	Control, sensor and switch
DISVEL	*.dvl	*.h5	*.abf	_dvl.csv	Distance and relative velocity between 2 points
DURINJ	*.durinj	*_durinj.h5	*_durinj.abf	_durinj.csv	Duration injury
ENERGY	*.energy	*.h5	*.abf	_energy.csv	Energy output
ENGGRP	*.enggrp	*.h5	*.abf	_enggrp.csv	Group Energy output
ENGMAT	*.engmat	*.h5	*.abf	_engmat.csv	FEM Material Energy output

The combination of all the factors previously mentioned and multiple other possibilities sets MADYMO apart from all other car crash environment simulators. Consequently, MADYMO is the perfect candidate to become the software package in which to base all calculations and simulations on Pixel AV304's crash test and model optimization.

2.1.2 SYSTEM CHARACTERISATION

System characterisation refers to the construction of the crash environment inside a simulation which contributes to an increment on the similarity between reality and

simulation, also referred to as gross-motion simulations. A gross-motion simulator comprises a series of obligatory elements to properly define the crash environment: a body dynamic sub-model, a contact sub-model, a restraint system sub-model - including seat belts, airbags and child restraint systems – and an injury criterion.[14] All physical elements are defined as different *system models*, which allows the bundling of components of similar nature and common goal. These different system models can be observed in Figure 2.1, where a whole system is divided into four different system models: vehicle (system model 1), seat (system model 2), steering wheel and airbag (system model 3) and dummy (system model 4). This aggregation of components in system models facilitates the comprehension of the file and the needed modifications to perform to the model in case of any unexpected behaviour in a certain element.[16]

The body dynamic sub-model allows the inclusion of any desired element which helps recreate the aimed situation, such as geometrical and structural components or even dummies or human models. These items can easily be to the model by assigning a geometry, a mass and an inertia to them. This body dynamic sub-model can be defined as a multibody element internally defined in MADYMO, which can be ellipsoids, planes or cylinders, or it can be an element designed externally in other programs such as SolidWorks, having meshed the sub-model prior to the addition to MADYMO. These FE models can be defined as facets, which is a mesh fully attached to a rigid body, or as finite elements, which become deformable according to element creation and the material's characteristic. In Figure 2.1, different bodies are classified as MB or FE inside each system model to highlight the importance of disparity in behaviour of each element depending on the type of body it is declared as. This image shows dummies are built as multibody components, whereas airbags are designed as FE components, due to the deformation these undergo during simulations, which is the reason why seat belts are also defined as finite elements.

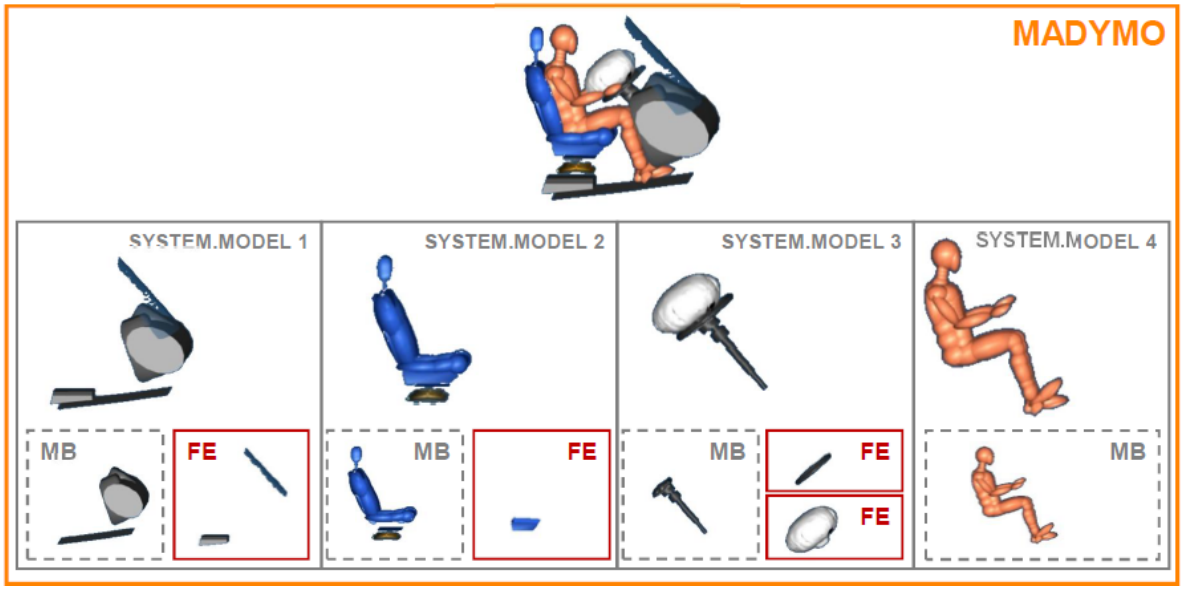

Figure 2.1 - Body-dynamic system models and subsystem classification. Source: Siemens AG, 2020

The finite element (FE) feature was included in version 5.0 in the late 90's and it allowed users to broaden the capacity to execute several actions in the program, enabling the improvement of the behaviour experienced by complex elements used in simulations such as airbags, deformable components and the interaction between these complex components and passengers. Nevertheless, the addition of FE models may result in an increase in computational energy and in total simulation time, as models might become more sophisticated and more calculations will be required to complete the simulation.

In this project, it has been necessary to resort to the use of a special FE model to recreate the behaviour of the motor vehicle impact test bench seat cushions. As previously mentioned, FE models can be used to define deformable complex components, such as cushions, given the deformation these undergo during car accidents. From all possible combinations of FE models available to emulate the test bench cushions, MADYMO offers the option of including a foam material, which can be used in cases similar to the one previously mentioned, in which the data on the foam deformation is already acknowledged, thus improving the precision of the simulation. When defining a foam material, the material parameters to include are the following: density, characteristic material (loading and

unloading stress-strain functions, hysteresis slope and elastic limit), poisson's ratio, stress-strain definition (log – logarithmic Cauchy curve – or nominal – engineering stress-strian) and the hysteresis model.[17] To declare a foam material, MADYMO offers two possibilities depending on the behaviour to recreate: solid foam material and Fu-Chang foam material, which can also be assigned in LS-PrePost. These materials follow a varying force-strain behaviour as it is shown in Figure. The solid foam material only requires the declaration of one material characteristic, whereas the Fu-Chang foam is governed by different material characteristics depending on the velocity of penetration. [18]

Furthermore, following the inclusion of a body to a simulation model, it is necessary to declare the degrees of freedom each element has by defining the so-called joints. These joint definitions enable the limitation of an element's movement in any axis, or even all of them. All elements must be linked to at least another element by a joint, creating a chain which links the movement and behaviour of all the simulation's components, guaranteeing a coordinated movement between elements. It should be mentioned that the first *system model* to be declared is a reference space and a reference plane, which is not linked to any other object when being created for it is the first and is defined as a fixed element with all movement restricted and is used as the foundations for the rest of the simulation model.

When building a simulation model in MADYMO, not only is it required to create and add al the bodies which compose the model, but also must all contacts be declared, resulting in the contact sub-model. This sub-model helps define the behaviour of various surfaces when establishing contact with one another by applying a force depending on the amount of penetration through a body or deformation suffered by those declared as deformable. Nevertheless, when calculating contacts between surfaces, there must always be a master surface and a slave surface, which defines the behaviour of the contact by specifying which body is deformed and which is penetrating. This crucial classification of surfaces is key to an optimal contact definition, as it helps ensure an appropriate behaviour of the elements according to that specified.

The definition of the contact depends on the type of body each has been defined as (multibody or FE). Contacts in MADYMO can be declared as MB_MB, MB_FE or FE_FE and each type of contact requires the definition of different aspects and even different types of contact. Table 2.3 summarises all the existing possibilities of contacts to declare and the element-type situation in which each can be used, being the most common configurations indicated with darker coloured cell.

Table 2.3 – Contact types and assignment criteria. Source: Siemens AG, 2020

CONTACT.			MB_MB	MB_FE	FE_FE
KINEMATIC				CONTACT_FORCE.KINEMATIC	
ELASTIC	CHARACTERISTIC based	FORCE	CONTACT_FORCE.CHAR CHARACTERISTIC.CONTACT CONTACT_MODEL = FORCE	CONTACT_FORCE.CHAR CHARACTERISTIC.CONTACT CONTACT_MODEL = FORCE	CONTACT_METHOD.NODE_TO_SURFACE_CHAR CONTACT_FORCE.CHAR CHARACTERISTIC.CONTACT CONTACT_MODEL = FORCE
		STRESS		CONTACT_FORCE.CHAR CHARACTERISTIC.CONTACT CONTACT_MODEL = STRESS	CONTACT_METHOD.NODE_TO_SURFACE_CHAR CONTACT_FORCE.CHAR CHARACTERISTIC.CONTACT CONTACT_MODEL = STRESS
	MATERIAL based	PENALTY			CONTACT_METHOD.NODE_TO_SURFACE or CONTACT_METHOD.SURFACE_TO_SURFACE CONTACT_FORCE.PENALTY
		ADAPTIVE			CONTACT_METHOD.NODE_TO_SURFACE or CONTACT_METHOD.SURFACE_TO_SURFACE CONTACT_FORCE.ADAPTIVE

Lastly, in order to correctly evaluate all output data from physical variables extracted from the occupant's specifically activated sensors, an injury criterion must be defined before executing a simulation. Thanks to the complex calculations MADYMO is capable of executing, it is also possible to obtain measurements of injury-based calculations of different criteria developed over the years. Some of these trauma standards are prestored in MADYMO's memory and the program performs the necessary operations to calculate these automatically unless the contrary is indicated. The predefined injury parameters in dummy models and the limb each is associated with, such as HIC or TTC, are presented in Table 2.4 and will be used during the project when evaluating the effect of recline angle variation in some of these measurements.[19]

Table 2.4 - Predefined injury parameters in dummy models in MADYMO. Adapted from: Siemens Ag, 2020

Body part	*Injury criteria*
Head	Head Injury Criterion (HIC)
Neck	Neck Injury Criterion (NIC_FORWARD) Neck Injury Predictor (N_{ij})
Thorax	3 ms criterion (3MS) Thoracic Trauma Index (TTI) Viscous Injury Response (VC)
Legs	Axial Loads Tibia Index

Although injury criteria are predefined for each occupant, both human model and dummy, they can still be modified on demand. The injury parameters can be adapted to the simulation's circumstances and context to adapt these parameters to its situation by modifying time intervals, threshold values and other specifications.

2.1.3 MADYMO SEAT BELT MODULE

One of the key components of motor vehicle impacts when it comes to injury prevention is the seat belts. Prior to the appearance of three-point belts, two-point seat belts were commonly used as a simple restraint system, equivalent to present lap belts, which ensured the attachment of the passenger's waist to the vehicle and increased the probabilities of survival in the case of a motor vehicle accident.[20] The three-point seat belt was first implemented by Volvo in 1959 and ever since its use has never ceased to increase worldwide due to the intrinsic value it offers to matters of safety.[21] It is for this reason that it was decided to include in MADYMO a specific module responsible for enabling the creation, fitting and modification of seat belts in models, facilitating immensely what should be a thorough and complicated task in case of the absence of this module.

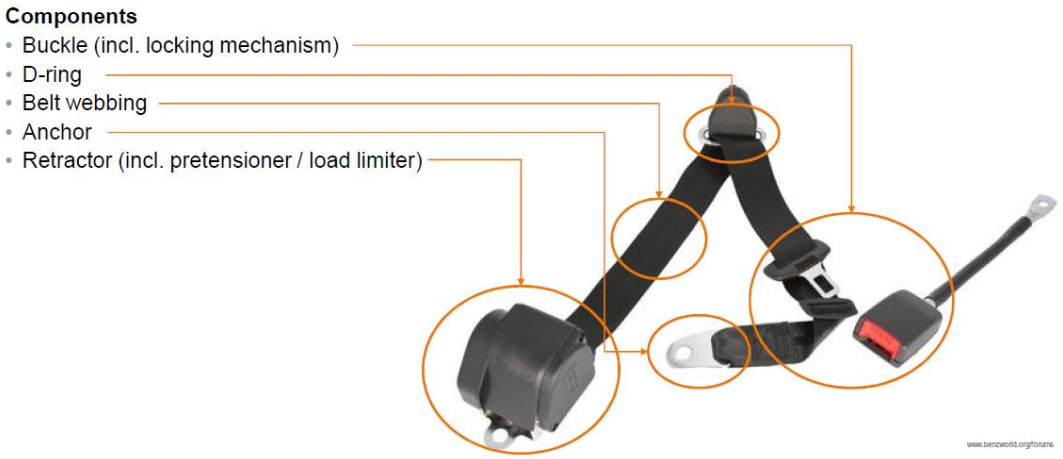

Figure 2.2 - Three-point seat belt components. Source: Siemens AG, 2020

Seat belts are typically comprised of five main components: buckle (locking mechanism), D-ring, belt webbing, anchor and retractor (that may include pretensioner and load limiter). All these elements can be modelled using the seat belt module offered by MADYMO and are presented in Figure 2.2. There are seven tools available to create a seat belt in MADYMO. These tools are the following: belt, for belt webbing definition; slip models, to calculate slipping forces between different belt segments; retractor model, for retractor definition; pretensioner models, which allow the declaration of a pretensioner in the model; load limiter, to declare a load threshold for the seat belt; fuse belts option, which allows to represent the tearing of belt stitches; and hybrid belt modelling, which enables the addition of truss or membrane finite elements to the seat belt to model complex behaviours during motor vehicle accidents.[22] However, in this project only hybrid belt webbing and slipping will be included as it can be observed in Figure 2.3. This is because the other elements were not needed to model seat belt behaviour in this project's simulations and these would increase the model's complexity unnecessarily. Moreover, the buckle and the D-rings have been also included in the model using the computational files available on elements stipulated by the R-129 regulation, using the material available online of a R-129 test bench.

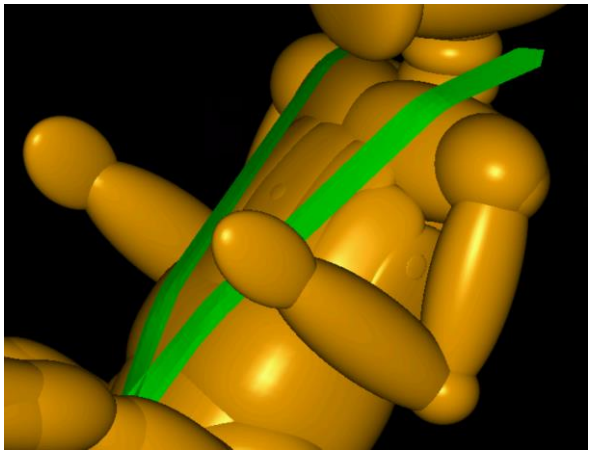

Figure 2.3 - Seat belt webbing model

Seat belt systems in MADYMO can be comprised of two different models: conventional MB belt model or hybrid MB-FE belt model. These different types of belt models can be visually differentiated in Figure 2.4. The combination of only unidimensional belt segments leads to the creation of a conventional MB belt model, thanks to the attachment of the belt's ends to any sort of component already created in the model (MB, FE node or the reference space), leading to a restriction of belt's slip only in the segment's direction. These standard MB models are easier to operate with and can be used to define simple seat belts which may only operate in one direction. On the other hand, hybrid MB-FE models are comprised of a conventional MB belt model and finite elements combined to recreate behaviour of slip and friction in various directions across the surface to which the belt model is attached. It is for this reason that hybrid belt models are more commonly used and are those used in the project. An example of a hybrid seat belt created in this project can be observed in Figure 2.3.

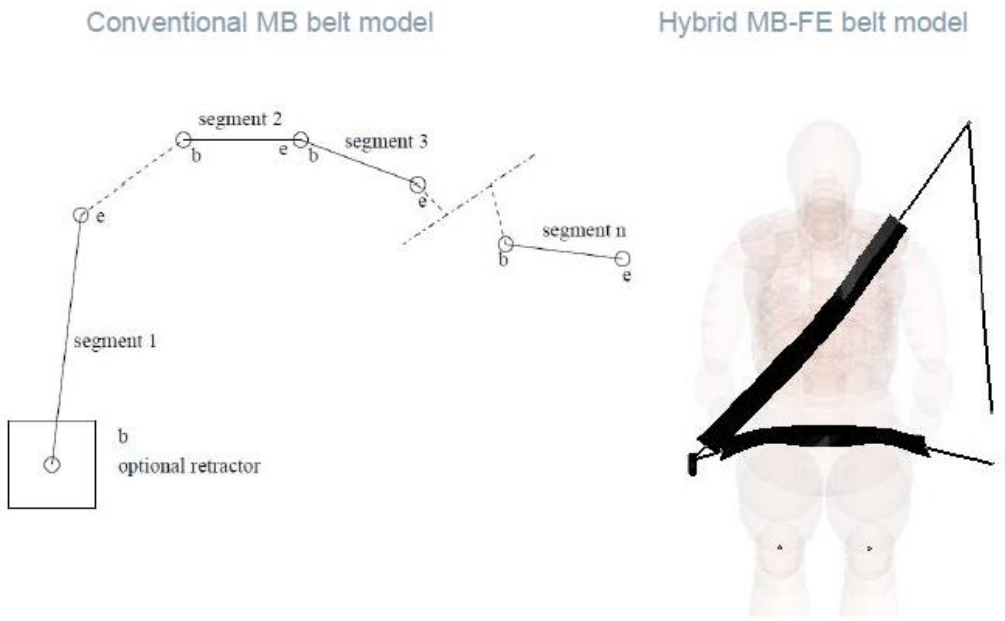

Figure 2.4 - Conventional MB (left) and Hybrid MB-FE (right) belt models. Source: Siemens AG, 2020

The behaviour adopted by seat belts during all types of motor vehicle accidents such as frontal impact or rollover can be excessively complex to be modelled using a simple traditional seat belt model. It is for this reason that the multidirectional friction behaviour the finite element component of hybrid MB-FE belt model offers makes it a far better option to choose. The most common type of extra elements used are membrane elements, although truss elements (unidimensional finite elements) can also be applied in seat belt definition. In addition, hybrid belt models' display is more appealing, resulting in a quicker recognition of the element in the model and of possible mistakes made during the creation of these. [22]

The necessary fields of data to complete when creating a hybrid belt, which are presented in Figure 2.5, are separated into two different categories: MB (conventional) belt segment and FE belt segment. The FE belt segment models the belt's part that will contact the occupant or, in this case, the CRS. On the other hand, the MB conventional belt segment simply ensures that information on velocity and displacement of each segment is transferred to other segments, ensuring the continuity of the belt and the transfer of forces between segments.

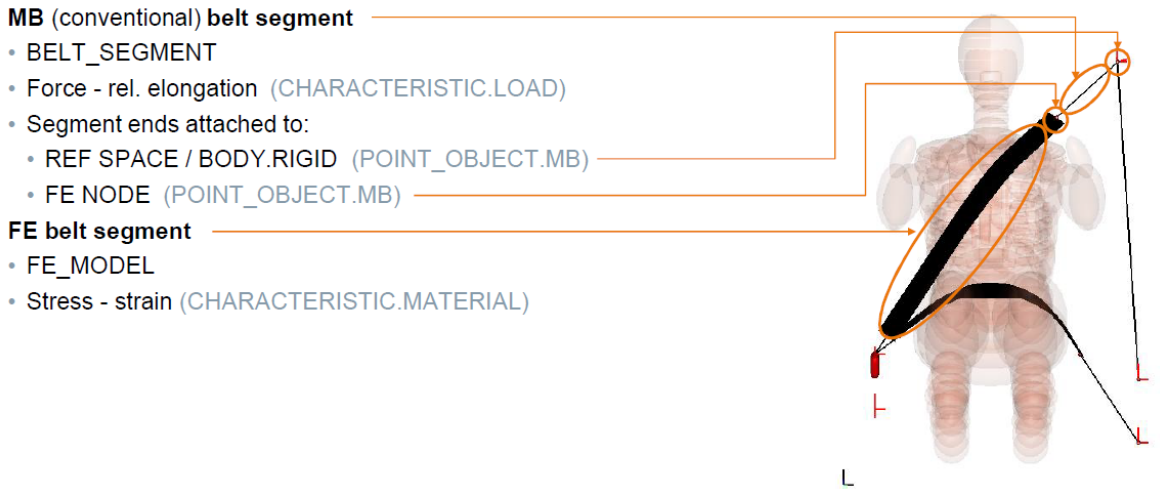

Figure 2.5 - Hybrid MB-FE belt model definition and components. Source: Simcenter MADYMO Introduction Training – Day 2, Ag. Siemens

The multibody element requires the declaration of a belt segment, a force vs relative elongation characteristic definition (*characteristic.load*) and the attachment points. The attachment point specification allows to select the bodies to which the seat belt is attached both in the begin and end point. In case of attaching one of the two points to another belt point, a slip characteristic must be declared as a belt tying, which will later be explained. The other key parameter to include is the *characteristic.load* field, which contains a force vs relative elongation function, defining the behaviour of the belt segment when subjected to strain.[22] Suffice it to say, when declaring the *characteristic.load*, MADYMO allows to declare different loading and unloading functions depending on the seat belt's state combined with a hysteresis model under which the transition from loading and unloading, and vice versa, is defined. There are 3 different hysteresis models in MADYMO depending on the characteristics of the model: model 1, in which the unloading curve must go through the origin and a hysteresis slope must be specified; model 2, which is more flexible than model 1 as it does not require the unloading curve to meet the origin; and model 3, which will not be used in this project and is characterised by the absence of a hysteresis slope parameter via the use of a shifted and scaled unloading curve for each coordinate.[23]

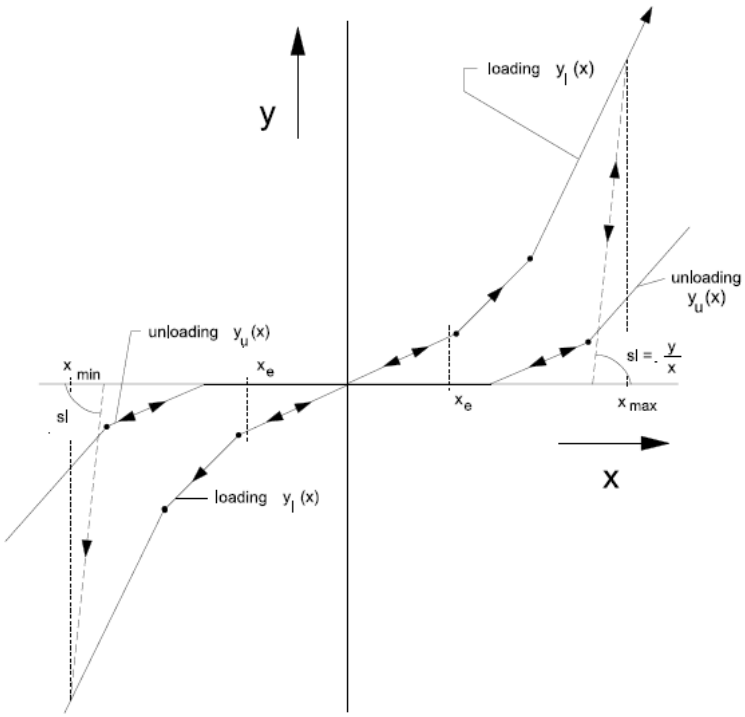

Figure 2.6 - Hysteresis model 1 in MADYMO. Source: Siemens Industry Software and Services BV, 2020.

Having all MB belt segments already defined, hybrid MB-FE belt models, as presented in Figure 2.5, require the definition of the other half of the model: the FE model. This FE model, as previously mentioned, is used to increase the precision of the seat belt model and its similarity to reality, by the multidirectional behaviour it provides, thus demanding the declaration of a truss or a membrane element to which a material data will be assigned. Information regarding the FE model of the seat belt will be explained later when presenting the belt fitting module available in MADYMO. Furthermore, similarly to the *characteristic.load* parameter specified in the MB belt segment, behaviour of the finite element part of the seat belt must be defined by specifying a material based field which will determine the seat belt's nature. This *characteristic.material* parameter can also include a hysteresis model which designates the loading and unloading characteristic of the finite element part of the seat belt. The hysteresis model used in this case in the project will be model 1, as no tension must be applied by the seat belt for null strain when being unloaded.

On the other hand, belt segments must be attached to different objects both in the begin and in the end. The elements to which they can be attached are MB elements, FE models and even to the reference system, other belt segments included. In order to model the performance of the union between two belt segments, a belt tying must be declared. The *belt.tying* command allows the attachment of two ends of a seat belt to one another and calculates the slip necessary between both elements. Depending on the forces applied by each belt segment and the Coulomb friction of the tying, the belt will remain unchanged or a slip will be experienced until the tying reaches the force equilibrium. The belt tying can be found in two different states: slip or stick, depending on whether belt equilibrium has been reached or not. MADYMO performs calculations in each time to determine each tying's state. In case of no possible slip between two belt segments, the belt must be divided into two different belts, just like it is done in the right example presented in Figure 2.7, and a Coulomb friction coefficient must be declared.[22]

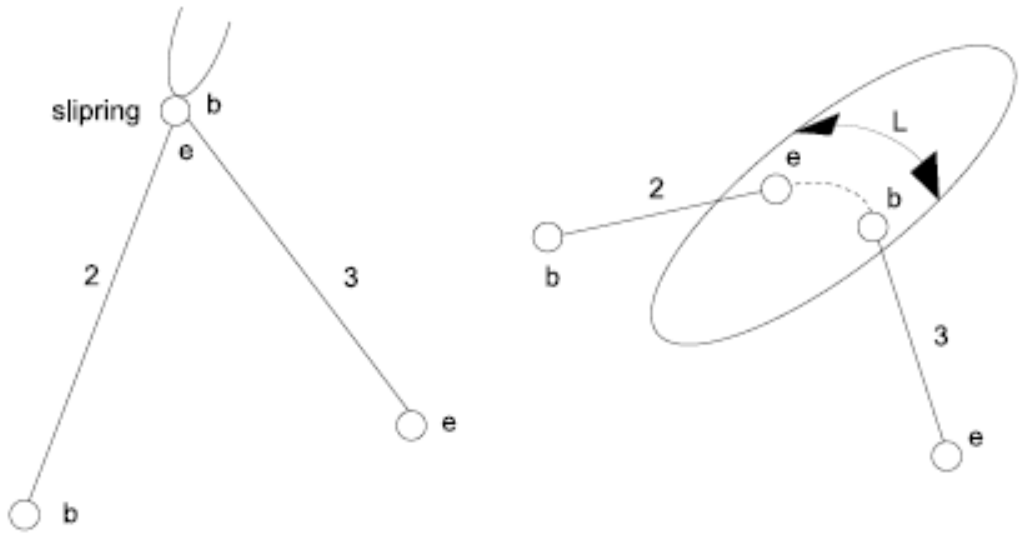

Figure 2.7 – Belt tying used to connect different belt segments and mechanism fllowed. Source: Siemens Industry Software and Services BV, 2020.

Moreover, seat belts can also be modelled using non-specific commands that simulate an elastic effort similar to that exerted by a retractor or a pretensioner. It is for this reason that simple belt models, such as those being used in this project, can be described with Kelvin restraints.[22] Restraint is referred to any force or effort applied to an object as a penalisation for a certain type of movement, which is different from a constraint, which represents a simple limitation of movement, blocking that degree of freedom despite any effort applied to it. There are different features that can be used in MADYMO to model a restraint: Kelvin, forces applied by a spring and a damper in a parallel configuration; Maxwell, forces applied by a spring and a damper in a series configuration; point restraint, elastic and damping forces calculated via the relative position of a point to that point's restraint coordinate system; joint restraint, elastic, frictional and damping force experienced by the relative motion in the kinematic joint to which it is applied; and cardan (flexion torsion restraint), torques applied to two objects as a result of the angular motion experienced by this in the restraint coordinate system.[24] In this project, the only restraint that will be added is that in charge of the activation of all belts of the system, acting as a pretensioner and retractor, therefore the only restraint used will be a Kelvin restraint. When declaring a Kelvin restraint, the user has to specify two points which will be linked through the restraint, as well as a *characteristic.load* parameter which declares the loading (and unloading in case it is necessary) function. The *characteristic.load* can also be followed by a damping coefficient which will specify the penalisation received due to the velocity's contribution between the two bodies linked. Nevertheless, although Kelvin restraints are valid for modelling strings and dampers in a parallel configuration, the stiffness function (*characteristic.load*) does not have to follow any fixed law, allowing the user to decide the applied load's variation. In this project, as a 7N compression in the shoulder and lap belt is set regulation as mandatory for impact tests performed following R-129 regulation, the Kelvin restraints included for these belt segments is a horizontal function which fixes the belts' tension to 7N independent of the strain experienced by the restraint.

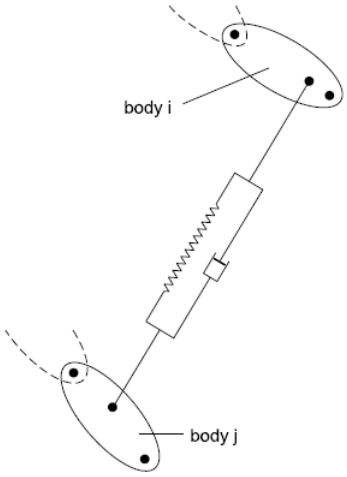

Figure 2.8 - Kelvin restraint in MADYMO. Source: Siemens Industry Software and Services BV, 2020

Lastly, as previously mentioned at the beginning of this section, one of MADYMO's most advantageous features when it comes to seat belt modelling is the belt fitting tool, which facilitates a usually tedious and thorough task. When defining a belt with the belt fitting tool, certain steps have to be taken in the following order to obtain a correctly fitted seat belt:

1. Open the Belt Fitting Wizard by pressing F10.
2. Choose a *system.model* to which the belt will belong, introduce a name, choose between truss and membrane hybrid seat belt and decide the geometrical features of the seat belt. Example presented in Figure 2.10.
3. Choose a *characteristic.material* and a *characteristic.load* previously defined to declare the FE and MB belt behaviour, respectively.
4. Select the start and end attachment points previously created.
5. Select the surfaces around which the belt should fit (surface, group or FE model).
6. Modify belt to adjust it correctly to surfaces and press Finish. Example presented in Figure 2.9.

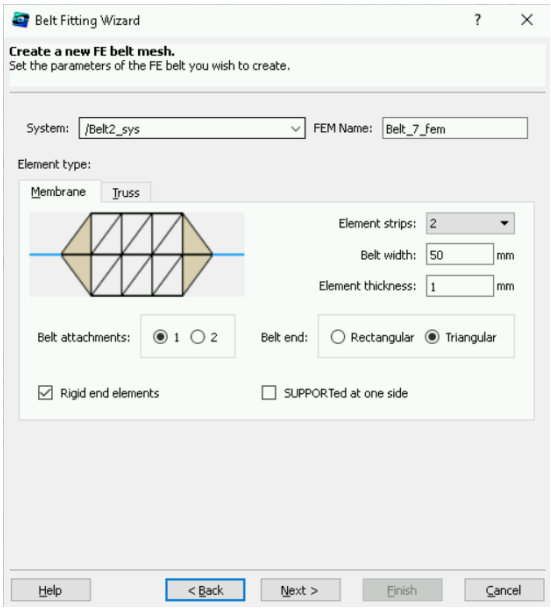

Figure 2.10 - Belt geometry definition using the Belt Fitting Wizard (step 2)

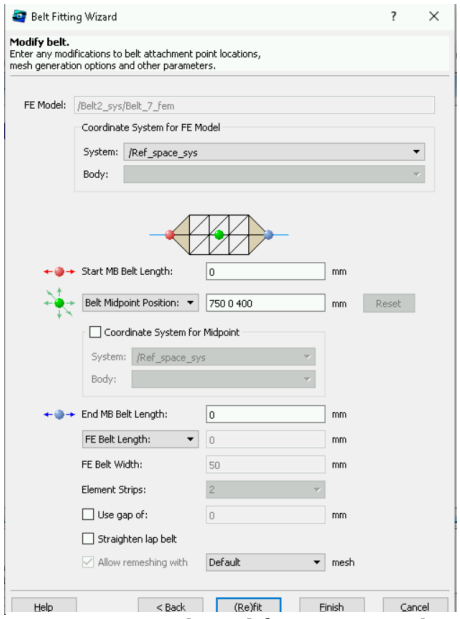

Figure 2.9 - Belt modification using the Belt Fitting Wizard (step 6)

After the definition of the belt and having made all modifications needed to ensure a correct fitting of the belt around all surfaces, the user must check that there are no visible errors and initial penetrations of any body through the seat belt, obtaining a correctly fitted seat belt (Figure 2.11). In case of incorrect fitting, it is recommended to change parameters such as finite element size (smaller elements are more precise but increases simulation times) or using a gap, which the distance which separates belt and near surfaces.

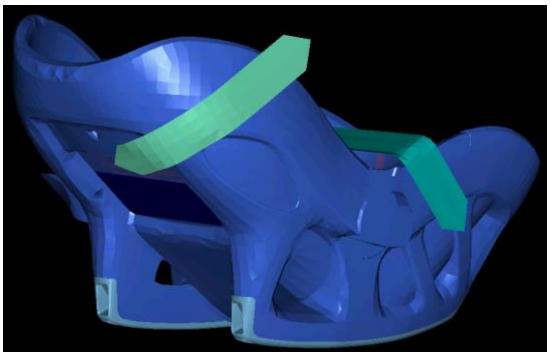

Figure 2.11 - Resulting seat belt example using Belt Fitting Wizard

2.1.4 MADYMO Q1.5 CHILD DUMMY

Anthropomorphic test devices (ATDs), also known as crash test dummies, are widely known to be one of the greatest contributions to road safety and the automotive industry in the latest years. They are used to evaluate newly designed restraint system or to study problems on already existing systems thanks to them being mechanical proxies of a human being.[25] As a result of the recurrent use they are given in the automotive industry, MADYMO developers decided to install a dummy data base in the program which already includes all the information necessary for every dummy model. This way users are exempted from the duty of dummy designing and modelling for each simulation, facilitating all kinds of work with dummies in MADYMO, as well as optimising the precision available for any simulation.

Dummy models in MADYMO can be of three types: ellipsoid models, facet models and finite element models. Difference between models lies in the techniques used to model both geometry and mechanical features. All models are chains of rigid bodies which have inertial properties already specified and are linked to one another via kinematic joints.[26] Nonetheless, given that ellipsoid models result in shorter simulation times and a lower computational memory usage, the dummy used in this project is an ellipsoid-based dummy model, therefore these dummies will be the ones this section will be focusing on. Besides, in the real-life frontal crash test performed by Karwala-Avionaut on Pixel AV304, a Q1.5 dummy was used and, consequently, the ellipsoid model available in MADYMO for this dummy is the ATD to be used in this project.

There are multiple dummy families which have been developed throughout the years divided into the test each will be used in: frontal impact, side impact, rear impact or rollover. Given that this project will only evaluate frontal impact data, this section will only focus on the dummy models available in MADYMO for frontal impacts. These families of dummies ideal for frontal impacts are Hybrid II, Hybrid III, CRABI infant dummies, THOR and Q series. All these dummy families have most of their models preinstalled in MADYMO, fulfilling a

wide demand of different anthropomorphic test devices for various age groups, which are presented in Table 2.5.

Table 2.5 - Frontal impact dummies available in MADYMO. Adapted from: Siemens Industry Software and Services, 2020

Dummy Family	*Dummies available*
Hybrid II	50^{th} percentile Part 572
Hybrid III	3-year-old
	6-year-old
	5^{th}, 50^{th}, 95^{th} percentile Q Dummy
	50^{th} percentile standing Q Dummy
	50^{th} percentile Base Model
	50^{th} percentile FAA Dummy (Aviation)
CRABI	CRABI child dummy (12-month-old)
THOR	THOR 50^{th} percentile adult male
Q	Q0 (newborn)
	Q1 (12-month-old)
	Q1.5 (18-month-old)
	Q3 (3-year-old)
	Q6 (6-year-old)
	Q10 (10-year-old)

In the real-life crash test performed by Karwala-Avionaut on the Pixel AV304, the dummy used was the 18-month-old dummy from the Q family, therefore the dummy information which will be explained onwards will only correspond to the Q1.5 dummy. This dummy was developed in 1993 by the Netherlands Organization of Applied Technical Research (TNO) and replaced the TNO P-series dummies, as a much more reliable and precise ATD for child occupants.[25]

Furthermore, ATDs have certain dimensions and weights which have been obtained from data massively acquired worldwide to create a standard model which best assembles a child's mechanical and geometrical behaviour. In Table 2.6, dimensions and weights of the Q1.5 dummy have been presented.

Table 2.6 - Q1.5 dimensions and weights per body region. Adapted from: Yoganandan et al, 2015

Property	*Body region*	*Value*
Key dimension (mm)	Shoulder width	227
	Hip width	194
	Buttock to popliteus	185
	Sitting height	499
	Standing height	800
Weight (kg)	Head & neck	2.8
	Torso	5.04
	Upper extremity	1.20
	Lower extremity	2.06
	Total	11.1

The Q1.5 child dummy model developed by TNO has been included in MADYMO following all the geometrical parameters that the real-life dummy has. The ellipsode model's geometry is comprised of 7 different body regions with similar characteristics, which add up to 11.1 kg. These regions are described according to the Madymo Model Manual:

- Head: comprised of two ellipsoids which model the dummy's head and face, respectively. The head's properties have been obtained from a head frontal and lateral impact tests performed and obtaining similar results on the simulation. A bracket joint links the head to the upper neck load cell.
- Neck: comprised of five ellipsoids which enable compression, extension, bending and torsion of the neck, given the nature of the ellipsoids' joints: triple-joint restraint

and a cylindrical joint combined with two universal joints. Neck validated in forward and lateral bending pendulum test.

- Shoulders and clavicles: flexible structural area which links arms and spinebox thanks to the clavicles being attached to the sternum by a point restraint and allowing the translational movement of the shoulders.
- Ribcage: deformable thin shell comprised of five ellipsoids connected to the sternum and the spinebox, as well as Cardan and point restraints linking the ribcage to the sternum. Bending and contact characteristics are determined from thorax validation examinations. Thorax validated in frontal and lateral pendulum tests.
- Lumbar spine and abdomen: a triple-joint restraint represents the lumbar spine, using a bracket joint for load measuring. The abdomen is divided into three ellipsoids (upper, middle and lower abdomen) which transfer loads to the lumbar spine and the pelvis. Lumbar spine validated in the same test as neck validation.
- Pelvis: comprised of four ellipsoids, which divide the pelvis into two sections: lower and rear pelvis near the seat and the pelvis wings.
- Limbs: two arms and two legs, each with three ellipsoids linked with rotational universal joints: arm-forearm-hand and thigh-calf/shin-foot.

Aside from the individual validation of some of the dummy's regions that have been previously stated, it is necessary to perform a full dummy validation test which, in this case, was executed in a frontal CRS sled test at 60, 53 and 47 km/h and in a lateral CRS sled test at 50 km/h. After all dummy components and the contacts' characteristics have been confirmed and validated, the model's precision and similarity to reality are confirmed and the computational model of the Q1.5 dummy is ready to be used.

In addition, some important pieces of information must be considered when using the Q1.5 dummy model to ensure a correct use. It is recommended to use a time step for the Q1.5 model smaller than 10^{-5} seconds. The dummy can be easily positioned at will in the simulation thanks to the joints available in the model by pressing F11 and using the Joint Positioning tool. The dummy has a total of 11 joints whose degrees of freedom available

vary from 1 to 6 depending on the joint that is being modified. Besides, dummy contacts are predefined in the model and some of which can be modified to change the behaviour of a certain region in case needed, although it is unrecommended.[27] In Figure, a Q1.5 dummy is displayed with all the components previously mentioned.

Figure 2.12 - Q1.5 child dummy from MADYMO. Source: Siemens Industry Software and Services BV, 2020

Furthermore, after a simulation is finished, it is possible to extract information on any body region provided with a sensor. These sensors are responsible for the measurement of a certain piece of information, such as the acceleration or displacement of the region each is installed at, and for the data's preparation in an output file. This information can be exported to a file and manipulated externally using any sort of data analysis program. In this project, the dummy's output signals are exported to CORA to obtain an objective insight on the similarity between the real-life crash impact performed by Karwala-Avionaut and that obtained in MADYMO.

Lastly, each dummy possesses predefined injury criteria, which were evidently defined by TNO, adapted to the corresponding age group. The injury criteria available in the Q1.5 child dummy model designed by TNO with different filtering frequencies are HIC15, HIC36, head acceleration (3MS and peak), neck (peak torque and tension), thorax acceleration and deflection (3MS and peak) and pelvis acceleration (3MS and peak).

2.2 CHILD RESTRAINT SYSTEM REGULATION (R-129)

Child restraint systems have been used since 1933, when a child seat was first introduced to control children's position during automotive trips.[28] Although, it was not until the early 1960's that a child restraint was first used in Sweden with the main goal of injury prevention and safety. Since then, CRS use has increased each year and so has the efficiency of these systems to prevent children from suffering any type of injury. [29]

These child restraint systems are subjected to certain rules and regulation depending on the country each is implemented. Some of the valid CRS regulations in the present time are the following: AS1754 in Australia, NZS5411 in New Zealand, FMVSS 213 in United States, CMVSS 213 in Canada and UNECE R-129 in Europe.[30] As this investigation has been carried out in Europe for a child restraint system designed and produced by a polish company, the regulation which dictates the conditions under which the impact tests are performed is the European R-129 regulation, thus being the one to be analysed from this point onwards in this section.

The valid European child restraint regulation used until 2013 had been the R44.04, which was agreed by the United Nations in 1958. Since its implementation, the R44 regulation had successfully contributed to the decrease in injured children and casualties due to motor vehicle accidents on the road via the control and homologation of child restraint systems. Nevertheless, a desire to improve road safety for children motivated the GRSP Informal Group committee to develop a new regulation, which led to the adoption of the R129 regulation (ECRS - Enhanced Child Restraint Systems) by the United Nations Economic Commission for Europe (UNECE) in July 2013. Nonetheless, despite the development of a new regulation, both regulations have been running in parallel until 2018.[31] As R129 is based on the previous regulation, it is important to first understand several aspects present in the R44, although this section will only focus on the aspects which are relevant for frontal impacts.

The R44 regulation divides child occupants into five different groups depending on the mass which are presented in Table. Further information on each age group's specifications have also been added to Table, to facilitate the display of information.

Table 2.7 – CRS mass groups according to R44. Adapted from: Domenech et al, 2018

Group	*Mass [kg]*	*Integrated Restraint System*	*Approved ISOFIX*	*Mandatory rearward facing*
Group 0	<10	Yes	Yes	Yes
Group 0+	<13	Yes	Yes	Yes
Group I	9 – 18	Yes (impact shield)	Yes	No
Group II	15 – 25	No	No	No
Group III	22 - 36	No	No	No

According to R44, frontal impacts tests must be carried out at a speed of 50km/h and the seat under evaluation must experience a deceleration pulse, simulating an accident. This acceleration is provided to the restraint system thanks to a sled these elements are placed on and attached to. The deceleration pulse to be experienced is not absolutely exact, although it must be comprehended between two thresholds, being the maximum deceleration accepted a value between 20g and 28g. The region in which the deceleration pulse must be included is presented in Figure 2.14.

Lastly, regulation R44 stipulates a series of thresholds on head and thorax data which must not be exceeded by the dummy during the system's homologation test. The maximum head displacements allowed are 550mm horizontally and 800mm vertically. On the other hand, regarding the thoracic acceleration, the peak of the signal must be lower than 3ms, with a resultant acceleration lower than 55g and a maximum vertical acceleration of 30g. These magnitudes are measured using sensors equipped on the dummy for data retrieval.

After 2013, a total of 60 countries started the implementation of the R129 regulation in the child restraint system homologation. This process was divided into 3 phases to ensure a correct transition: Phase 1 on ISOFIX Universal Integral CRS (i-size), phase 2 on boosters and phase 3 on belted integral CRS. The main aspects improved in R129 compared to R44 regarding child safety in frontal impacts are presented below and in Table 2.8. [32]

Table 2.8 - Differences between R44 and R129. Source: P. Lesire et al, 2013

Item	ECE Reg. 44	New ECE Reg.
CRS homologation types	Universal, semi-universal, restricted, vehicle specific	Universal (called i-size), vehicle specific
CRS classes	Fixed weight classes	CRS manufacturer defines the suitability of the product based on the child's stature
Requirements for CRS orientation	CRS classes 0 and 0+ may not be used FF	Children up to 15 months old may not be FF
Anti rotation device ISOFIX	TopTether universal for group I FF, TopTether for other CRS and support leg semi-universal	TopTether and support leg universal with special criteria for the support leg w.r.t. position in car X and Z orientation
Test bench	 relatively soft bench foam	 relatively stiff bench foam
Test procedure frontal impact	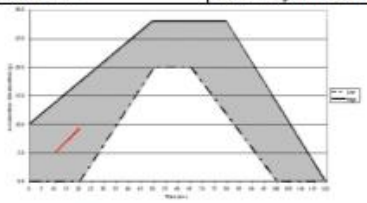 generel test layout similar, differences exist w.r.t. test bench, dummies etc.	
Dummy criteria frontal impact	Head displacement < 550 mm (500 mm for ISOFIX, 600 mm RF), a3ms chest < 55 g; a3ms chest Z < 35 g	Head displacement < 500 mm (700 mm RF); HPC < 600 or 800; a3ms head < 75 g or 80 g; a3ms chest < 55 g
Test procedure rear impact	For RF CRS	For RF CRS test conditions comporable to R44 except test bench, dummies etc.
Test procedure roll over	Quasi static roll over along X and Y axis	Quasi static roll over along X and Y axis, comporable with ECE R44
Test procedure lateral impact	No test	Test procedure with flat door and linear intrusion
Child dummies	P dummies (P0, P3/4, P1.5, P3, P6, P10)	Q dummies (Q0, Q1, Q1.5, Q3, Q6, Q10 in preparation)
Geometric requirements for space for the child (internal dimensions)	P dummies	Geometrical checks considering 5th and 95th percentile of seating hight, shoulder hight, shoulder width, pelvis width
Geometric requirements external dimensions	For ISOFIX CRS different CRF (F1, F2, F2X, R1, R2, R3, L1, L2)	Universal maximum F2x (B1) or R2 (D)
Chest clip	Not allowed	Not forbidden

- Rear-facing position up to a minimum of 15 months old instead of the previous 9 months old.
- New generation dummies which improve the data retrieval process (Q dummy).
- Easier ISOFIX installation and instructions to avoid incorrect positioning and attachment of CRS to vehicle (Figure 2.13).
- Improved compatibility between car seats and i-size CRS.
- Seat classification according to class (integral or non-integral), category and occupant stature.
- Support leg system incorporation which is attached to the CRS's base and transmits loads to the vehicle's structure.

Figure 2.13 - ISOFIX installation in vehicle. Adapted from: Fundación Mapfre, "Children's road safety"

Furthermore, it is important to mention that the R129 states absolutely all the relevant conditions under which the homologation tests for child restraint systems must be performed. It is for this reason that the regulation states information on the sled in which the CRS is placed, the seat belts, the foam material used for the sled's seating or even the deceleration pulse suffered by the sled. The deceleration experienced by the sled during a frontal impact test can be observed in Figure 2.14.[33] where a narrow path delimits the values that the deceleration pulse must fulfil. The same happens with other CRS standards previously

mentioned and whose deceleration pulses can be observed in the same image. In frontal impact tests, sled must be travelling at 50km/h and experience a deceleration pulse contained inside of the corresponding region in Figure 2.14 for R44 (same conditions in R44 and R129).

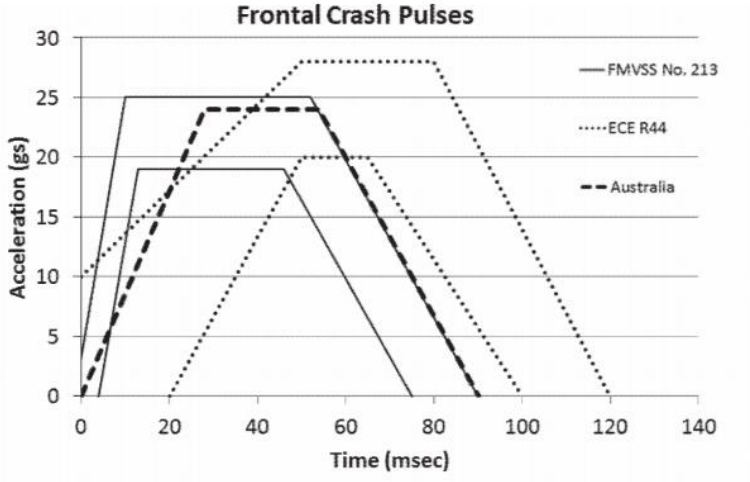

Figure 2.14 - Frontal impact test deceleration pulse profile for CRS standards. Source: NHTSA, 2020

There are many other instructions and restrictions to consider when executing a vehicle crash test following R129, which can all be consulted in the R129 official regulation document. From all the information available, it is important to mention some aspects which will be key during the execution of the project:[34]

- Sled dimensions and mass, as well as bench test configuration are all fixed and have to fulfil certain requirements. It is for this reason that a CAD model of the bench test can be found online (Figure 2.15), in order to ensure the fulfilment of the R129 regulation in an impact test performed in a computational simulator, such as MADYMO.

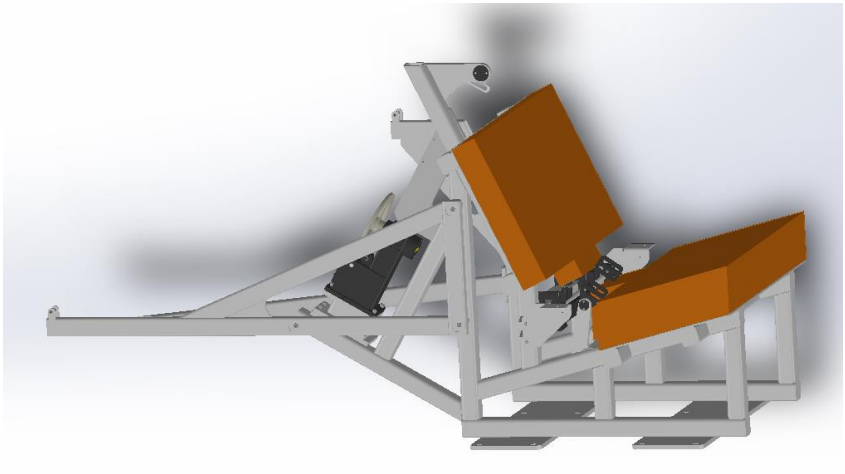

Figure 2.15 - CAD model of R129 test bench

- Seat belts properties are predefined and must meet geometrical and loading values. For instance, belt width and seat belt pretensioning of 50N have fixed values.
- Back and seating must be covered with polyurethane foam. This polyurethane's properties are presented in Table 2.9 and determine the behaviour of both the back and the seating of the test bench. Unfortunately, there is not a CAD model available of this foam with its properties included. Foam characterisation can be performed following a standardised impact test on the seating by recording the penetration experimented by a 2.75kg headform (Figure 2.16) through the cushion after a 500mm free fall.

Table 2.9 - Foam cushion properties following R129. Source: United Nations, 2013

Group	*Value*	*Unit*
Density	68-74	Kg/m^3
Compression resistance	13	kPa
Indentation Load Deflection	500 (+/15%)	N
Tensile strength	≥150	kPa
Ultimate elongation	≥120	%
Compression set	≤3	%

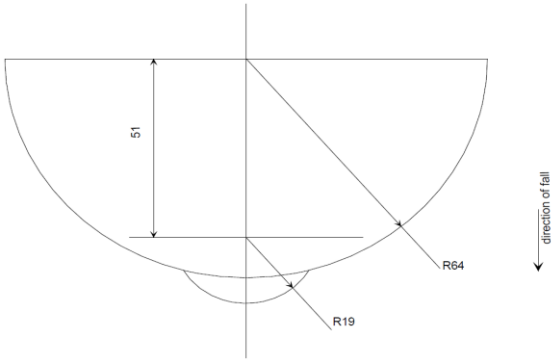

Figure 2.16 - Foam characterisation test headform. Source: United Nations, 2013

Lastly, motor vehicle crash test standards include certain injury thresholds which cannot be surpassed during the test. These thresholds are presented in Table 2.10 and had already been mentioned at the beginning of the section. In case these variables do not exceed the presented thresholds, the child restraint system can be commercialised and its homologation process reaches the end.

Table 2.10 - Injury criteria following R129 for Q1.5 dummy. Source: R129, 2013

Criterion	*Abbreviation*	*Unit*	*Value (Q1.5 dummy)*
Head performance criterion (only in case of contact)	HIC (15)	-	600
Head acceleration 3 ms	A head 3 ms	g	75
Upper neck tension Force	Fz	N	Monitoring purpose
Upper neck flexion Torque	My	Nm	Monitoring purpose
Chest acceleration 3 ms	A chest 3 ms	g	55

2.3 CORA

The CORrelation and Analysis (CORA) software was developed near 2002, when the Partnership for Dummy Technology and Biomechanics (PDB) was founded by German car manufacturers. These companies partnered together with the intention of harmonising content and procedures in the motor vehicle safety sector by combining experience and knowledge in the dummy, simulation and biomechanics areas. One of the most important contributions the PDB has offered is the CORA software, which is ideal for the road safety sector.[35]

CORA is a time-history signal analyser which calculates the similarity in time between the specified signals. It requires a minimum of two curves to perform the evaluation, which are a reference curve (obtained from a test) and a simulation curve to be graded. This makes it useful in injury studies as a tool to classify the acceptability of a simulation model which aims to emulate a real-life test performed. [13] This way, the CORA rating calculated for a signal being compared to another helps objectivise these curves resemblance, isolating the decision from mere opinions and impressions, which depend on, for example, the analyst's mentality or the scientist's state of mind, shedding light on the true similarity between both signals.

The CORA rating is calculated combining two different methods which measure different aspects which may denote resemblance between curves: corridor metric and cross-correlation metric. The corridor method is based on signal alignment and the proximity of the simulation curve to the real test signal in each time unit. On the contrary, the cross-correlation analysis is comprised of three different metrics which may even reward phase-shifted signals, given that the behaviour may be similar although not coincident in time. The combination of both of this metrics result in a number between 0 and 1, resulting a higher value of CORA rating in a greater signal resemblance.

Due to the multiple uses this technique can be given and the versatility it offers, there is not a certain rule or regulation which dictates a minimum CORA rating value to be achieved when performing simulations and result analysis. The absence of this criteria leaves the interpretation of results to the analyst's judge. Nevertheless, the criteria presented in Table 2.11 will be taken to consideration to evaluate the resulting CORA ratings in this project.[36]

Table 2.11 - CORA rating grading. Source: S. Eshragi et al, 2018

Overall Rating (CORA)	*Grade*
CORA > 0.94	Excellent
0.8 < CORA ≤ 0.94	Good
0.58 < CORA ≤ 0.8	Fair
CORA 0.58	Poor

Prior to the explanation of the different correlation methods CORA uses, it is important to mention that the analysis is only carried out to a certain interval of time called the *interval of interest*. The analysis is performed strictly using information in the interval of interest except for the case of phase-shifted correlation calculation, for which information outside of this region is necessary. Furthermore, it should be considered that most parameters are user-customizable, although the modification of these parameters may result in an increase in subjectivity.

Firstly, the corridor component is calculated defining inner and outer corridors surrounding the test curve. These corridors are typically limited with curves that run parallel to the test curve, creating a closed region with parallel boarders, although the corridor curves may also be defined by the user. The default setting is that inner and outer regions are defined as percentages of the test curve using customizable parameters (a_0 for the inner and b_0 for the outer corridor). In case of the simulation curve being inside the inner corridor, that time point receives a value of 1. If it is found outside the outer corridor, the time point receives a value of 0. On the other hand, a penalty is applied if the simulation curve is contained inside

the outer corridor and outside the inner corridor. This penalty is calculated proportionally to the distance to each threshold and is a number between 0 and 1. The CORA rating for the corridor method is the average of all values obtained for each time point inside the interval of interest using this method.

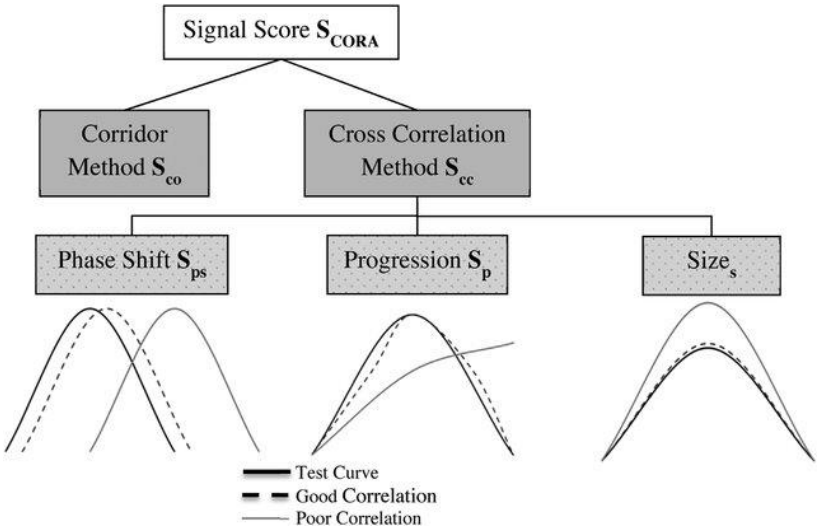

Figure 2.17 - CORA rating methods and scores. Source: Putnam et al, 2015

On the other hand, the cross-correlation analysis is comprised of three different calculations: shape, phase and size ratings, and requires a previous calculation of the maximum cross-correlation. The maximum cross-correlation is obtained by shifting left and right the test curve until it reaches the maximum phase shift permitted (m_{min} to the left and m_{max} to the right) and calculating the cross-correlation (K_{xy}) parameter for each shift following E. 2.1. The biggest value of cross-correlation from all allowable shifts is the maximum cross-correlation.[37]

$$K_{xy}(m) = \frac{\sum_{i=0}^{n-1} x(t_{min}+(m+i)\cdot\Delta t)\cdot y(t_{min}+i\cdot\Delta t)}{\sqrt{\left(\sum_{i=0}^{n-1} x^2(t_{min}+(m+i)\cdot\Delta t)\cdot\sum_{i=0}^{n-1} y^2(t_{min}+i\cdot\Delta t)\right)}} \qquad \textit{E. 2.1}$$

Once the cross-correlation parameter is defined, all three derived methods can be explained. Firstly, the progression rating (V) can be calculated using the maximum cross-correlation value from all shits available as presented in E. 2.2. The progression rating rewards

simulation curves for a similarity in increase and decrease intervals as well as a resemblance in behaviour of tendencies (Figure 2.17).[37]

$$V = \left(\frac{1}{2}\left(K_{xy,max} + 1\right)\right)^{k_v} \quad E.\ 2.2$$

Secondly, the phase shift rating is obtained using the phase shift value (δ) used in the maximum cross-correlation curve. Prior to the analysis, a minimum (δ_{min}) and maximum (δ_{max}) values of phase shift are selected as a percentage of the interval of interest. If $\delta < \delta_{min}$, the phase score is one. If $\delta > \delta_{max}$, the phase score is zero. If neither is true, the phase score is calculated using *E. 2.3*. This score rewards simulation curves which are similar to test curves, but do not coincide in time (Figure 2.17).[37]

$$P = \left(\frac{|\delta_{max} - |\delta||}{\delta_{max} - \delta_{min}}\right)^{k_p} \quad E.\ 2.3$$

Thirdly, the size rating rewards simulation curves which coincide with the test curve in range of values and size (Figure 2.17). This value is obtained comparing the test curve in the interval of interest and the optimally phase-shifted portion of the reference curve by following *E. 2.4* and *E. 2.5*.[37]

$$\frac{F_x}{F_y} = \frac{\sum_{i=1}^{n} x^2(t_{min} + \delta + i \cdot \Delta t)}{\sum_{i=1}^{n} y^2(t_{min} + i \cdot \Delta t)} \quad E.\ 2.4$$

$$G = \begin{cases} \left(\frac{F_x}{F_y}\right)^{k_G} & if\ F_x > F_y \\ \left(\frac{F_y}{F_x}\right)^{k_G} & if\ F_y < F_x \end{cases} \quad E.\ 2.5$$

Lastly, once all four scores have been calculated, using these values and their respective user-customizable weights (*E. 2.6*), the final overall CORA score can be obtained and thus a more objective metric on the resemblance between the test curve and the reference curve.[38]

$$C_3 = g_1 \cdot C_1 + g_2 \cdot (g_v \cdot V + g_p \cdot P + g_G \cdot G) \quad E.\ 2.6$$

Having explained all the main aspects of the CORA rating method, it is important to highlight that all parameters can be user-customized. Nonetheless, the customization of these parameters may increase the level of subjectivity of the analysis, but it can also be beneficial in case of a correct justification on in the reason for the change of parameters depending on the purpose of the study. The default values for parameters are presented in Table 2.12, which match with those used in this project in the MADYMO model's validation process following the R129 regulation and Karwala-Avionaut's frontal impact test performed with the Pixel AV304 and a Q1.5 dummy.

Table 2.12 - CORA rating parameters' default values. Adapted from: D. Albert, 2020

Parameter	*Definition*	*Default setting*
K	Exponent factor for calculating corridor rating	2
A_0	Inner corridor width percentage	0.05
B_0	Outer corridor width percentage	0.5
G_1	Weighting factor of corridor rating	0.5
D_MIN	Determines minimum desired phase shift	0.01
D_MAX	Determines maximum desired phase shift	0.12
INT_MIN	Defines the maximum time shift used by cross-correlation method	0.8
K_V	Exponent factor for calculating progression rating	10
K_P	Exponent factor for calculating phase rating	1
K_G	Exponent factor for calculating size rating	1
G_V	Weighting factor for progression rating	0.5
G_P	Weighting factor for phase rating	0.25
G_G	Weighting factor for size rating	0.25
G_2	Weighting factor for cross-correlation rating	0.5

2.4 OTHER TECHNOLOGIES

The previous technologies described require a thorough explanation due to its relevance to the project. However, other technologies have been used that, although being of small relevance to the project and being widely used in the industry, require a brief explanation on the use each tool was given.

Firstly, the tool which has made possible the modification of the recline angle of the back of the restraint system based on the original CAD of the Pixel AV304 is LS-PrePost. It also permitted the obtention of a valid model of the R-129 test bench cushion, as its behaviour and loading and unloading functions must be introduced in MADYMO, so that the program can replicate its behaviour in the simulation, thus providing a more exact model and higher CORA ratings which consolidate the similarity between tests. However, LS-PrePost is a very common program to use in the field, thus being unnecessary to dedicate a separate section to explain its fundamentals. Besides, its use in this project is considered secondary as its only purposes were mesh creation, element addition, recline angle modification and physical properties calculation, which are considered to be basic operations.

Secondly, Matlab was used to analyse information provided by Karwala-Avionaut on the frontal impact homologation test. The deceleration pulse to which the test bench was subjected was manipulated using Matlab. In addition, the data extracted from the foam impact test performed on the R129 seat cushion was also manipulated using Matlab.

Furthermore, a code on Python was used to manipulate and automatise the output information manipulation and data comparison between the real-life frontal impact test and the MADYMO validation model results.

Lastly, Microsoft Excel was used to manipulate output data from the alternative models simulated in MADYMO, organising information in tables with conditional formatting, which helped obtain more visual results, and displaying the biomechanical results measured by the dummy in MADYMO in simple graphs and diagrams.

Chapter 3. STATE OF THE ART

3.1 MOTOR VEHICLE RELATED PEDIATRIC INJURIES

Since the automotive industry started to develop in 1886, road safety has always been a main concern. Despite this concern, one of the main contributions to road safety, the three point seat belt, was not introduced in production until 1959 when Volvo first implemented it in a car in Sweden. [21] Since 1959, many inventions and studies have contributed to the reduction of casualties and injuries in motor vehicle accidents, such as airbags or child restraint systems.

Focusing on children and in the USA, the number of fatalities registered between 2000 and 2009 in motor vehicle accidents suffered by people aged 0-19 experienced a reduction of 41% and ceased to be the leading cause of unintentional death between children aged 1-4 years old in 2007, as shown in Figure 3.1.[39]

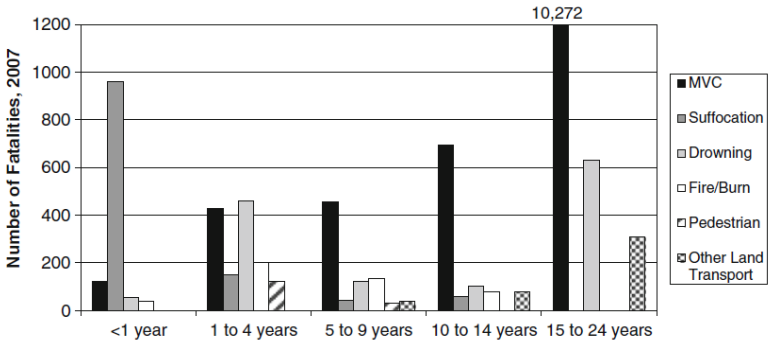

Figure 3.1 – Top five causes of unintentional fatality for children in the USA in 2007. Source: CDC NCIPC WISQARS, 2010

Similarly in Europe, Figure 3.2 shows the reduction in the number of child fatalities during vehicle crashes compared to the total reduction in road fatalities in the EU from 2006 to 2015, which proves the steady improvement of pediatric road safety in high-income countries. In this statistic, children are any human being aged below 15. Interestingly, child

fatalities descended from 1300 to 654 in 2015, which represents a 50% reduction, whereas total road deaths experienced a reduction of only 39% [40]. This reduction can be largely attributed to the use of child restraint systems, and therefore, these figures serve to prove the steady improvement of child restraint systems and its effect on child safety. Nevertheless, Lee et al [41] carried out a study in which still 52% of the fatally injured children were inappropriately restrained, due to either an incorrect CRS installation or an inconvenient CRS selection for the occupant's age or size.

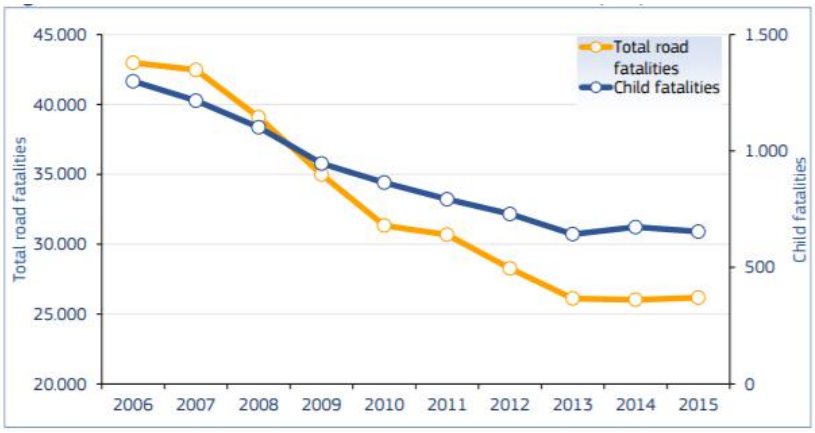

Figure 3.2 – Number of child and all road in the EU, 2006 – 2015. Source: European Road Safety Observatory, 2017

Even when the CRS is not 100% perfectly used, in comparison to unrestrained children, the risk of death or serious injury when using a rearward-facing child restraint system is a 71% lower and a 54% lower when it comes to forward-facing restraint systems.[42] More specifically for younger children from 0 to 2 years old, rearward-facing restraint systems have an injury rate registered which is 0.57 times the injury rate registered for that of forward-facing systems. In addition, rear-facing restraints are 5.57 times safer in side impacts and 1.23 times safer in frontal impacts compared to front-facing restraints.[43] These studies prove the convenience of rearward-facing child restraint systems over those forward-facing for infants, as injury and death rates are lower for the first. Nevertheless, increase in mass and size of children is suggested by some researchers as a limiting factor for the use of rear-facing CRS although this concern has more to do with comfort issues more than with safety facts. In this regards, the National Highway Traffic Safety

Administration (NHTSA) recommends four steps to follow as the child grows: rear-facing system with incorporated harness (newborn to 3 years old), forward-facing system with harness (1 to 7-year-olds), three-point seat belt combined with child restraint system booster (4 to 12 years old) and, finally, conventional seat belt without any additional restraint system (8-year-olds or older). [44] The coincidence of certain recommended systems in time is explained by the effect of size and mass in the effectiveness of these, thus depending the ideal CRS to use not only on the child's age, but also on size and mass.

Nevertheless, in Sweden rear-facing systems are recommended for the first 4 years of life as it was reported that children up to 4 years old experienced a reduction of 90% risk for AIS 2+ injuries in comparison to those unrestrained.[4] This results in a usage of rearward-facing CRSs in Sweden between 64% and 79% for children between 1 to 3 years old. [47], [48]

3.2 IMPORTANCE OF SEATBACK ANGLE IN REAR-FACING CRS

The main goal of all CRSs is to couple as tightly as possible the child's body to the vehicle in order to distribute all loads suffered by the occupant across the biggest surface possible, increasing the amount of time the system is put to work.[49] For this reason, rear-facing CRSs help distribute load across the infant's back, increasing the surface on which it is applied. [50]

According to N. Yoganandan et al[49], child restraint systems' ability to properly restrain the occupant to the vehicle diminishes if the recline angle exceeds 45º to the vertical axis, as a result of the force exerted by the seat projecting the infant upwards becoming greater than resulting force exerted by the back of the restraint system. This means that a smaller recline angle of the back of the CRS increases the security and protection provided. On the other hand, newborns' head must be prevented from hanging forward, given that this could result in airway obstruction, as children are not able to hold their heads erect and steady enabling postural control in a seating position until 2-3 months old.[51] This way, N. Yoganandan et al [49] conclude that a recline angle of 45º from vertical provides the best compromise

between both aspects, not recommending an angle smaller than 30º [52] (Figure 3.3). Nevertheless, it is not specified whether this conclusion was obtained using a base underneath the restraint system installed or not, as well as the variables tracked and analysed.

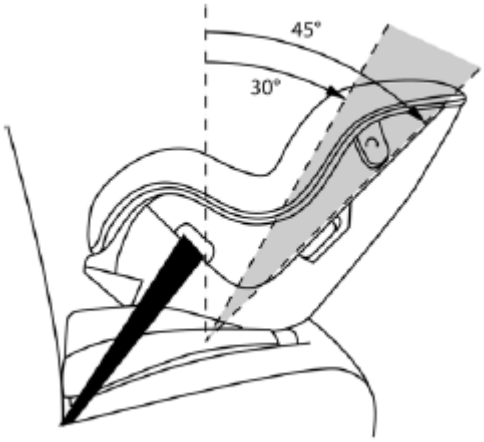

Figure 3.3 - Recommended recline angles of back of rear-facing CRSs from vertical. Source: N. Yoganandan et al, 2015

Sherwood et al [67] concluded once again in an experimental test performed with a CRABI 12-month-old dummy and a Q1.5 that rearward-facing child restraint systems offer a greater protection than forward-facing. However, no conclusions were drawn on the most convenient recline angles which optimizes the occupants' safety.

Sherwood et al [68] compared the performance of various child restraint systems with different configurations (rear-facing or forward-facing) using a CRABI 12-month-old dummy. This study concluded the higher security offered by rear-facing system, but failed to determine any influence of the recline angle of the CRS, as models were different. Nevertheless, angles of the CRSs specified ranged from 38º to 48º from vertical.

Lastly, Whitman et al [52] carried out a study with three different child restraint models and multiple configurations. The recline angles of the back of the systems were 35º, 42º, 45º and 46º from vertical. However, the disparity between model configurations makes inconvenient the extraction of conclusions on the effect of different recline angles of the back of the CRS.

3.3 PEDIATRIC INJURY BIOMECHANICS AND ASSESSMENT

Pediatric biomechanical studies help develop the child restraint system industry, thus contribute to the improvement of infant protection during motor vehicle crash accidents. The injury criteria to which injury risk graphs and Injury Assessment Reference Values (IARVs) are translated for Q-dummies are the only ones used in pediatric injury analysis. These criteria are Head Injury Criterion (HIC), Head Acceleration for 3ms (Head ACC3ms), Upper Neck tension (Fz), Upper Neck bending moment in flexion (My) and Chest deflection (Dchest).[53] These criteria coincide with some of those registered by MADYMO dummies as previously mentioned in Chapter 2.1 [19], as well as with those stated as injury criteria for infants in the R-129 regulation stated in Chapter 2.2 [34]. However, injury criteria are usually calculated and developed based on evaluations performed to just one dummy and they are later translated to other dummies via scaling. This has led to the inclusion of specific injury criteria calculation for each dummy, improving the reliability of these criteria.[10]

Moreover, the mentioned criteria can be calculated in motor vehicle computational simulations or in real-life impact tests, but in real-life road accidents it is practically impossible to take these measurements. It is for this reason that different medical injury metrics are used, so that information gathered by doctors can be used. [54] The most important injury metrics used in MVC are the Abbreviated Injury Scale (AIS), which grades injury severity from 1 (minor) to 6 (maximal), and the Injury Severity Score (ISS), which is calculated using the AIS scores from the three most severely injured body parts after an accident.[55] On the other hand, the KABCO scale is also used by law enforcement in the US, but its use is not recommended, given its disagreement with medically-based metrics. [56]

Furthermore, several countries have developed international collaboration projects in which the main objective was to broaden the child occupant injury understanding in motor vehicle crashes. The most important projects carried out by the European Union so far have been CREST (Child Restraint System in Cars) in 1999 and 2000, CHILD (Child Led Injury

Design) from 2002 to 2006 and CASPER (Child Advanced Safety Project for European Roads) from 2009 to 2012. [57] These projects are responsible for the review of current regulations, as well as of performing an analysis on massive data samples of motor vehicle crashes. Lesire et al [32] concluded that the R129 combined with the CASPER project discoveries will help improve compatibility between cars and child restraint systems, as well as facilitating a correct CRS installation and use, which is one of the main problems all three projects identified. However, K. D. Klinich et al [58] concluded in an experimental study with 31 different CRS models that there were no combinations of vehicle and CRS in which LATCH belt tightening was physically impossible. Furthermore, the CASPER project also aimed to improve the efficiency of child safety, which included the development of specific injury risk curves for the Q-dummy family. [59] This way, all three projects continued the development of injury criteria for child dummies which had already been demanded, as adult data scaling had been proven to be imprecise. [60]

3.4 THE Q-FAMILY OF PEDIATRIC CRASH TEST DUMMIES. EXPERIMENTAL CRASH TESTING AND COMPUTER SIMULATED TESTS

The child restraint system to optimize in this project is a rear-facing system given that it is recommended by the manufacturer for children under 13 kg [45] and this usually corresponds to children under 2 years old. This particular CRS is properly assessed using the Q1.5 dummy model, which is specifically designed for infants under 13kg. [46] This sets the Q1.5 dummy apart from all other ATDs to perform the homologation test of Karwala-Avionaut's rear-facing child restraint system subject to study: Pixel AV304.

The Q-Dummy family, presented in Figure 3.4, was developed using the R44 regulation and CREST and CHILD project results to generate child ATD models which can gather more reliable information and to which injury criteria can be adapted. After that, the R129 regulation states that Q-dummies are preferable when it comes to child injury risk

assessment. [46] The dummy which corresponds to an 18-month-old with 11.1 kg of mass is the Q1.5, which is used in PIXEL AV304's impact test.

Figure 3.4 -The Q-dummy family: (from left to right) Q1.5, Q3, Q0, Q6, Q1 and Q1 without suit. Source: K. de Jager et al, 2005

Similarly to this project, various studies require the design of a computational model which represents a real-life road accident or impact test. In order to confirm the reliability of the computational model and its results, it is necessary to perform a continuous validation and verification of the simulation's similarity to reality. [14] In case of having the real-life frontal impact test results, it is convenient to compare these to the metrics obtained in the simulation model. For this purpose, CORA rating is widely used as an objective metric of time-history similarity. [13], [36]–[38] Hence, a higher CORA rating will contribute to a much more reliable results and conclusions.

The MADYMO (MAthematical DYnamic MOdel) software is widely used in the automotive industry and allows to build a computational model of a motor vehicle crash using multibody three-dimensional technology combined with FE models. Many studies carried out in the recent years used MADYMO as the ideal impact simulator software to perform the experiment. [61]–[65] Nevertheless, most MADYMO models developed tend to have a predominant proportion of multibody components over FE elements, as FE components in MADYMO substantially increase simulation time and memory usage. For FE models, LS-DYNA and PAM-CRASH are also commonly used. [66]

Lastly, a general review of similar studies carried out on the field is beneficial to understand the method followed during the project or its justification. Wismans et al [63] performed MADYMO 3D simulations of Hybrid III dummy sled tests to recommend dummy model improvements. They did this by comparing model and experimental test acceleration-time histories, which can help determine the similarity between reality and simulations. Yuanzhi Hu et al [64] modelled the effects of seat belts on occupant kinematics and injury risk. Unfortunately, occupants were adults and the impact analysed was a rollover. Nonetheless, injury evaluation was performed using HIC, N_{ij} and CTI. On the other hand, Menon et al [62] carried out a similar project to the present although analysing seating angles of high back booster seats following FMVSS 213, which does not cover children under 2 years old in the EU. Despite the mentioned dissimilarities, MADYMO was the mathematical model used and a multibody bench seat was used, instead of an FE model with foam behaviour.

Chapter 4. JUSTIFICATION AND OBJECTIVES

4.1 JUSTIFICATION

According to Yoganandan et al [49], in rear-facing child restraint systems, achieving the optimal recline angle is critical. An excessively upright system may lead to airway obstruction if the infant's head tips forward, and an excessively reclined system will not be able to restrain the occupant adequately. For this reason, the correct execution of this study will allow to optimize the Pixel AV304's efficiency and child protection offered, improving the already existing and commercialised item.

Furthermore, investigation carried out so far in child restraint system configuration and installation are mainly focused on seat belt installation or rear-facing and forward-facing orientation comparison. However, studies which make mention of different recline angles experiment with different CRS models with different characteristics. For this reason, conclusions on optimal recline angles of the systems may not be fully reliable, as dimensions, materials and other aspects may distort the comparability of all configurations. This project only uses one model with various recline angles, which facilitates the comparability of results and increases the reliability of the conclusions drawn.

In addition, the different angle configurations analysed in the project offer a total range of +10º/-10º with respect to the recline angle with which Pixel AV304 has been initially designed. This 20º variation analysis allows to evaluate the recommended range of recline angle for rear-facing child restraint systems between 30º and 45º from vertical. The progression followed between models in this project will provide information on changes in biomechanical variables measured in a Q1.5 dummy model for each angle. No other study has been found which offers the mentioned data obtained with a progressive variation of the recline angle of the same CRS model with absolutely no other alteration.

A proper execution of the project will shed light on the effect of rear-facing CRS recline angle on child protection and injury prevention. The conclusions drawn from this study may help improve automotive safety for newborns and infants, thus helping reduce the number of infant casualties recorded in the following years. This justifies the alignment of this project with the Sustainable Development Goals (SDG) related to child health and industrial innovation: good health and well-being (SDG 3); industry, innovation and infrastructure (SDG 9); and sustainable cities and communities (SDG 11). [69]

4.2 OBJECTIVES

This section presents the objectives that have been set at the beginning of the project, whose consecution will lead to a satisfactory completion of the project.

1. ***Generation of a validated simulation model of the CRS under study in a frontal impact test following R129 in MADYMO.*** No valid results and conclusions can be obtained without generating a computational model of a frontal impact test in MADYMO as similar as possible to the real-life homologation test performed on the Pixel AV304 by Karwala-Avionaut following the R129 regulation. This first objective requires the achievement of the following partial objectives:

a) ***R129 test bench modelling.*** The homologation test is performed using a test bench and pre-defined seat belt conditions. The R129 is the European regulation which dictates the conditions under which all homologation tests performed on CRSs must fulfil. The generation of a valid test bench and seat belt model in MADYMO enables the possibility of re-using the model for further investigations performed under the same regulation. This includes a proper characterisation process of the seat cushion's material, obtaining the foam's loading and unloading functions for instance.

b) ***Pixel AV304 model inclusion and Q1.5 dummy positioning.*** The main purpose of the study is the evaluation of the Pixel AV304 rear-facing child restraint system. This requires a correct CRS meshing and inclusion in the MADYMO model, including possible modifications of the uncomplete CAD model provided by Karwala-Avionaut. Furthermore, a correct dummy positioning and interaction between CRS and dummy will increase the reliability of the results obtained.

c) ***Final validation model CORA rating over 0.6***. The CORA rating helps measure the resemblance between the computational model created and the real-life frontal impact test performed by Karwala-Avionaut. The goal is to obtain a minimum CORA rating of 0.6 during the first 175ms of the impact test. The CORA rating will be

calculated including all the real-life test signals provided by Karwala-Avionaut: head accelerations, upper neck axial force and moments, thorax accelerations and chest displacement (global CORA rating).

2. ***Analysis on effect of recline angle variation of the back of a CRS in occupant's security.*** After the validation process, alternative models of the Pixel AV304 with different recline angles will be introduced to the validation model replacing the original CRS model.

a) ***Generation of alternative CAD models of the Pixel AV304 with different recline angles***. In order to perform the analysis on recline angle variation, the CAD model of the Pixel AV304 will be modified using LS-PrePost to obtain the desired recline angles. The study will be based on simulating 9 different models with a maximum variation of 10º (from 34º to 54º from the vertical direction) in intervals of 2.5º between models.

b) ***Evaluation of injury criteria of all alternative models.*** To evaluate the convenience of certain recline angles of the back of the CRS, it is necessary to analyse the fulfilment of the injury criteria available for Q1.5 dummies in frontal impacts. The injury criteria that will be taken into consideration are: peak head resultant acceleration during 3ms, peak thorax resultant acceleration during 3 ms, Head Injury Criterion (HIC), maximum neck axial force and the neck injury criterion (N_{ij}).

c) ***Evaluation and analysis of possible correlation between CRS recline angle and occupant protection.*** The change of head and thorax acceleration, upper neck axial force and moment, and lumbar forces and moment will be analysed depending on the value of the recline angle. Possible correlations between physical properties and recline angle will be evaluated numerically and graphically.

3. ***Recommendation of an optimal recline angle of the back of the Pixel AV304 child restraint system which maximises the occupant's security and protection.*** Main objective of the project and original purpose of the study.

Chapter 5. METHODOLOGY

In this section, the methodology followed during the execution of the project is presented. It has been organised in the clearest manner possible to allow an easier understanding of the actions taken and the reasons behind each decision. Firstly, the validation process which has been followed throughout the project and the CORA rating analysis executed are explained. Secondly, it is important to perform a thorough description of the validation model's different elements and their key properties. Later, the interactions between the model's components are presented, which is vital for MADYMO models. Lastly, it is important to explain how the recline angle was varied and the conditions under which all the alternative models were simulated, which led to the obtainment of an optimal recline angle and the finalization of the project.

5.1 MODEL VALIDATION

5.1.1 VALIDATION OF THE MODEL. CORA RATING.

The main aim of this project is to obtain an optimal recline angle of the back of a rear-facing child restraint system, which maximizes occupant safety and ergonomics. The child restraint to be optimized is the Pixel AV304 produced by Karwala-Avionaut. In order to carry out the project, instead of manufacturing different CRS models with different recline angles and test them in crash impact tests, which is extremely expensive, the study is carried out using MADYMO, a mathematical passenger model, and performing simulations with models obtained from modifying the Pixel AV304 design.

To ensure that the conclusions obtained in the MADYMO simulations correlate to the results which would be obtained in real-life crash impact tests, before producing any recommendation, it is necessary to perform a model validation prior to the recline angle variation. With this in mind, Karwala-Avionaut provided a series of time-history curves

obtained from the experimental frontal impact crash test performed to homologate the Pixel AV304 model. These time-history functions were measured by a Q1.5 dummy, which was used as the occupant, given that the rear-facing model is aimed for children under 13kg.

In addition to the time-history curves, Karwala-Avionaut provided a set of multimedia documents which include pictures of the homologation test, both before and after the execution of the test, as well as two videos of the experiment from a lateral and an overhead view (Figure 5.1). These photos and videos were provided a fully representative image of how the test was performed: seat belt positioning, test bench used and dummy positioning, CRS positioning. Furthermore, the video helps compare the model's and dummy's kinematics during the test to that observed in the simulated test.

Figure 5.1 – Pixel Av304 homologation test by Karwala-Avionaut. Source: Karwala-Avionaut, 2020

Taking into account that a properly validated simulation model increases the validity and reliability of the conclusions drawn after the consecution of the project, it is crucial to obtain a validation model which maximizes its similarity to the real-life impact crash test. In order to measure the level of resemblance between impact test and simulation, it has been decided to make use of the CORA rating, which has been previously explained in detail in Chapter

2.3. The CORA rating offers a more objective metric to measure the level of similarity between two time-history curves. In this case, using the time-history of some of the physical variables measured by the sensor's placed in the Q1.5 dummy used in Pixel AV304's frontal impact test and those registered by MADYMO's Q1.5 dummy in the computational frontal impact simulation, a CORA rating can be obtained which offers an objective insight on the validity of the tested model.

The time-history curves provided by Karwala-Avionaut are displayed in Table 5.1. On the other hand, MADYMO's Q1.5 dummy model has many sensors, which generate up to 32 different channels. Having identified the signals available from Karwala's impact test, it is very simple to only select the corresponding signals from MADYMO's dummy. However, as it can be observed in Figure 5.2, the dummy was not placed perfectly aligned with the X axis, which resulted in a complex behaviour in the Y axis which can be hardly emulated in MADYMO. For this reason, it was decided to eliminate all signals which represented behaviour in the Y axis, as it can be observed in Table 5.1, in which these signals have been assigned a weight of 0 for the CORA rating calculation. Nevertheless, displacements and rotations experienced during the test as a result of an imperfect dummy positioning are still considered in the analysis of resemblance between tests.

Figure 5.2 - Dummy positioning and misalignment with X axis. Adapted from: Karwala-Avionaut, 2020

Table 5.1 - CORA signals compared and weights for analysis

Variable	*Axis*	*Cora Signal Identifier*	*CORA rating weight*
Head Acceleration	X	**11HEAD0000Q2ACXA**	0.2
	Y	11HEAD0000Q2ACYA	0
	Z	**11HEAD0000Q2ACZA**	0.2
Neck Force	X	11NECKUP00Q2FOZB	0*
Neck Torque	X	11NECKUP00Q2MOXB	0
	Y	**11NECKUP00Q2MOYB**	0.2
	Z	11NECKUP00Q2MOZB	0
Thorax Acceleration	X	**11THSP0000Q2ACXA**	0.2
	Y	11THSP0000Q2ACYA	0
	Z	**11THSP0000Q2ACZA**	0.2
Chest Displacement	X	11CHST0000Q2DSXB	0

**Although neck axial force was initially considered relevant for the CORA rating calculation, the reason why it was ruled out of the process will be explained in Chapter 6.1*

Considering all the information provided, the validation of the model has been performed using two metrics. Firstly, a CORA rating obtained from the signals and weights presented in Table 5.1 was used. As it was previously explained in Chapter 2.3, the CORA rating can be obtained modifying all the parameters used, including the importance given to corridor and cross-correlation methods. With the objective of obtaining the most unbiased result possible, the parameters that have been used are those set as default in CORA and presented previously in Table 2.12. Secondly, the lateral and overhead view videos have been used to perform a more subjective evaluation on the dummy and CRS movement experienced during the impact test. The main aspects of these videos to which attention has been paid are CRS penetration and displacement on the seat cushion and dummy's head rotation around Z axis and displacement in all directions.

5.1.2 VALIDATION MODEL'S COMPONENTS

After explaining how the validation process works and the tools used to obtain a valid simulation model, it is necessary to describe all the simulation components which have been inserted in MADYMO. this section focuses on model and simulation conditions description, as well as component positioning.

5.1.2.1 Frontal Impact Test Conditions

The frontal crash test performed by Karwala-Avionaut lasted a total of 300ms, which is the amount of time in which dummy data was gathered and the provided videos were recorded. However, most signals start obtaining low values after approximately 175ms, which leads to considering that the actual impact only lasts 175ms, thus becoming the *interval of interest* for CORA rating the first 175ms of the test. This time interval has been reduced to 175ms to avoid the obtainment of higher CORA ratings, as the tendency to lower values registered after 175ms can be easily replicated by the model and the truly relevant time interval of the impact has already occurred. This is a common practice in the field of impact biomechanics.

On the other hand, when performing MADYMO simulations, it is required to leave a time prior to the impact, allowing all the elements of the simulation to comfortably interact with one another and begin the simulation from equilibrium. For this reason, taking t=0 as the moment in which the acceleration pulse begins, initiating the impact test, the initial time has been chosen to be -400ms. In this period of 400ms between the beginning of the simulation and the acceleration pulse, the dummy must comfortably sit on the child restraint system, the CRS has to be placed on top of the cushion, the seat belt buckle and anchors have to be unlocked and the seat belts have to be refitted using elastic force. All these events and their activation times are presented in Table 5.2. However, when performing small modifications which did not affect the pre-simulation time, MADYMO allows the user to import the position of all joints of an existing simulation at a certain time. This allowed to reduce the simulation time when performing small changes by importing a similar simulation's joint positioning and only having 50ms of pre-simulation before the acceleration pulse occurred.

Table 5.2 - Simulation events and respective times and goals

Simulation period	*Event*	*Goals*	*Time (s)*
Pre-simulation (-400ms, 0ms)	Gravity activation	Pixel Av304 positioning Q1.5 dummy positioning	-0.400
	Seat belt tensioning	Lap belt and shoulder belt positioning around CRS (50N)	-0.200
	Seat belt buckle and anchors unblocking	Freedom of movement for buckle, D-ring and anchor	-0.150
	Seat belt blocking	Lap belt and shoulder belt blocking	-0.015
Impact crash test (0ms, 175ms)	Acceleration pulse activation	Impact crash test following Karwala's real-life test	0

Furthermore, it is important to explain the two acceleration fields to which the model is subjected: gravity and acceleration pulse. Firstly, the gravity included in the model has a value of 9.81 m/s^2. It affects all elements in the simulations used for model validation. Nevertheless, in simulations performed with child restraint systems with different angle configurations, in case of having a more horizontal back, the seat belt slipped under the system and adopted an incorrect position after tensioning. For this reason, gravity was disconnected for lap belt and shoulder belt for these simulations to avoid a mispositioning of the seat belt. Secondly, the acceleration pulse included in the model begins at t=0 and corresponds to the impact crash test deceleration pulse. This information has been provided by Karwala-Avionaut and corresponds to the same pulse used in the real-life impact crash test performed on the Pixel AV304. Suffice it to say, this deceleration pulse fulfils the R129 regulation requirements which were previously presented in Chapter 2.2. The acceleration pulse must be contained inside an acceptance region which is shown in Figure 5.3. On the

other hand, the deceleration pulse with which all simulations were performed is presented in Figure 5.4 and fulfils the R129 regulation requirements with a 60Hz filter.

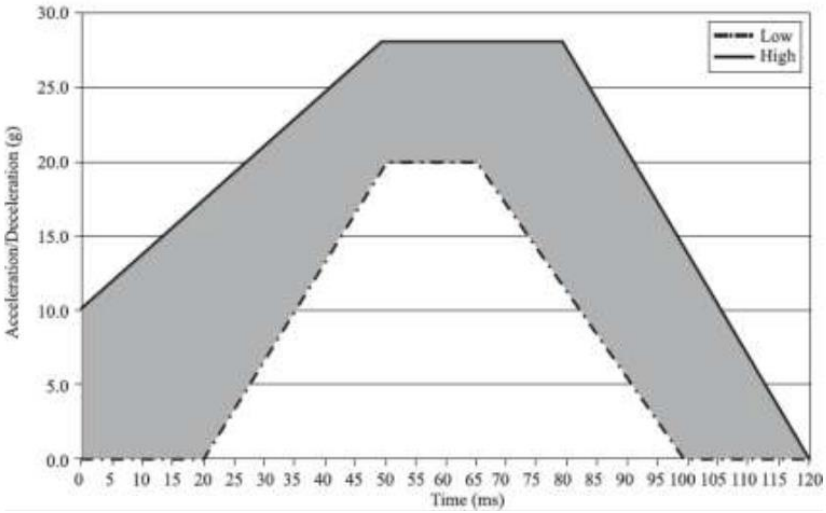

Figure 5.3 - R129 acceptance region for frontal impact deceleration pulse. Source: United Nations, 2013

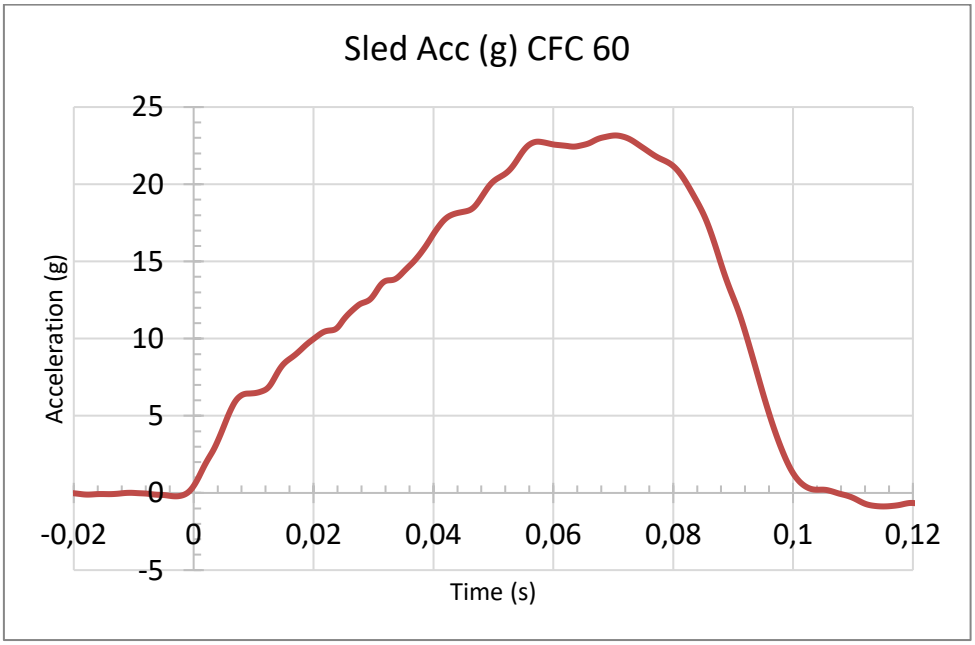

Figure 5.4 - Sled acceleration pulse of Pixel AV304 impact crash test

However, although the regulation defines the acceptance region for positive values of acceleration measured in g's (1g=9.81m/s^2), the acceleration pulse must be included in MADYMO measured in SI base units (m/s^2 in this case) and with negative values, as the vehicle is decelerating. Furthermore, the pulse must be declared at least from -400ms to 175ms, as these will be the times in which the experiment will be carried out. Values registered before t=0, the acceleration pulse was approximated to 0, to avoid noise in the signals and to ensure a correct pre-simulation. The resulting deceleration pulse introduced in MADYMO is displayed in Figure 5.5.

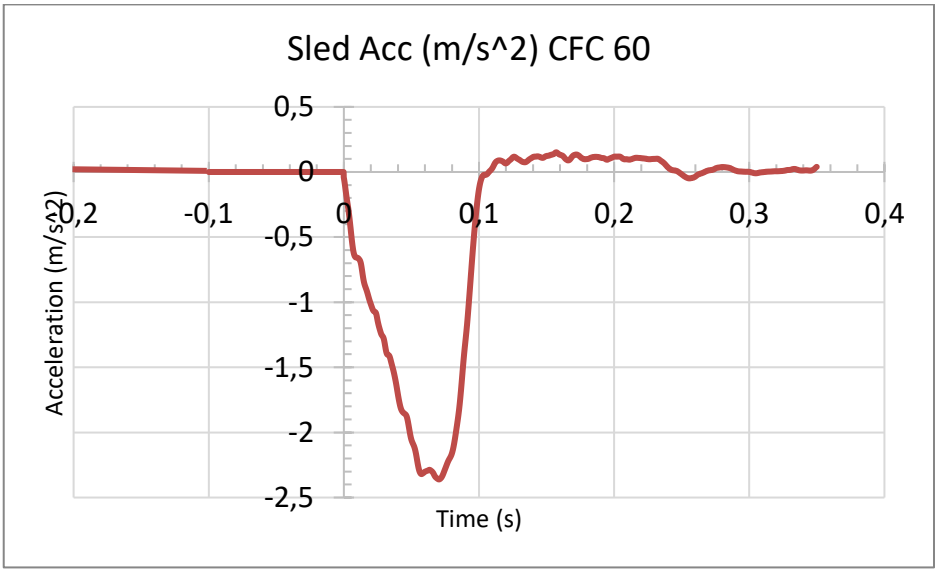

Figure 5.5 - Sled acceleration pulse introduced in MADYMO

5.1.2.2 Pixel AV304 CRS Model

One of the main components of the MADYMO model is evidently the Pixel AV304 child restraint system produced by Karwala-Avionaut, as the main goal of this project is the optimization of the recline angle of this CRS model. To correctly include the Pixel AV04 in the MADYMo simulations, it is necessary to obtain a CAD model of the element, pre-process it using LS-PrePost to create a mesh and simplify the surfaces, add the FE model to MADYMO, define physical properties and perform the necessary modifications.

Firstly, Karwala-Avionaut provided a CAD model of the Pixel AV304, as well as a real-life sample of it. Prior to preprocessing the model, it was necessary to calculate the restraint system's physical properties: mass, inertias and centre of gravity. The mass was determined weighting the real-life sample in the laboratory, obtaining a total mass of 2.443kg. In addition, a visual inspection of the sample and the CAD model allowed to notice that the CAD model only possessed the system structural shell, but the foam which separates child and shell was missing, thus being necessary to perform some modifications to the model. The first modification was the addition of extra elements which filled all the gaps in the model which could lead to irregularities on the surface. The other main modification performed was the recreation of the headrest's foam as a replica of the headrest's shell scaled and moved 5 cm away. The resulting meshed CAD model in LS-PrePost shown in Figure 5.6 was introduced in the MADYMO model by adding all the corresponding nodes, elements and parts.

Figure 5.6 - Meshed CAD model of Pixel AV304 in LS-PrePost with gaps filled and headrest support

On the other hand, inertias and centre of gravity were calculated using the CAD model available and the *Measure* tool in LS-PrePost. As the model had been modified and some components were not included in the CAD model, an iterative process had to be performed varying densities until the total mass value matches that measured experimentally. All internal structural elements were assigned a density of 900kg/m^3, which corresponds to high density polyethylene, the shell elements' density was calculated iterating density values. The final density obtained was 1920kg/m^3, which allowed experimental and computational masses to match, thus obtaining the final value of inertias and centre of gravity (Table 5.3).

Table 5.3 - Pixel AV304 physical properties calculated using LS-PrePost

Property	*Unit*	*Axis*	*Value*
Centre of gravity (measured from origin of reference system)	m	X	-0.404
	m	Y	0
	m	Z	0.2015
Mass	kg	-	2.443
Inertia	kg·m^2	Ixx	0.0532
	kg·m^2	Iyy	0.0486
	kg·m^2	Izz	0.0986
	kg·m^2	Ixy	3.2·10^{-6}
	kg·m^2	Iyz	0.7·10^{-6}
	kg·m^2	Ixz	0.0181

Following the CRS model inclusion in MADYMO and its physical properties definition, it two other final modifications were performed in the model in MADYMO. The first modification was the addition of two belt subjections which are present in the real-life model but are missing in the CAD model. These subjections were included symmetrically to the model and guide the lap belt and avoid its misplacement in the model. They were defined

using simple surface ellipsoids and matching dimensions with those measured experimental in the Pixel AV304 sample available.

On the other hand, the second modification performed was the addition of two MB surface ellipsoids between dummy and CRS. These elements were included as a continuation of the scaled headrest included in LS-PrePost to ensure a correct dummy positioning. One ellipsoid was added between the dummy's back and the CRS's back as an extension of the head rest foam model. The other ellipsoid was added between the dummy's upper legs and the seat of the CRS as an extension of the back ellipsoid. These two modifications can be observed in Figure 5.7, where the original model is compared to that with the CRS foam ellisoids.

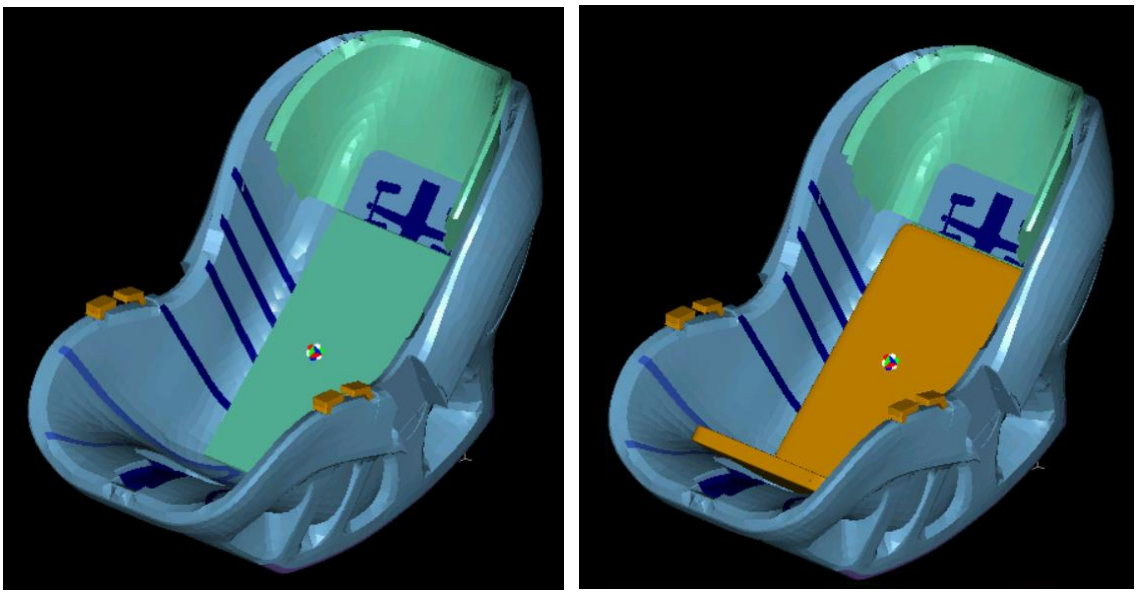

Figure 5.7 - Final MADYMO validation model of Pixel AV304. Left: Original. Right: Modified Model

Finally, some contact characteristics must be included to define the surfaces interaction with other elements. In addition, different groups of elements and nodes must be defined in the model, which will be used when declaring the surfaces with which certain elements will make contact. All these aspects will be explained in the interactions section in Chapter 5.1.3.

5.1.2.3 Q1.5 Dummy

Firstly, it is important to know the dummy that was used during the homologation test of the Pixel AV304 child restraint system. As it is a rear-facing system, the recommended maximum weight for an occupant is 13 kg, hence Karwala-Avionaut performed the frontal impact crash test using a Q1.5 dummy. This dummy, which corresponds to an 18-month-old child, is characterised for a total mass of 11.1kg, a standing height of 80cm and a sitting height of 49.9cm.

As it has already been explained in Chapter 2.1.4, MADYMO has a dummy database preinstalled with multiple dummy models and their physical characteristics. In this case, the Q1.5 dummy corresponds to the *"d_q32yel_inc.xml"* file.

Once the file has already been identified and included to the model, it is necessary to adequately place and orient the dummy in the reference space to ensure a correct simulation. The Joint Positioning tool (press F11) helps place the dummy in the most according way possible to emulate the impact test performed by Karwala-Avionaut. However, the dummy model in MADYMO is endowed with certain states of equilibrium for each joint. This does not allow the dummy to be positioned in the exact same way as it was placed on the CRS during Karwala-Avionaut's test. As it has already been mentioned, the dummy in the real-life test was not perfectly aligned with the X-axis, which results in a position mismatch. This combined with the state of equilibrium to which the neck rotation is limited, prevents from a correct dummy positioning. However, it is possible to perform a rotation of the whole dummy around the Z-axis of 1º, resulting in a better initial dummy positioning.

On the other hand, the dummy's limbs were placed in the model in the most similar way possible to that in the real-life crash test. Firstly, both legs must be placed symmetrically to the XZ plane and fully extended with the lower and upper leg ellipsoids parallel to one another. In addition, both feet must be making contact with the back seat cushion before the deceleration pulse begins. Furthermore, both arms are positioned at a 90º angle, which corresponds to its state of equilibrium in MADYMO, and placed above the lap belt. To sum

up, the resulting initial position of the dummy in the MADYMO simulation is shown in Figure 5.8.

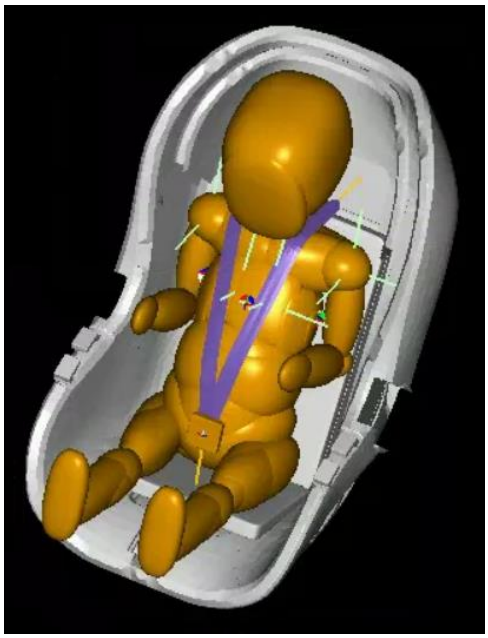

Figure 5.8 – Q1.5 dummy positioning in MADYMO

Lastly, two aspects on dummy positioning in validation and varied angle simulations must be considered. Firstly, as the validation model is to be compared with real-life frontal impact test data, conditions between both tests must be as similar as possible. However, once the validation process has been finished and the final base model has been obtained, the tests performed with CRS with recline angles varied will be simulated at a neutral position with no initial Z-axis rotation. For this reason, an extra simulation will have to be performed with the base model in order for results to be comparable to those obtained with the present recline angle of the Pixel AV304. On the other hand, comparability between simulations with recline angle varied will be granted by locating the dummy's H-point in the same position on the horizontal plane. This will make test the more unbiased and the similarity between initial conditions will be granted.

5.1.2.4 Seat and Back Cushions of the ECE R-129 test bench

The seat and back cushions are critical elements in the model, as they are responsible for the energy absorbed during the impact and the movement experienced by the CRS and, consequently, the dummy. Cushions' physical properties such as mass and dimensions are not that relevant to the simulation, as these elements are attached to the test bench and do not rotate or move respectively to it. The only physical properties relevant to the project are density, foam behaviour and load vs unload functions, which defines the foam's deformation and allowed penetration depending on the force exerted. Two options were initially considered during this project to model the seat and back cushions: an FE model with foam properties defined or a MB model with the foam's behaviour included in the respective contact characteristic. The R129 regulation specifies some of these properties, which are presented in Table 5.4. However, foam materials are not easily defined, as its elastic behaviour varies drastically depending on the level of penetration (Figure 5.9), hence being the foam characterisation process very complex, as three regions can be observed: linear elasticity, plastic deformation and densification.[70]

Table 5.4 - Foam cushion properties following R129. Source: United Nations, 2013

Group	*Value*	*Unit*
Density	68-74	Kg/m^3
Compression resistance	13	kPa
Indentation Load Deflection	500 (+/15%)	N
Tensile strength	≥150	kPa
Ultimate elongation	≥120	%
Compression set	≤3	%

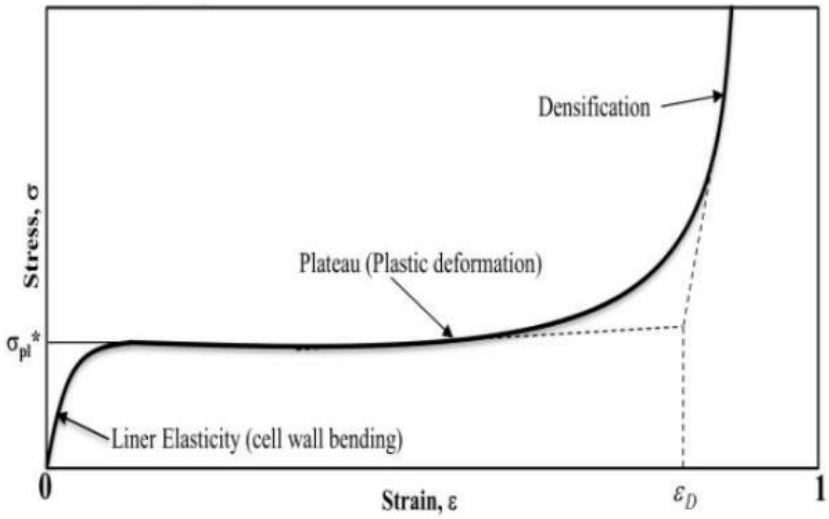

Figure 5.9 - Stress vs Strain curve of foam materials. Source: S. Haidar et al, 2018

At the beginning of the project, a simple MB ellipsoid was used as a surface to support the CRS and dummy, but no specific property was provided to it. Further in the project, it seemed beneficial to change the MB model to an FE model with foam characteristics. MADYMO offers the possibility to define an FE model as a foam using *material.foam* or *material.foam_fu_chang*. These commands allow to model an element's behaviour similar to that of a foam, with a similar characteristic of deformation and finite element displacement. The main difference between these two commands is that the Fu Chang foam models a velocity dependant behaviour, modifying the material's characteristic, whereas the other foam model has a simple and constant material's characteristic.

To model the foam's behaviour, it is necessary to perform an impact test in a real-life R129 test bench and record the impactor's displacement. This test is performed with a 2.75kg headform following certain instructions stated in Annex 13 of the R129 regulation [34], which was previously explained in Chapter 2.2. In this project, the resulting impactor displacement obtained from a foam impact test performed on a seat cushion was provided thanks to a personal communication with a researcher of the Universidad de Zaragoza, one institution that performs routinely crash tests with CRS. Once the desired displacement was known, a parametric test was performed in LS-DYNA recreating the impactor's penetration

in an FE modelled seat cushion with the objective of obtaining a similar displacement recorded in the LS-DYNA simulation. (Figure 5.10)

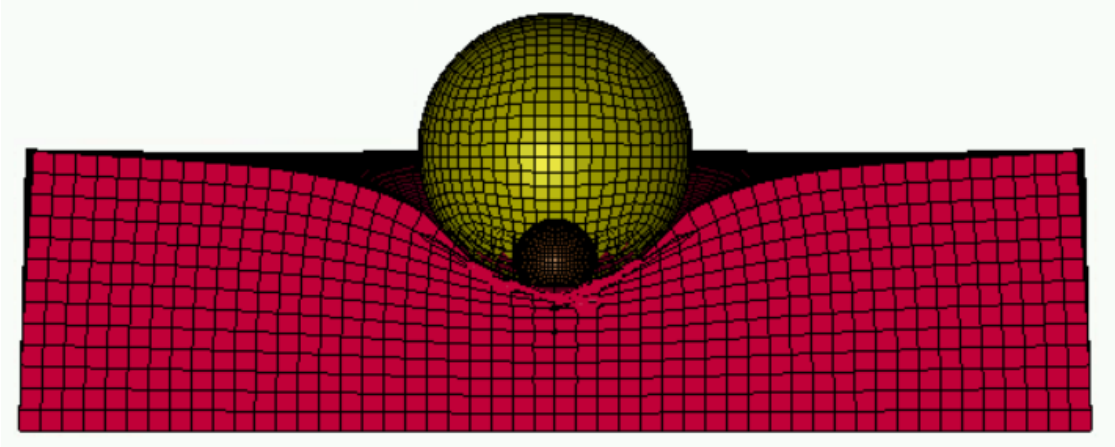

Figure 5.10 - Foam impact test in LS-DYNA before penetration

After multiple modifications on the foam's physical parameters (damping, curve scaling, compression resistance, etc…), the loading and unloading processes were finally modelled and a similar foam to that used in real-life test benches was obtained. In Figure 5.11, the data provided by the real-life foam impact test and the final displacement obtained in the LS-DYNA post processor with the computational foam model are compared. As it can be observed, the unloading did not perfectly match that measured in the experimental test, which leads to possible modifications on the unloading curves obtained.

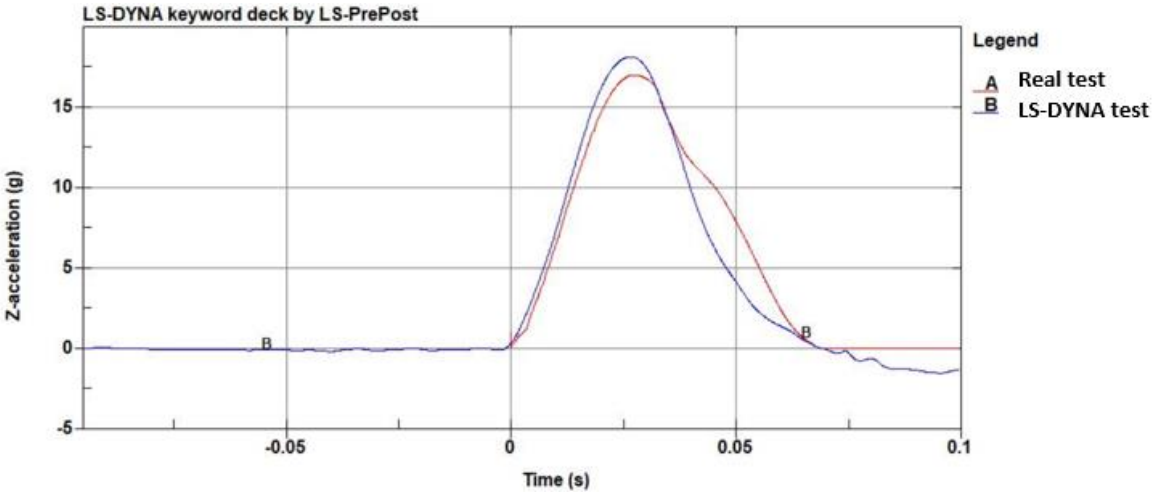

Figure 5.11 - Impactor's acceleration recorded during foam validation test. Red: real-life cushion impact test. Blue: LS-DYNA foam impact test

Once the foam modelling in LS-DYNA was finished, the foam characteristic was included in MADYMO as a velocity dependant foam material (*material.foam_fu_chang*). After several validation simulation tests, the Fu Chang foam material seemed to offer a more similar cushion model than the simple foam constant foam (*material.foam*). However, the model's complexity rose substantially, as well as the memory usage per simulation, which resulted in total simulation times of more than 24 hours. In addition, both foam material characteristics failed approximately 25% of the times due to infinite energy or hysteresis model failure. For these reasons, it was decided to model both seat and back cushions using the MB model previously mentioned. To do this, the material cannot be defined the same way as an FE model, as the foam characteristic is not available for MB models. With this in mind, a load and an unload function had to be declared to define the cushions' behaviour depending on penetration. Additionally, damping and friction may also be added to the model. All of this will be explained later in Chapter 5.1.3.2, where all information on the contact declared between CRS and seat cushion is explained and the contact characteristics are presented.

Once the seat and back cushions were added, simulation times diminished to 2 hours, instead of 26 hours with the FE cushion model. Unfortunately, FE foam model was obviously more precise, hence the CRS and dummy behaviour worsened after this modification. Nevertheless, changing some of the contact characteristics and cushion parameters, results obtained with the MB cushions improved considerably. Although contact modifications are explained in Chapter 5.1.3.2, two geometrical modifications were applied to the seat cushion: increase in thickness and length. The increase in thickness was performed due to high penetration of the CRS in the cushion, which led to almost reaching the plane of symmetry and MB in MADYMO modify their characteristics when reaching this region. The increase in length is induced by a large CRS excursion on the cushion, which leads to the CRS losing contact with the seat cushion due to the MB cushion not being deformable during the simulation. (Figure 5.12)

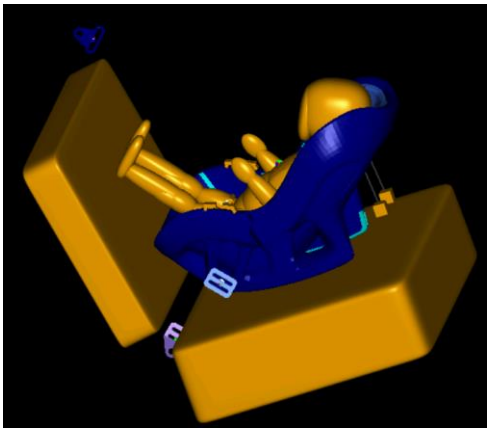

Figure 5.12 - Discarded test bench cushions model with thicker MB ellipsoid modelling seat cushion

However, after performing multiple tests with the MB surface ellipsoids as test bench cushions, it was decided to analyse the impact of swapping the seat cushion's ellipsoid for a surface plane, given all the problems the MB ellipsoid was giving. As a result, the CORA rating obtained in the validation model rose considerably (from 0.544 to 0.637), thus justifying a final modification on the seat cushion (Figure 5.13). The contact definition was not changed, as surface planes are considered MB elements, but the uniformity of the surface helped eliminate noise from all signals and obtain better results.

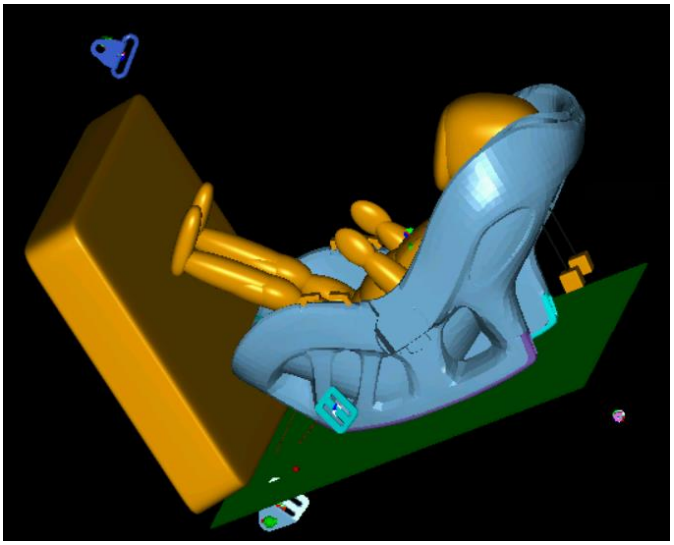

Figure 5.13 - MB back cushion and surface plane modelling seat cushion

5.1.2.5 Test Bench Buckles and Anchor points

The test bench buckles and anchor points system is comprised of all the elements which are connected through shoulder belt and lap belt and contribute to set the geometry of the seatbelt and facilitate an easier belt fitting. These elements are the following: D-ring, anchor and buckle. The positions of these points were obtained from a CAD model of the R44 test bench manipulated with SolidWorks. However, this model of the test bench did not match with that used in Karwala-Avionaut's frontal impact test, as the D-ring appeared on the wrong side of the bench in the R44 test bench and the buckle was not placed in the exact same position (Figure 5.14).

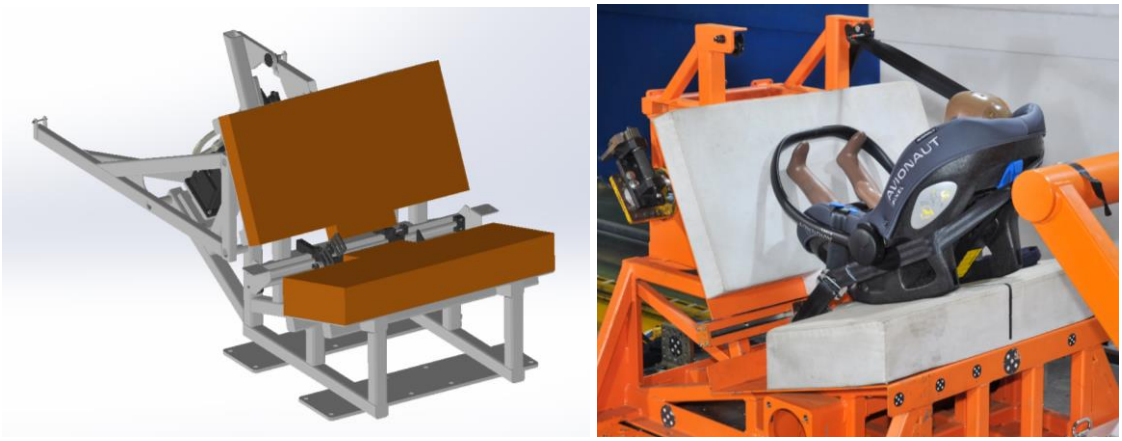

Figure 5.14 - CAD model of R44 test bench in SolidWorks vs Karwala-Avionaut test following R129

Only the D-ring and the buckle positions were slightly modified from those provided in the CAD model of the test bench. The D-ring was moved symmetrically to the other side of the test bench and its position was checked superimposing an overview picture of the real-life impact test and the MADYMO model. The buckle's position was modified using the same method as that used for the D-ring, although using a lateral view.

Lastly, once the buckles' positioning has been executed, some physical properties must be provided to MADYMO. These properties are the mass, inertia and centre of gravity and they will define the dynamical behaviour of each element. After assigning steel as the buckles' material, each buckle's properties were evaluated using SolidWorks and its *Mass Properties* function.

Once all inertial properties have been calculated, all four buckles can be included in the MADYMO model and their joints can be defined. D-ring, anchor and the buckle's anchor are assigned a *joint.revo* with only one rotational degree of freedom. On the other hand, the floating element, which corresponds to the buckle and the latch plate is defined with all degrees of freedom, being only restricted by a MB conventional belt segment linked to the buckle's anchor.

The resulting buckle configuration can be observed in Figure 5.15, where test bench cushions, shoulder belt and lap belt have also been displayed to obtain a better overview of

the test bench configuration. Nevertheless, the seat cushion has been displayed with the real-life dimensions, instead of the length and thickness dimensions augmented as previously explained in Chapter 5.1.2.4. Furthermore, the seat belt and shoulder belt modelling and inclusion in model are explained in the following section in Chapter 5.1.2.6

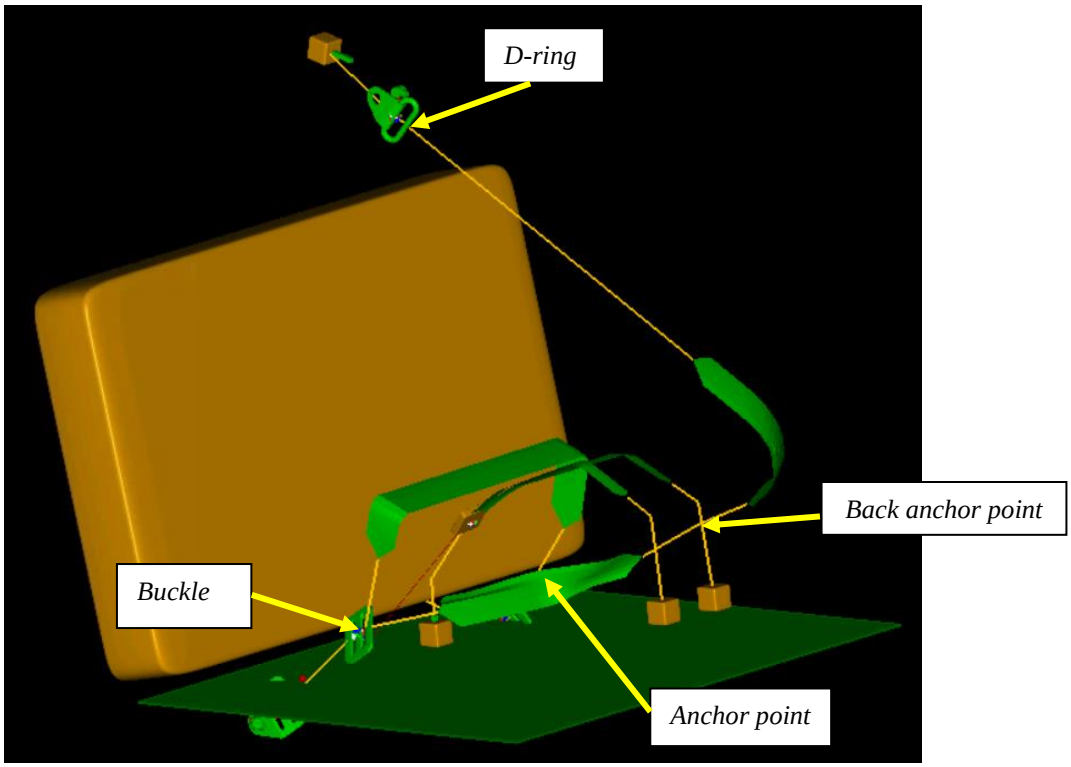

Figure 5.15 – Buckles positioning relative to lap belt and shoulder belt routing in MADYMO model

5.1.2.6 Test Bench Seat Belt

The test bench seat belt is used to attach the child restraint system (CRS) to the test bench cushions, both seat and back. In this case, the frontal impact crash test is performed using a rear-facing child restraint system, which implies the seat belt's installation in a specific manner. The shoulder belt must be routed behind the restraint system making contact with its back. In addition, Pixel AV304 is provided with an anchor point in the centre of the back across which the shoulder belt must be routed (Figure 5.16). On the other hand, the lap belt

must be routed over the dummy's legs contacting the CRS. In order to ensure the lap belt's correct attachment to the CRS during trips and specially during accidents, the Pixel AV304 model is provided with two subjections on both sides across which the lap belt must be routed. It is important to mention, as it was previously explained in Chapter 5.1.2.2, that both of these elements (back anchor point and lateral lap belt subjections) were not included in the original CAD file provided by Karwala and they had to be introduced to the model manually using MADYMO ellipsoids and point object definitions. Once the seat belt's routing path has been specified, it can be added to the MADYMO model. Note that the seatbelt attachement was done in the MADYMO model accordingly to the specifications provided by the manufacturer in the CRS installation manual.

Figure 5.16 - CRS back anchor point for shoulder belt (blue piece)

According to the R129 and R44 regulations, certain parameters and conditions must be fulfilled to ensure the validity of an impact crash test. In regard to seat belt installation, both regulations define parameters such as belt width, belt pre-tensioning or belt material characteristics. Using the real-life impact test and the parameters stated in R129 regulation, lap belt and shoulder belt were introduced in the MADYMO model with the Belt Fitting Wizard tool available in MADYMO.

The seat belts were created as hybrid belts with conventional MB element to which an FE model attached is attached. After specifying the geometrical parameters as shown in Figure

5.17a, it is necessary to assign a material characteristic for the FE part and a belt segment load characteristic to define the seat belt's stiffness. Followingly, after defining the beginning and the end point of the seat belt (buckle, D-ring, anchor or CRS back anchor point) and the surfaces and bodies with which the belt is to make contact, the seat belt can be fitted and even modified using the Belt Fitting Wizard tool.

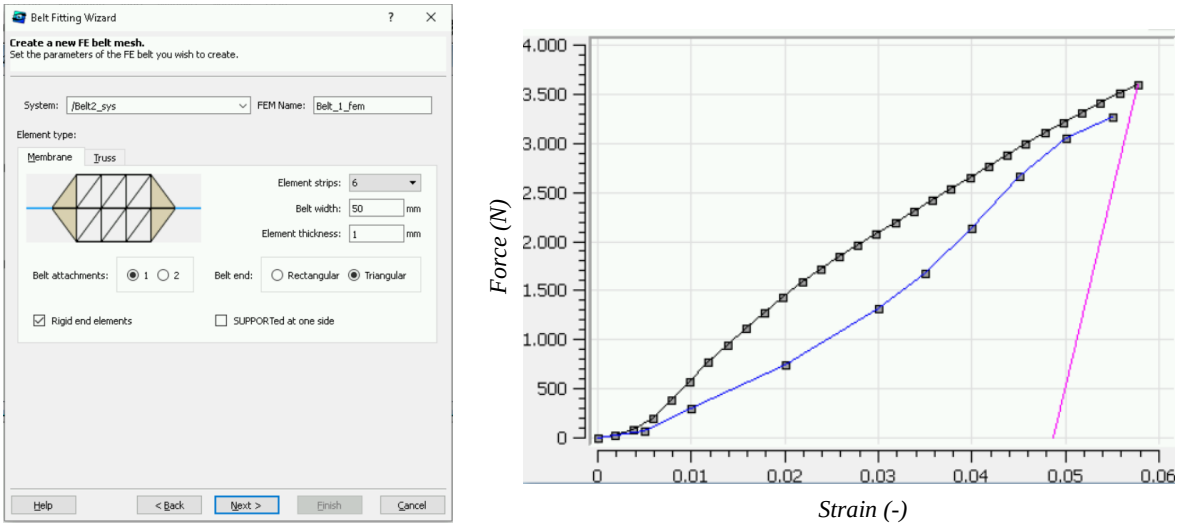

Figure 5.17 – a) Lap belt and shoulder belt geometrical configuration
b) Load characteristic of lap belt and shoulder belt (load and unload)

The material (FE) and load characteristics (MB) were obtained from a belt characterisation test. Both characteristics follow a hysteresis model with a load function and an unload function, as well as a hysteresis slope. The maximum values for load characteristic of 4000N at approximately 66.7mm extension were obtained from R. Menon et al [62], resulting in a 3200N force at 5% strain that can be observed in Figure 5.17b. The material characteristic was obtained by dividing the load characteristics by the area.

Once the seat belts had been defined, the only thing left in the seat belt model was to include a component which acted as a retractor. Due to the complexity of adding a retractor to the model and due to a constant belt pre-tension during the test, a simple spring attached to a small mass could serve as a retractor. For this reason, a 10 g mass was linked to the D-ring on top of the test bench, working as a retractor, and another identical mass was attached to

the anchor point. Both of these masses were linked to their respective adjacent bodies with a *restraint.kelvin* model which simulates a spring. The load characteristic defined for this Kelvin restriction was a horizontal line at 7N, so that a constant pre-tension is applied to the model.

The resulting lap belt and shoulder belt can be observed in Figure 5.18. It is important to mention that the shoulder belt was divided into two sections to model the behaviour of the joint point located in the back of the CRS. Otherwise, the Belt Fitting Wizard would not generate a seat belt routed across the surfaces and bodies in the desired way.

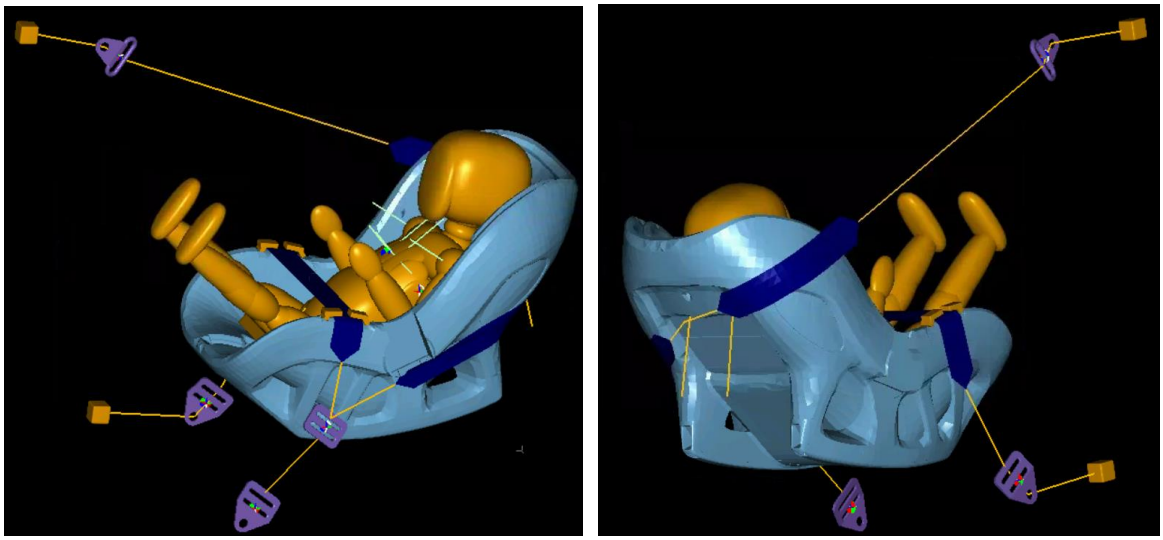

Figure 5.18 - Shoulder belt and lap belt routing invalidation model

5.1.2.7 Dummy Harness Belt

The dummy's seat belt is used in this impact test to attach the Q1.5 dummy to the CRS and ensure the dummy never loses contact with the restraint system. The harness is composed of an anchor and 3 segments which meet at the anchor, placed on top of the child's hip. With the objective of modelling the CRS's harness, another belt system model has to be defined in MADYMO with certain parameters which differ from those used to model the lap belt and shoulder belt previously mentioned. The harness installed in the Pixel AV304 can be

observed in Figure 5.2, where the belt anchor and the top segments can be differentiated, and all three segments meet again at the back of the CRS as it is shown in Figure 5.16. In addition, the rear-facing system possesses different holes for adjusting the harness routing to the optimal height depending on the child's size. In this case, the harness has been routed using the top hole, as the dummy being used corresponds to the biggest child allowed.

The harness routing in the model is performed using as reference points the top holes of the back of the CRS, the belt routing hole located beneath the child's pelvis and the pelvis anchor which serves as meeting point for the 3 belt segments making contact with the dummy's abdomen and pelvis. Furthermore, it is important to mention that the top harnesses are modelled using hybrid MB-FE belt segments and these are set to contact the abdomen, clavicles, ribcage and shoulder. On the other hand, the lower harness segment's small size allows to model it using only MB conventional segment, which reduces memory usage and simplifies the model, thus having only to specify begin and end point.

After a similar geometrical definition of the top segments to that previously performed for lap belt and shoulder belt (Figure 5.17), although using 4 element strips and an FE belt width of 20mm; it is necessary to declare a material characteristic and a load characteristic. These were obtained from those used for lap belt and shoulder belt modelling, although scaled proportionally to the belt width: 20/50.

Furthermore, a belt tension must be declared in the harness to ensure the dummy's attachment to the restraint system. With this goal in mind, once again a Kelvin restraint has been added joining a small mass and the MB belt segment, avoiding the use of a retractor. These springs have been defined at all three ends of the harness and have a constant load characteristic. According to the R129 regulation, in impact crash tests the harness is fitted using a tension of 250N and placing a surface between harness and dummy that is later removed. This is not possible to model in MADYMO, as this test cannot be performed as such. As the rationale of this procedure in the regulation is to eliminate any slack between the dummy and the seatbelt, it was decided to use a constant tension for the harness with

value 7N, which models the behaviour of a tense harness that only acts when the child experiences a displacement.

To sum up, the resulting harness obtained is comprised of two hybrid belt models, which are routed from the pelvis to two small masses over the dummy's shoulder on either sides, and a MB conventional belt segment, which is routed from the pelvis to a small mass located beneath the CRS. Belt segments and all three masses are linked using springs with a constant load, which avoids the dummy from losing contact with the CRS. All three segment meet at the dummy's pelvis, where a pelvis anchor has been introduced. The resulting harness is presented in Figure 5.19.

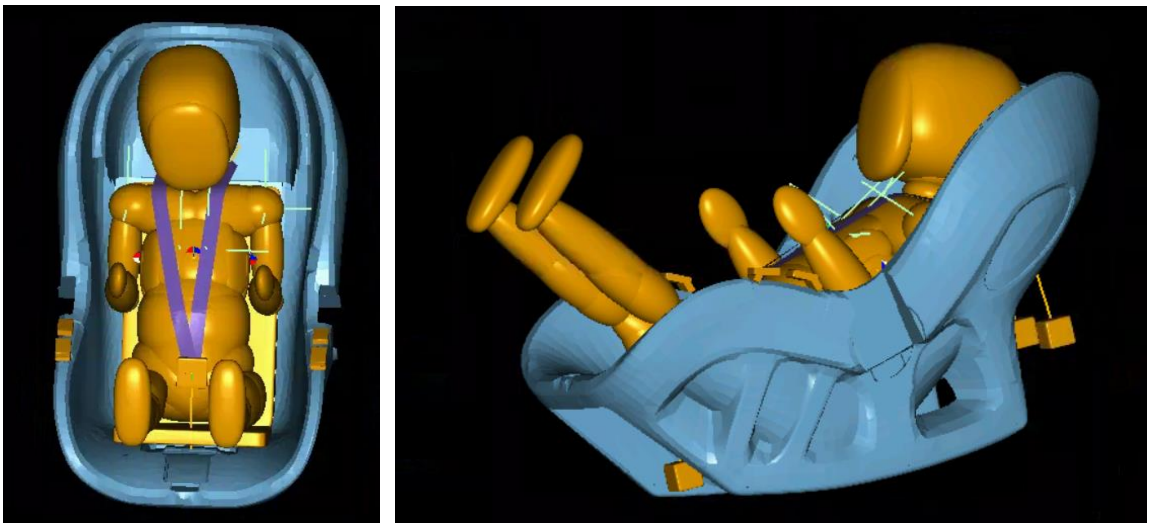

Figure 5.19 - Dummy harness modelled in MADYMO with Kelvin-restraint retractor

5.1.3 VALIDATION MODEL'S INTERACTIONS

One of the key elements when creating MADYMO files and executing simulations are the contacts declared between elements and the interactions these define. In this section, contacts declared and the characteristics under which these are defined in the validation model are explained. However, these interactions will be declared exactly the same way in the models with recline angle variation, so everything will apply in the same way for those models.

5.1.3.1 Dummy to CRS

One of the main contacts present in the MADYMO model is that declared between dummy and the Pixel AV304, which defines the behaviour of both surfaces when contacting. It is important to remember that 3 elements were added to the CRS to model the existing foam between CRS and dummy. These three elements were the modified headrest, obtained from scaling the nodes that make contact with the dummy's head; the added surface ellipsoid at the back of the CRS, to make contact with the dummy's back; and the added surface ellipsoid underneath the dummy's legs, to make contact with the pelvis and upper legs. For this reason and to extract useful information on the contact forces recorded during different tests, 9 different contacts were declared between dummy and CRS, which are briefly explained hereafter. Suffice it to say, in MB-FE contacts the MB surface is declared as master surface and the FE model as slave surface. In addition, it is important to point out that friction values, damping coefficients and curve scale values were obtained after a parametric test using MADYMO and comparing model's kinematics and CORA ratings.

- Arms to original CRS nodes: arms and shoulders can possibly make contact with any node of the CRS's FE model. For this reason, a single contact for arms and shoulders was declared with the whole FE model. This contact's characteristic is predefined by the dummy's characteristics and includes a friction coefficient of 0.7.
- Head to headrest nodes: the headrest's mission is to model the CRS's foam bringing the dummy forward and improving the head's lateral displacement and rotation. The contact characteristic is user-defined as the *HeadCnt_chr* and was defined from scaling by 4 the *BackCnt_chr*, which was obtained from an impact test performed on the dummmy's back. A friction coefficient of 0.4 was added to this contact to obtain a correct head's torque in the Y-axis and a damping coefficient of 200Ns/m was included.
- Head to CRS nodes: this contact is declared in exactly the same way as the previous, although with the original CRS's nodes (without head rest and pelvis foams). The addition of this contact aims to add an extra contact force in case of excessive head's

penetration in the headrest. The contact characteristic is also *HeadCnt_chr* and the friction coefficient's value is 0.4.

- Arms to foam modelling ellipsoids: this contact is declared in exactly the same way as the first, although with the pelvis ellipsoid foams. The contact characteristic is defined by the dummy and a friction coefficient of 0.7 was added.
- Back and pelvis to pelvis foam modelling ellipsoids: this contact is declared using the *BackCnt_chr* with a damping and friction coefficients of 10Ns/m and 0.7, respectively. The surfaces involved are the back and pelvis of the dummy and the two surface ellipsoids added to the CRS to model its foam.
- Legs and abdomen to pelvis foam modelling ellipsoids: this contact is declared using the *BackCnt_chr* with a damping and friction coefficients of 10Ns/m and 0.7, respectively. The surfaces involved are the legs and abdomen of the dummy and the two surface ellipsoids added to the CRS to model its foam.
- Lumbar spine to pelvis foam modelling ellipsoids: this contact is declared using the *BackCnt_chr* with a damping and friction coefficients of 10Ns/m and 0.7, respectively. The surfaces involved are the dummy's lumbar spine and the two surface ellipsoids added to the CRS to model its foam.
- Neck to pelvis foam modelling ellipsoids: this contact is declared using the *BackCnt_chr* with a damping and friction coefficients of 10Ns/m and 0.7, respectively. The surfaces involved are the dummy's neck and the two surface ellipsoids added to the CRS to model its foam.
- Ribcage to pelvis foam modelling ellipsoids: this contact is declared using the *BackCnt_chr* with a damping and friction coefficients of 10Ns/m and 0.7, respectively. The surfaces involved are the dummy's ribcage and the two surface ellipsoids added to the CRS to model its foam.

The *BackCnt_chr* characteristic was added due to excessively high contact forces recorded in the dummy's back and lumbar spine. Due to the dummy's contact characteristic being

encrypted, an impact test as that shown in Figure 5.20 was performed to obtain the contact characteristics.

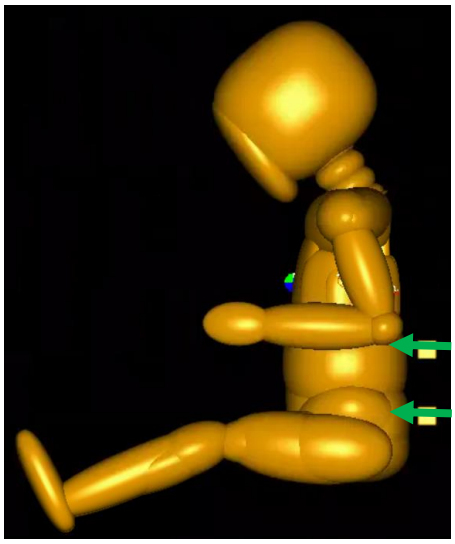

Figure 5.20 - Back impact test to obtain dummy's contact characteristics

After the impact test being performed, the resulting pelvis and back contact forces displayed in Figure 5.21 were obtained and the *BackCnt_chr* was defined using the first slope of both curves, as they match. As a result, instead of having a contact characteristic divided into different intervals, the same stiffness was defined for any penetration: 100N at 0.01 strain. The *HeadCnt_chr* was obtained from scaling the *BackCnt_chr*, which led to an improvement of the model, improving CORA ratings from 0.54 to 0.64. This contact was declared as four times stiffer than the original *BackCnt_chr*, which resulted in 400N at 0.01 strain.

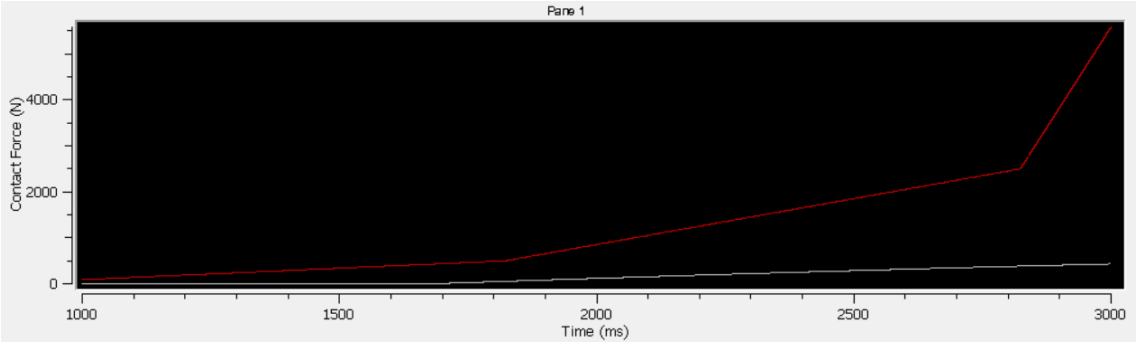

Figure 5.21 - Pelvis (red) and back (white) contact forces obtained from back impact test on Q1.5 dummy

5.1.3.2 CRS to Seat Cushion

Several calculations showed that the interaction experienced between CRS and seat cushion is the most important in the entire model, as it is the contact force that determines all the kinematics and dynamics of the CRS and dummy. It is for this reason that a correct definition of the foam's behaviour and the contact characteristic is crucial to obtain a valid model. As it has already been mentioned in Chapter 5.1.2.4, an initial FE model of the seat cushion with Fu Chang foam material was dismissed due to 26-hour-long simulations. The FE model was replaced by a MB surface ellipsoid, reducing memory usage considerably and simulation times to 2 hours approximately. However, it was discovered that with a MB surface ellipsoid, output signals were full of noise and steep peaks were observed (Figure 5.22), which justified dummy accelerations and forces with undesired peaks.

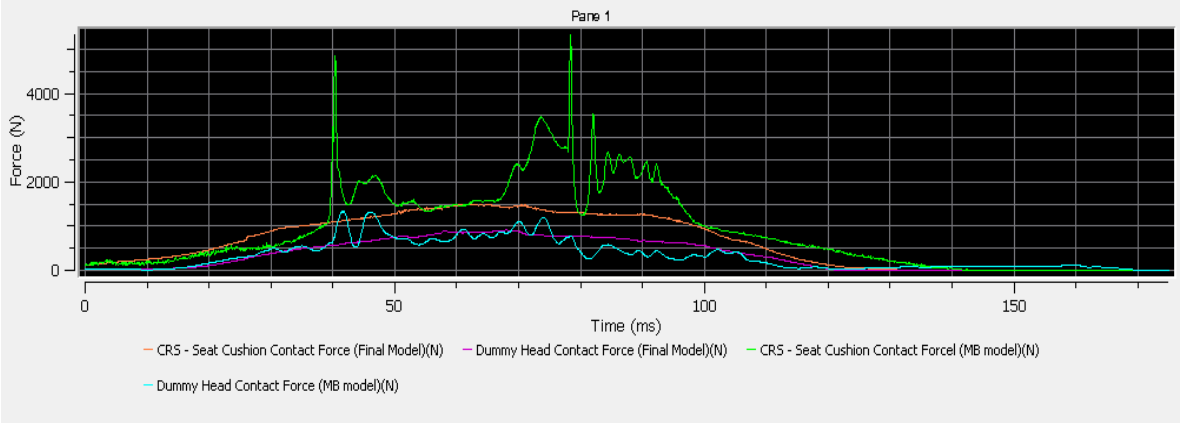

Figure 5.22 – Contact forces registered with MB seat model and Final model

After augmenting the ellipsoid's dimension to reduce these negative aspects, it was decided to model the cushion as a surface plane, as the results obtained were not sufficiently clean despite using a 60Hz low-pass filter to analyse results. The surface plane allowed to obtain a considerably better CORA rating (from 0.54 to 0.64) as a result of the reduction of peaks observed in contact forces registered in the interaction between CRS and seat cushion (Figure 5.22). However, it is important to explain the process followed in the declaration of this contact.

As it has already been explained, the first step was the foam characterisation performed in LS-DYNA using the Fu Chang foam material and comparing simulation results to impactor test results following the R129 regulation (Figure 5.10 and Figure 5.11). To improve the cushion's behaviour and with the intention of obtaining cleaner signals, the same impact test was performed with the characterised foam substituting the spherical impactor with the CRS's supports (the parts of the CRS that make direct contact with the test bench seat cushion) (Figure 5.23). The force vs penetration curve obtained from this experiment was then introduced as the contact characteristic in MADYMO. This would contribute to model more correctly the contact characteristic, as contact between both surfaces was declared only to the sled's nodes, instead of to all CRS's nodes.

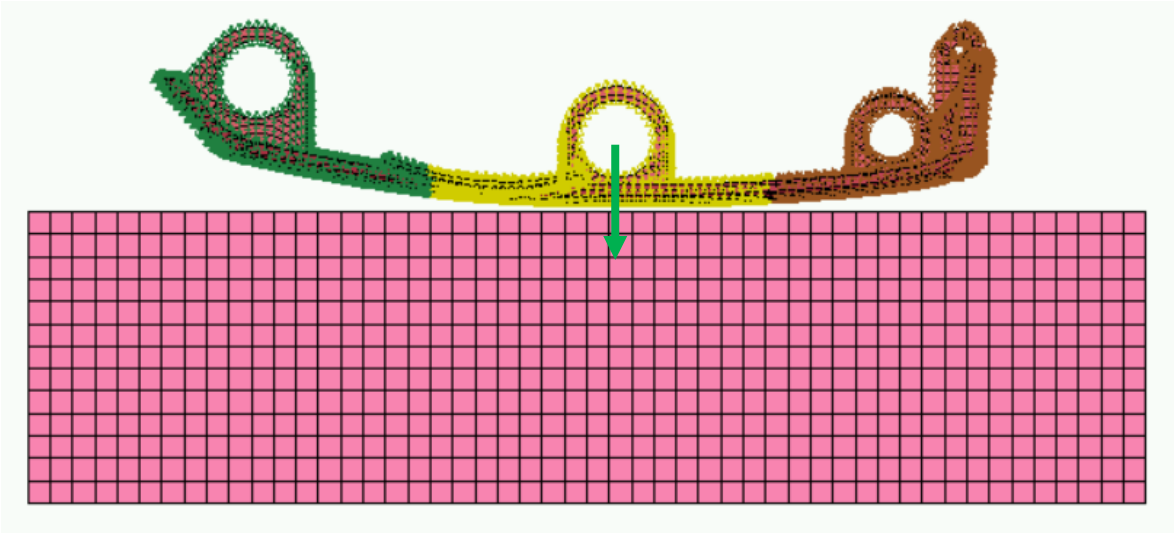

Figure 5.23 - Foam impact test performed with CRS sled

Furthermore, as it can be observed in Figure 5.23, both sleds can be divided into three sections with different orientations. For this reason, the test was repeated and the contact characteristics obtained for the front and back sections were similar to that recorded for the middle part although scaled by 0.5 (Figure 5.24). Considering this information, it was decided to separate the contact between CRS and seat cushion into 6 different contacts, differentiating between left and right sled and between front, back or middle sections.

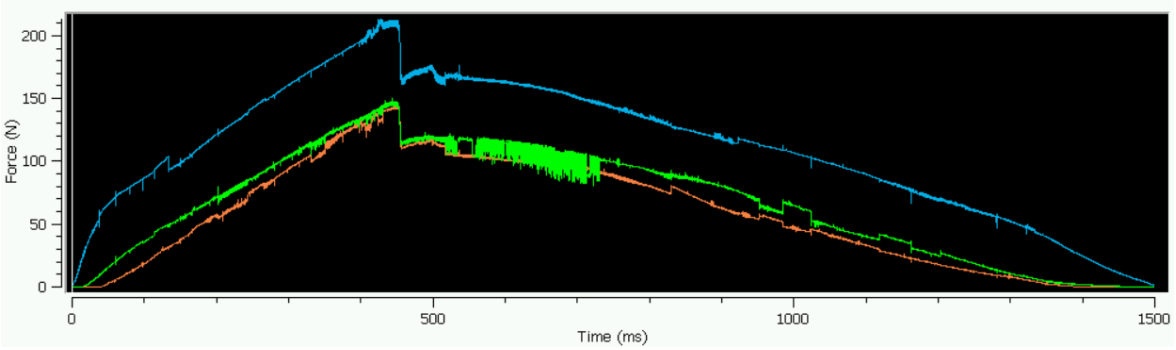

Figure 5.24 - Contact force in sled impact test. Blue: middle section. Green: back section. Blue: front section

In addition, the central part of the Pixel AV304 located beneath the system also penetrates through the cushion, but, due to a bad interaction with the FE model, contact with this region had been eliminated. For this reason, a contact with the central lower part of the CRS was added with a contact characteristic obtained from scaling by 2 the *Foam_chr*, given the greater area of contact and a surface parallel to the cushion.

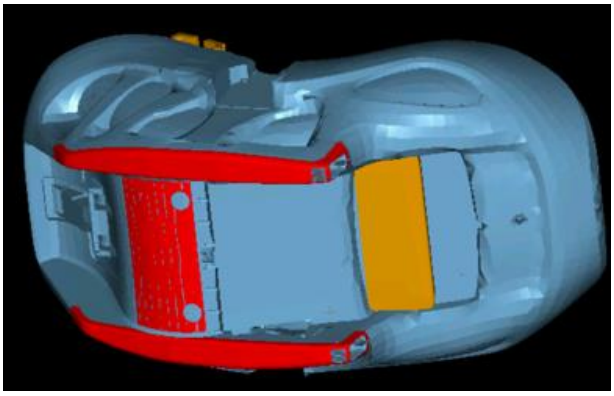

Figure 5.25 - Elements for contact declared with seat cushion

Lastly, although the contact had initially been declared with the components' nodes, a better behaviour was identified when the contact was defined with surface elements. For this reason, all 7 contacts defined between CRS and seat cushion were performed using the CRS's (Figure 5.25). This way, contact force is dependent on surface penetration rather than using node penetration, which can reduce noise levels in the output signals.

To sum up, contact between CRS and set cushion was divided into 7 different contact, distinguishing between the middle section, right sled (front, middle and back) and left sled (front middle and back). The contact characteristic used of type force was obtained from an impact test performed with the CRS's sled and the damping coefficient used was 150Ns/m and the friction coefficient's value was 0.7.

5.1.3.3 CRS to Back Cushion

The CRS to back cushion contact must be declared, as the CRS and test bench back cushion meet when shoulder belt and lap belt are tightened. However, this contact is secondary, as it only exists at the beginning of the deceleration pulse. After the first 10ms, both objects cease making contact with one another and this contact becomes irrelevant for the rest of the simulation.

The contact characteristic used is the *Foam_chr*, which was previously included in the CRS to seat cushion contact, hence its principles have already been explained. The MB-FE contact is declared with a force characteristic following the *Foam_chr* and a friction coefficient of 0.7.

In case of deciding to model the back cushion as a plane instead of as a surface ellipsoid, the same way it was done with the seat cushions, it is not required to change the contact characteristic, as the behaviour does not change. The only difference between these two models would be the noise obtained in the output signals.

5.1.3.4 Dummy to Back Cushion

The simplicity of this contact radicates in the small time these surfaces make contact. In addition, only one contacthas to be defined to model this behaviour. As both are MB elements, a force characteristic is used with a friction coefficient of 0.3. The force characteristic used is that previously between CRS and seat cushion (*Foam_chr*). As the only part of the dummy that will be making contact with the back cushion are both legs, these are the only elements added as master surfaces and the back cushion as the slave surface.

However, this contact does not have a noticeable effect on the results registered, so its relevance is not very high.

5.1.3.5 Seat Belt to CRS

As previously explained, due to the Pixel AV304 being a rear-facing CRS, the test bench's shoulder belt is routed behind the CRS's back and the lap belt is routed over the child's legs and the CRS horizontal half. As a result of the CRS's configuration, the shoulder belt had to be divided into two different segments with the back anchor point as the connector. On the other hand, the lap belt must be routed over the dummy's legs and abdomen and is guided with two MB subjections located at either side of the CRS, which ensure that contact between lap belt and system is not lost at any time.

The contact established between the belt subjections is declared as an MB-FE contact with a kinematic force characteristic, which resulted as better seat belt behaviour, [71] and a friction coefficient of 0.3, which allows the lap belt to slide through the subjections with a slight restriction opposed to the movement.

On the other hand, the contact characteristic declared between shoulder and lap belt with the Pixel AV304 are exactly the same, as no difference in the system's surface has been considered. The contact has to be defined as an FE-FE as both belt and CRS are FE models. The contact method chosen was *surface_to_surface* with an adaptative force. The contact was provided a friction coefficient of 0.3 and a low damping coefficient of 0.05Ns/m. The Initial_Type-Check was activated to avoid any initial penetrations and the gap was defined at 2.5mm. The belt's characteristic load has been previously explained in Chapter 5.1.2.6, so it will not be explained again in this section.

5.1.3.6 Harness Belt to Dummy

The harness belt is comprised of a MB segment, attaching the MB harness buckle to the lower part of the CRS, and two hybrid belt models located at either sides of the dummy, routed from shoulder to abdomen, where the harness buckle is located. There are two

contacts declared between harness and dummy: dummy to harness buckle (MB_MB) and dummy to belt (MB_FE).

The dummy to harness buckle contact is declared between buckle and dummy's pelvis and the contact characteristic predefined for Q1.5's pelvis contacts is applied. The contact type is declared as force contact characteristic with a friction coefficient of 0.3. This contact declaration does not have a big impact on the model, thus becoming a secondary contact.

On the other hand, the harness belt to dummy contact is much more relevant, as it will affect the chest deflection and the thoracic accelerations registered. The load characteristic was previously defined in Chapter 5.1.2.7 and it had been obtained from scaling the 50mm wide shoulder belt's characteristic to the new belt width value of 20mm. Once the belt's load characteristic and material behaviour have been defined, as well as the constant retractor tension of 7N, the contact established between dummy and harness can be defined. It was decided to declare a force-based contact with a friction coefficient of 0.2, which ensures a correct belt positioning once the simulation has begun. In addition, the harness belt segments are usually found covered in a foam material which reduces friction.

Lastly, a contact between lap belt and dummy was declared in case the dummy's abdomen made contact with the lap belt at some point in the simulation, which was noticed when simulations with a smaller recline angle from vertical were executed. The contact definition was copied from that created between harness and dumm.

5.2 *RECLINE ANGLE VARIATION*

Once the validation process has been completely explained and all the elements' properties have been defined, the final angle variation and simulation process has to be performed.

In this section, the original model will be presented and summarised. After that, the methodology followed in the horizontal and vertical models will be explained, describing in detail the steps followed to obtain a model with a recline angle and to prepare the MADYMO

simulation file to obtain the final results, as well as the method followed to analyse the outcoming signals and to evaluate the CRS's security with the corresponding injury criteria.

To ensure the comparability between simulations with different recline angles of the back of the Pixel AV304, these tests were performed with dummy aligned with the X axis (suppressing the 1º initial rotation considered in the validation process) and with the dummy's back parallel to the back of the CRS. Furthermore, using the dummy's H-point as the dummy's coordinate system's origin, its coordinates must meet in all simulations performed to grant comparability between simulations.

On the other hand, all simulations were subjected to the same deceleration pulse obtained from Pixel AV304 frontal impact test performed by Karwala-Avionaut. Simulations began at t=-400ms and the deceleration pulse was applied at t=0, stopping the data gathering at t=175ms, just like it had been previously performed in the validation simulations (Table 5.2). This was done to ensure that the modified CRS would comply with the requirements of the regulation.

Lastly, the only differences between the original model and the recline angle-varied models are the recline angle of the CRS, the dummy's back recline angle and the belt's routing, as a belt refitting must be performed prior to each simulation. However, the seat belt routing was performed using the same elements as reference to apply the belts' forces in the same area and elements.

5.2.1 ORIGINAL MODEL

The original model coincides with that with the existing recline angle of the back of the Pixel AV304, which is currently commercialised and corresponds to a recline angle of 44º from vertical (Figure 5.26). Once the final validation model was obtained after analysing both the model's kinematics and the CORA ratings and outputs, the original CAD model is subjected

to the same impact test although with the Q1.5 dummy positioned symmetrically. This grants comparability between results obtained with different recline angles.

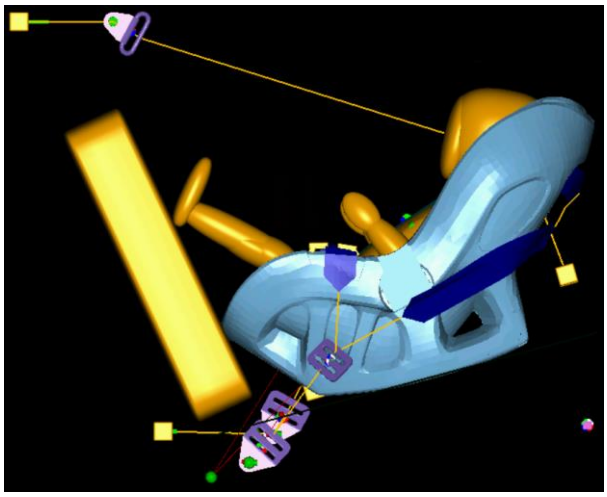

Figure 5.26 - Lateral view of MADYMO model of original Pixel AV304

The MADYMO simulation file is comprised of the same 9 *system.models* created for the validation process: reference space, Q1.5 dummy, Pixel AV304 child restraint system without recline angle modification, dummy's harness's buckles, dummy's harness, test bench cushions, buckles and lap and shoulder belts. The characteristics defined for each component have been previously explained in Chapter 5, as well as the contact characteristics used to model the interaction between elements. To perform the original model's simulation using the validation model as reference, it is only necessary to position the dummy symmetrically about the X-axis, as it had been positioned with a 1º rotation about the Z-axis, and to perform a refit of lap belt, shoulder belt and dummy's harness (Figure 5.27).

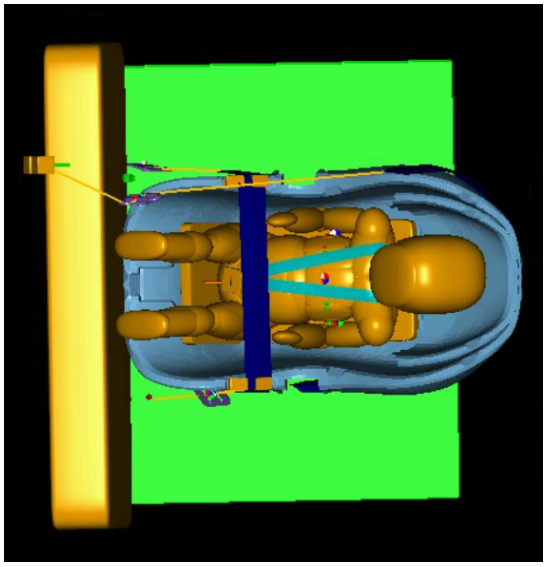

Figure 5.27 - Top view of MADYMO model of original Pixel AV304

After the original model simulation has been completed (Figure 5.28) and biomechanical signals have been measured (head acceleration, neck axial force, neck torque, thoracic acceleration, etc…), two different analyses were conducted to assess the suitability of the Pixel AV304's original recline angle. These analyses were based on studying different injury criteria and on evaluating the dummy's movement and kinematics.

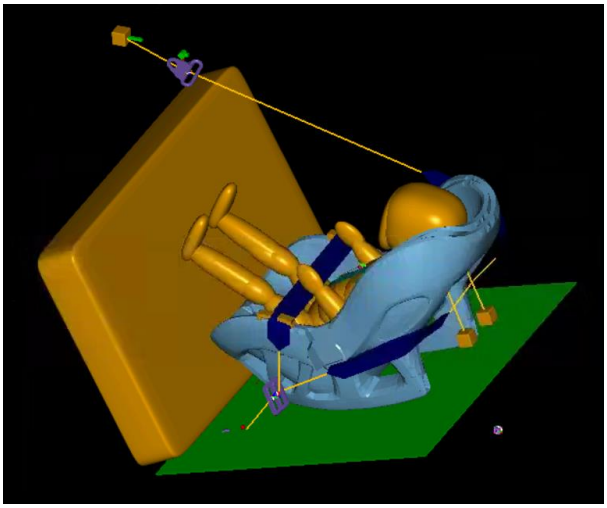

Figure 5.28 - MADYMO model of original Pixel AV304

5.2.2 HORIZONTAL MODELS

The main goal of this project is to obtain the optimal recline angle of the back of the Pixel AV304 rear-facing child restraint system to maximise the infant's security. As it has already been explained, once the MADYMO model validation has been finished, it is time to replace the original CRS's model by an alternative model with different recline angles. To that end both more horizontal and more vertical CRS were created in MADYMO. This section focuses on the angles that were greater than the original one of the studied CRS (more horizontal seatback of the CRS than the original one).

The current recline angle installed in the Pixel AV304 is 44º from vertical and the biggest recline angle tested was 54º (+10º from original), resulting in a more horizontal dummy position. The MADYMO model created with the alternative CRS models was exactly the same as that used in the initial test with the original model, except that the CRS was changed and that the dummy's back was re-positioned parallel to the CRS's back. In addition, for the horizontal models, lap belt and shoulder belt were not subjected to gravity during simulations to avoid an incorrect routing of the shoulder belt before belt tightening at t=-200ms. However, it is important to explain the process followed to obtain a recline angle-varied model starting from a CAD file of the original Pixel AV304 model using LS-PrePost.

Starting from the meshed CAD model of the Pixel AV304 which Karwala-Avionaut provided, the best option considered to generate alternative models with different recline angles was modifying the model's mesh using LS-PrePost. Firstly, it was necessary to rotate the nodes correspondent to the back of the CRS. As it is shown in Figure 5.29, the nodes selected were subjected to a rotation of the corresponding degrees in the negative direction (*Rotate* -). The origin of rotation selected for all models was the node 35332 and is marked with a green circle in Fig. However, the rotation was not applied at once to all selected nodes, as some complex shapes located near the CRS's sleds would prevent the shoulder belt from gently slipping over the system's surface. For this reason, for recline angle variations over 5º were performed in two steps, deselecting the nodes lower nodes.

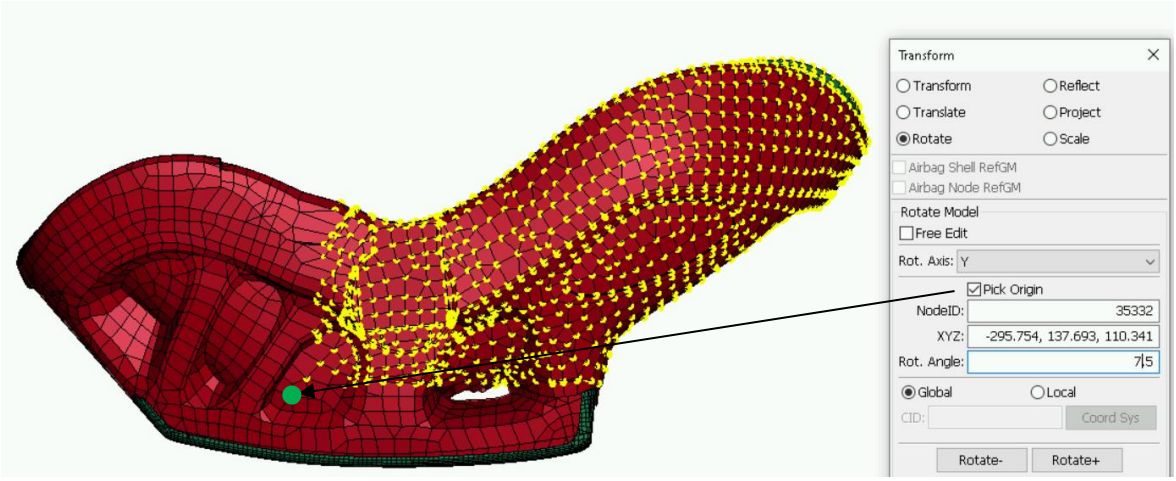

Figure 5.29 - Node rotation in LS-PrePost on 7.5º horizontal model

After all desired nodes have been rotated the corresponding angle, it is compulsory to recalculate the model's physical properties, which may have a considerable impact on the impact test simulations performed. Using LS-PrePost's *Measure* tool, it is possible to calculate the model's mass, centre of gravity and moments of inertia. These values were later introduced in the *Body.Rigid* field of the corresponding model in MADYMO. However, to be able to calculate all necessary physical properties, a material must be assigned to each component with the corresponding density. In this case, all components were divided into two groups, which would help obtain a valid model: high-density parts and unknown parts. The high-density parts are shown in Figure 5.30a and correspond to all components located in the interior of the CRS, which are made of high density polyethylene. The density used for high density polyethylene was 940kg/m^3, according to GRANTA EduPack.[72] On the other hand, the unknown parts correspond to the CRS's main body, the back's support and the elements manually added to smooth out surfaces (Figure 5.30b). The density assigned to these elements was obtained after an iterative process which finished when the model's mass matched with that measured experimentally: 2.448kg. Density values varied between alternative models, but the mean value of density used was 1976kg/m^3. It is beneficial to remember that the CAD model is not provided with the foam observable between dummy

and CRS, which justifies the iterative process of density calculation. Furthermore, the headrest modelled scaling part of the CRS's main body was not included to calculate physical properties as it was a simple surface with an element thickness of 1mm, which would not bring any relevant information.

Figure 5.30 – a) High-density components of CAD model of Pixel AV304
b) Unknown-density components of CAD model of Pixel AV304 without headrest

This process was repeated for all the alternative models with negative recline angle variations. It was decided to analyse the effect of recline angle change, resulting the most horizontal model in a 10º variation starting from the original model. A total of 4 alternative models were evaluated with an increment of 2.5º between models (2.5º, 5º, 7.5º and 10º) and the physical properties calculated for each model are presented in Table 5.5. All this information was included in the MADYMO file after changing the table of nodes and coordinates. Furthermore, it was necessary to recalculate the coordinates of the back anchor point, which links both segments of the shoulder belt. This point was located 2cm away from a reference point, which helped make the separation of the back anchor point match to that measured experimentally. Lastly, the belt subjections included at either side of the CRS had not to be moved, as the elements to which they were attached were not modified during the node rotation process.

Table 5.5 - Horizontal model alternatives and physical properties

Horizontal recline angle variation		*Unit*	*Original*	*2.5º*	*5º*	*7.5º*	*10º*
Density for unknown parts		kg/m^3	1860	1976	2160	1843	1927
Mass		kg	2.443	2.448	2.445	2.448	2.448
Centre of gravity	*x*	m	-0.404	-0.406	-0.413	-0.416	-0.415
	y	m	0	0	0	0	0
	z	m	0.202	0.187	0.188	0.179	0.169
Inertia	*Ixx*	kg·m^2	0.053165	0.04917	0.04842	0.04591	0.04503
	Iyy	kg·m^2	0.084642	0.08118	0.08256	0.08369	0.08278
	Izz	kg·m^2	0.098558	0.09459	0.99304	0.04268	0.10084
	Ixy	kg·m^2	0.000003	-0.000008	-0.000015	-0.000014	-0.000008
	Iyz	kg·m^2	0.000001	-0.000014	-0.000008	-0.000007	-0.000015
	Ixz	kg·m^2	0.018027	0.015244	0.013776	0.013485	0.009877

In addition to the model's pre-processing, some further modifications were necessary to complete the alternative model in MADYMO. After changing the CRS's mass, inertia, centre of gravity, as well as the back anchor's coordinates, the ellipsoid created to model the CRS's foam at the back of the CRS had to be rotated the exact same degrees as the CRS's back. Consequently, the dummy's back was positioned parallel to the ellipsoid, although avoiding any initial contact and the dummy's H-point was not moved to grant comparability between simulations thanks to being subjected to similar initial conditions.

Secondly, lap belt, shoulder belt and dummy's harness were to be refitted with the same properties as in the original model's simulation file. Nevertheless, before refitting the dummy's harness, the harness's buckle had to be repositioned in case of initial penetration through the dummy's abdomen and pelvis, as well as the harness's end points.

Lastly, the shoulder belt tightening was set at t=-200ms, leaving 200ms for the dummy to comfortably sit on the CRS. In this period of time, the belt would change its position and acquire an incorrect position when being tightened. For this reason, it was decided not only to deactivate the effect of gravity to lap belt and shoulder belt, but also to apply an acceleration field of 4m/s^2 upwards, which ensured a correct shoulder belt's routing after being tightened at t=-200ms. The resulting MADYMO model for the alternative Pixel AV304 model with 54º of recline angle from vertical is shown in Figure 5.31.

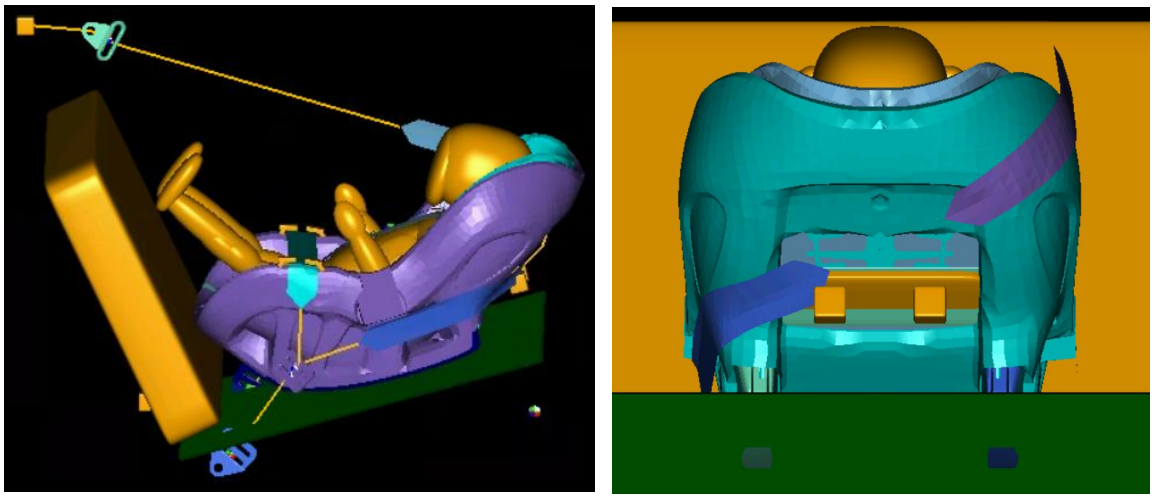

Figure 5.31 - Resulting MADYMO file of +10º recline angle alternative model

Once the MADYMO simulation files were executed, results for each recline angle had to be analysed and put to evaluation. In this project, two different assessments were performed for each simulation: kinematics' analysis and injury criteria application. The first aspect corresponds with a more subjective evaluation of events and dummy movement during the simulation, which may be useful to identify excessive dummy excursions or unwanted dummy rotations. On the other hand, the injury criteria that will be applied are those related to head acceleration, thorax acceleration and neck forces and torques. These values can be easily obtained using three output files generated by MADYMO with the following file extensions: *.lac*, *.peak* and *.injury*.

5.2.3 VERTICAL MODELS

The more reclined alternative models have already been explained and now vertical alternative models must be explained too. The current recline angle installed in the Pixel AV304 is 44º from vertical and the lowest recline angle tested was 34º (-10º from original), resulting in an erect vertical dummy position. The MADYMO model created with the alternative CRS models was exactly the same as that used in the initial test with the original model, except that the CRS was changed and that the dummy's back was re-positioned parallel to the CRS's back. In addition, in this case, it was not necessary to eliminate the gravtiy's effect on lap belt and shoulder belt, as the incorrect belt routing problem only appeared for horizontally reclined models. Furthermore, the process followed to obtain these models was practically identical to that followed for the alternative models previously explained in Chapter 5.2.2, but some operations were performed differently.

Starting from the meshed CAD model of the Pixel AV304 which Karwala-Avionaut provided, the best option considered to generate alternative models with different recline angles was modifying the model's mesh using LS-PrePost. Firstly, it was necessary to rotate the nodes correspondent to the back of the CRS in the same way that it was performed for the more reclined models, as it is shown in Figure 5.32. However, in this case the nodes selected were subjected to a rotation of the corresponding degrees in the positive direction (*Rotate +*). The origin of rotation selected for all models was the node 35332 and is marked with a green circle in Figure 5.32. In addition, the problem of excessive edges on the lower surfaces of the CRS did not occur for the vertical alternative models, as this area's elements were stretched instead of compressed. This allowed to perform all necessary rotations in one step, contrarily to the node-deselection method that had to be performed for the horizontal alternative models.

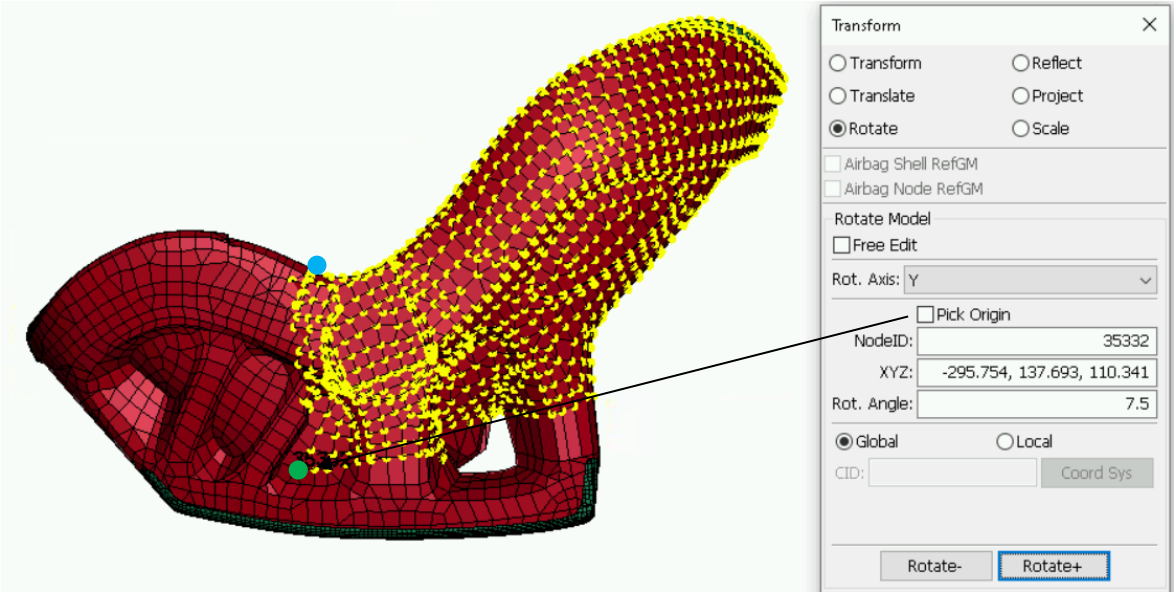

Figure 5.32 - Node rotation in LS-PrePost on 7.5º vertical model

After all desired nodes have been rotated the corresponding angle, it is compulsory to recalculate the model's physical properties, which may have a considerable impact on the impact test simulations performed. The physical calculation procedure to follow was exactly the same as that used for the horizontal alternative models. The high-density parts are shown in Figure 5.33a and correspond to all components located in the interior of the CRS, which are made of high density polyethylene. The density used for high density polyethylene was 940kg/m^3, according to GRANTA EduPack.[72] On the other hand, the unknown parts correspond to the CRS's main body and the back's support (Figure 5.33b). The density assigned to these elements was obtained after an iterative process which finished when the model's mass matched with that measured experimentally: 2.448kg. Density values varied between alternative models, but the mean value of density used was 1936kg/m^3. It is beneficial to remember that the CAD model is not provided with the foam observable between dummy and CRS, which justifies the iterative process of density calculation. Furthermore, the headrest modelled scaling part of the CRS's main body was not included to calculate physical properties as it was a simple surface with an element thickness of 1mm, which would not bring any useful information.

Figure 5.33 – a) High-density components of CAD model of Pixel AV304
b) Unknown-density components of CAD model of Pixel AV304 without headrest

In addition, the compression experienced by the elements located at the top of the lateral area led to unwanted edges where the lap belt is routed (blue circle in Figure 5.32), which could have led to incorrect belt positioning after tightening. For this reason, it was necessary to create additional elements to smooth down surfaces and grant a correct lap belt and CRS interaction, as it can be observed in Figure 5.33b with the golden elements created in the mentioned section.

This process was repeated for all the alternative models with negative recline angle variations. It was decided to analyse the effect of recline angle change, resulting the most vertical model in a 10º variation starting from the original model. A total of 4 alternative models were evaluated with an increment of 2.5º between models (2.5º, 5º, 7.5º and 10º) and the physical properties calculated for each model are presented in Table 5.6. All this information was included in the MADYMO file after changing the table of nodes and coordinates. Furthermore, it was necessary to recalculate the coordinates of the back anchor point, which links both segments of the shoulder belt. This point was located 2cm away from a reference point, which helped make the separation of the back anchor point match to that measured experimentally. Lastly, the belt subjections included at either side of the CRS had not to be moved, as the elements to which they were attached were not modified during the node rotation process.

Table 5.6 - Vertical model alternatives and physical properties

Vertical recline angle variation		*Unit*	*Original*	*2.5º*	*5º*	*7.5º*	*10º*
Density for unknown parts		kg/m^3	1860	1955	1940	1930	1920
Mass		kg	2.443	2.447	2.447	2.442	2.448
Centre of gravity	*x*	m	-0.404	-0.401	-0.398	-0.395	-0.389
	y	m	0	0	0	0	0
	z	m	0.202	0.195	0.201	0.204	0.209
Inertia	*Ixx*	kg·m^2	0.053165	0.052603	0.054297	0.056178	0.058276
	Iyy	kg·m^2	0.084642	0.080008	0.079101	0.078391	0.076913
	Izz	kg·m^2	0.098558	0.089681	0.086821	0.084096	0.080811
	Ixy	kg·m^2	0.000003	-0.000011	-0.000021	-0.000005	-0.000016
	Iyz	kg·m^2	0.000001	-0.000015	-0.000024	-0.000012	-0.000015
	Ixz	kg·m^2	0.018027	0.017401	0.018162	0.018787	0.018845

In addition to the model's pre-processing, some further modifications were necessary to complete the alternative model in MADYMO. After changing the CRS's mass, inertia, centre of gravity, as well as the back anchor's coordinates, the ellipsoid created to model the CRS's foam at the back of the CRS had to be rotated the exact same degrees as the CRS's back. Consequently, the dummy's back was positioned parallel to the ellipsoid, although avoiding any initial contact and the dummy's H-point was not moved to grant comparability between simulations thanks to being subjected to similar initial conditions.

Lastly, lap belt, shoulder belt and dummy's harness were to be refitted with the same properties as in the original model's simulation file. Nevertheless, before refitting the dummy's harness, its buckle and end points had to be repositioned to avoid initial penetration through the dummy's abdomen. The resulting MADYMO model for the alternative Pixel AV304 model with 54º of recline angle from vertical is shown in Figure 5.34.

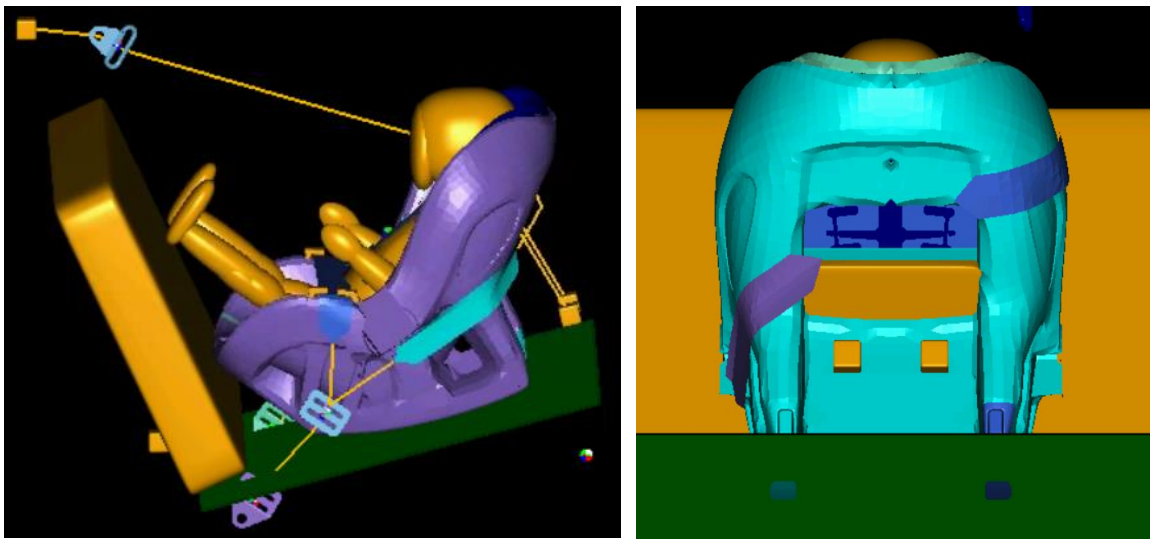

Figure 5.34 - Resulting MADYMO file of -10º recline angle alternative model

Once the MADYMO simulation files were executed, results for each recline angle had to be analysed and put to evaluation. In this project, two different assessments were performed for each simulation: kinematics' analysis and injury criteria application. The first aspect corresponds with a more subjective evaluation of events and dummy movement during the simulation, which may be useful to identify excessive dummy excursions or unwanted dummy rotations. On the other hand, the injury criteria applied are those related to head acceleration, thorax acceleration and neck forces and torques. These values can be easily obtained using three output files generated by MADYMO with the following file extensions: *.lac*, *.peak* and *.injury*. The *.lac* file can be manipulated using MADPost, MADYMO's post-processing tool, and displays the linear acceleration's time-history of head, thorax and pelvis registered during the simulation. The *.peak* file calculates and provides the peak values of some variables such as forces and acceleration, including the display of the HIC15 and HIC36 values (Head Injury Criterion), as well as the calculation of the 3MS injury criteria previously presented in Table 2.4. Lastly, the *.injury* file can also be manipulated using MADPost and displays the time-history of different forces experienced by the dummy, which in this dummy's case were lumbar and cervical forces and torques.

5.2.4 RESULT COMPARISON

Once the validation model has been completed and the alternative models have been simulated, the last step left to do in this project is the comparison of variables measured for each of the recline angles of the back of the Pixel AV304 analysed. As it has been previously explained two different comparisons can be performed to analyse the convenience of a certain recline angle over others: a kinematic analysis and a physical analysis. The kinematic analysis corresponds to a more subjective visual evaluation of the impact simulation test. It helps visualise the displacements experienced by each element, as well as certain rotations experienced by the dummy which may be unwanted. However, after the execution of this visual analysis, conclusions cannot be drawn as objective data on loads and acceleration is necessary. Taking this into consideration, after analysing each model's kinematics, the physical evaluation must be performed.

The physical analysis evaluates the time-history of physical variables measured in the dummy, which are used to identify the level of security each configuration offers. To perform this analysis, the variables that have been chosen as representative and relevant are head acceleration, thorax acceleration, pelvis acceleration, neck axial force, lower neck torque, lumbar axial force and lumbar torque. Some of these values used correspond to injury criteria stated by the R129 regulation or recommended by previous studies. These variables are Head 3MS, Thorax 3MS, Head Injury Criterion (HIC), neck axial force (Fz) and neck torque (My). As it had already been presented in Table 2.4, MAYDMO automatically calculates these values so that the analysis of results can be done quicker. However, the N_{ij} criterion had to be added manually as the Q1.5 dummy did not have it included automatically. The most critical N_{ij} parameters that were studied were the N_{TE}, which corresponds to the tension-extension region in the normalized SNPRM (Supplemental Notice for Proposed Rulemaking) neck injury criteria diagram (Figure 5.35), and the N_{CE}, which corresponds to the compression-extension region. As the neck was almost permanently experiencing an extension torque (<0 in Y axis), the only region in which the neck's tensional state is found is on the left side of the neck injury criteria diagram.

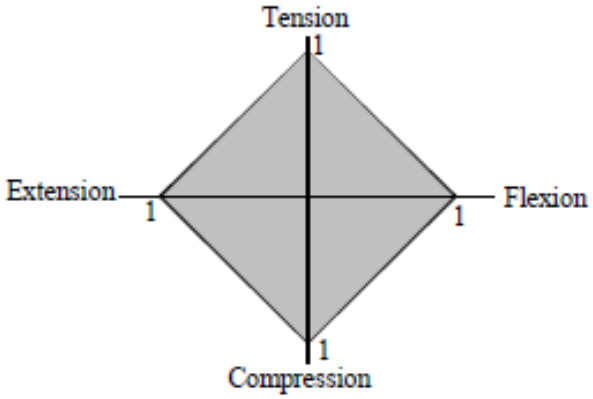

Figure 5.35 - Normalized SNPRM neck injury criteria for all dummy sizes. Source: R. Eppinger et al, 1999

It is beneficial to state that, during the validation process performed with the original model of the Pixel AV304, the signals that were taken into consideration for the final CORA rating were head acceleration (X axis and Z axis), neck torque (Y axis) and thorax acceleration (X and Z axis). Furthermore, the final model that was considered valid was that with the highest CORA rating for the neck axial force registered by the baby, thus enabling the use of information on neck axial force to evaluate injury risk. However, the lower area of the dummy corresponding to legs and lumbar area was not validated in any way, given the absence of reference signals registered by Karwala-Avionaut during the real-life frontal impact test. For this reason, lumbar forces and lumbar torque may be used to analyse the convenience of each recline angle; although information gathered in this area is not validated and, consequently, it should not be used as crucial evidence for reaching conclusions.

The thresholds for the Q1.5 dummy model selected for the injury criteria analysis were obtained from the R129 regulation and are presented in Table 5.7. This regulation originally states that neck axial force and neck torque are used for monitoring purposes only. However, injury criteria are permanently under review and the development of the N_{ij} injury criteria demands the addition of a threshold for neck axial force and for neck torque. In this case, the thresholds for these two variables were obtained from a study carried out by R. Eppinger et al with the CRABI 12-month-old dummy. [73] It has been decided to use the CRABI's thresholds for the Q1.5 injury criteria due to the absence of limits for this dummy's neck

injury criteria. According to C. P. Sherwood and J. R. Crandall [67], neck injury thresholds for both dummies are very similar and, consequently, given the absence of reference values to perform the study, the set of thresholds used for the neck injury criteria (N_{ij} and peak tension/compression) have been obtained from the CRABI 12-month-old.

Table 5.7 - Injury criteria and thresholds used during project

Criterion	*Abbreviation*	*Unit*	*Threshold for Q1.5*
Head Injury Criterion	HIC (or HPC)	-	600
Head acceleration 3 ms	A head 3 ms	g	75
Chest acceleration 3 ms	A chest 3 ms	g	55
Upper neck peak tension	Tz	N	780*
Upper neck peak compression	Cz	N	960*
Tension Intercept (N_{ij})	T - N_{ij}	N	1460*
Compression Intercept (N_{ij})	C - N_{ij}	N	1460*
Flexion Intercept (N_{ij})	E - N_{ij}	Nm	43*
Extension Intercept (N_{ij})	F - N_{ij}	Nm	17*

**These values correspond to thresholds for CRABI 12-month-old dummy and have been selected unmodified for the Q1.5 dummy.*

Lastly, the kinematic analysis was performed to obtain a subjective overview of the dummy's behaviour during the frontal impact test simulation. Conclusions cannot be drawn from this information due to its subjectivity and the absence of a clear knowledge of the optimal behaviour that should be visually observed. Nonetheless, this analysis was performed as it did not call for a tedious process and it could also be useful in case of an uncommon performance of the model due to the incorrect definition of an element.

Chapter 6. ANALYSIS OF RESULTS

In this section, the corresponding relevant results obtained in the project will be presented and analysed. The results to be analysed can be divided into two different sections. The first one is the final validation model's CORA rating evaluation and output signals analysis, as well as the CRS's and dummy's kinematics analysis. On the other hand, the second section compares all the different injury criteria calculations and output signals considered between the original model and the alternative models designed with different recline angles.

6.1 FINAL VALIDATION MODEL CORA RATING

As it has previously been explained multiple times, the main method used throughout the validation model evaluation was the CORA rating. The CORA rating allows to obtain an objective metric that may be useful to evaluate the resemblance between different time-history curves. In this case, it was used to compare the output signals obtained in MADYMO with the validation model and the real-life frontal impact test performed by Karwala-Avionaut with the original Pixel AV304 model. The CORA rating was constantly used to understand what effect certain modifications performed to the model had on the level of similarity of the MADYMO model to the real-life test. However, it is important to mention that the CORA rating sometimes could lead to an incorrect evaluation of the convenience of a modification, as sometimes high scores may be obtained by chance due to the methods used by CORA to measure correlation between curves. All these methods have already been explained in Chapter 2.3.

The validation model was built exclusively to increase the reliability of results and conclusions obtained in this study. The more valid the model is, the more possible it is for results obtained to be reflected in real-life impact tests. For this reason, both tests had to be exact replicas geometrically and physically. As it has already been stated and portrayed in

Figure 5.2, the Q1.5 dummy was not symmetrically positioned in the CRS during Karwala-Avionaut's real-life frontal impact test, which led to possible incongruity in variables measured transversally. For this reason, out of all the output signals provided by Karwala-Avionaut (Table 5.1), only head acceleration (X and Z axis), thorax acceleration (X and Z axis), neck axial force and neck torque (Y axis) were considered. However, the transversal movement and forces experienced by all components in the simulation were taken into consideration by performing a subjective general analysis on the simulations' kinematics, which would help to rule certain modifications out throughout de validation process. Furthermore, the validation process was performed for a frontal impact test, in which the most relevant variables are those considered, which boosts the assumption's validity.

Unfortunately, out of the 6 output signals that were initially considered to be relevant to the validation process with a total CORA rating of 0.167 for each variable, it was discovered that neck axial force emulation would be a very difficult task, due to the insignificant values registered, as well as the complexity of the function with noise and multiple peaks and valleys. The maximum values registered in the axial force in the real-life impact test were +65N of tension and -60N of compression, which corresponds to an 8% of the injury criteria threshold used for the Q1.5 dummy with 780N for peak tension and a 6% with 960N for peak compression.[67] It is for this reason that it was decided to eliminate neck axial force from the CORA rating, thus resulting in each output signal with a CORA rating weight of 0.2 each, as it had already been presented in Table 5.1. However, when performing the evaluation of neck axial forces with alternative models with different recline angles, this force's values must be checked, in case values come anywhere near the criteria's threshold.

Once the validation model was almost finished and on the verge of completion, the general appearance and behaviour of both CRS and dummy was very similar to that observed in the videos provided by Karwala-Avionaut, with similar head displacement, CRS excursion and CRS penetration through seat cushion. As the final step to obtain the definite validation model, a parametric test was performed varying 4 different coefficients (Table 6.1). This provided 54 different simulations with their respective results and parameter combinations.

Table 6.1 - Final parametric test performed on validation model

Coefficient	*Meaning*	*Initial Value*	*Final Value*	*Increment*	*Steps*
Cnt_coef	Scaling factor for CRS to seat contact	1.3	1.4	0.1	1
HeadFric_coef	Friction coefficient between dummy's head and headrest	0.4	0.6	0.1	2
HeadCnt_coef	Scaling factor of dummy's head and headrest contact	4	6	1	2
HeadDamp_coef	Friction coefficient between dummy's head and headrest	100	200	50	2

Out of all 54 simulations obtained after the parametric test performed, three simulations stood out as the best options with 3 different criteria. The first simulation was that with the highest CORA rating obtained without considering neck axial force: 0.765. The second simulation was that with a considerably high CORA rating of 0.713 and with the highest level of correlation obtained for the neck axial force: 0.345. On the other hand, although obtaining a final CORA rating (only 5 signals) of 0.691, the third simulation resulted in the highest CORA rating considering all signals with the same weight: 0.611. These three simulations and the parameters they were obtained with are presented in Table 6.2, where the CORA rating obtained from only the five relevant signals is referred to as "Final CORA rating". These five signals considered are head acceleration in X and Z axis, thorax acceleration in X and Z axis and neck torque in Y axis. The remaining signals were used to calculate the "Global CORA rating" and were previously presented in Table 5.1.

Table 6.2 - Final validation model candidates with parameters and CORA ratings

Property	*Highest CORA rating (5 relevant signals)*	***Highest neck axial force rating***	*Highest global CORA rating (all signals)*
Identifier	ID1	**ID2**	ID3
Cnt_coef	1.3	1.3	1.4
HeadFric_coef	0.5	0.4	0.5
HeadCnt_coef	5	4	5
HeadDamp_coef	100	200	200
Neck axial force CORA rating	0.198	**0.345**	0.275
Gobal CORA rating	0.594	0.594	**0.611**
Final CORA rating	**0.765**	0.713	0.691

The first simulation to be discarded out of the final three candidates was that identified with ID3. Although accomplishing the highest general CORA rating out of all simulations performed throughout the project, this model aims to resemble to a frontal impact test. These tests are characterised by a considerable difference between the relevance of longitudinal variables and that of transversal variables. For this reason, it was decided to discard this simulation due to unsuccessfully modelling the neck axial force and the variables which are considered relevant for the project's purpose.

Furthermore, ID1 and ID2 surprisingly obtained exactly the same general CORA rating: 0.594. As it has already been mentioned, the best general CORA rating obtained throughout the project was 0.611, which is only 0.017 away form those obtained with simulation models ID1 and ID2. However, the differences in final CORA ratings obtained in ID1 and ID2 compared to ID3 are far more notable: 0.087 and 0.035, which denotes a significant improvement in relevant variables' similarity and strengthens this assertion.

On the other hand, a different criterion had to be applied in order to decide which simulation was more appropriate to use as the final validation model: ID1 or ID2. For this purpose, it is beneficial to mention that, although neck axial force had been ruled out of the final CORA rating calculation, its importance is far from irrelevant and the validation model should at least obtain similar values and shapes of cervical loads to those registered during the real-life test. As it can be observed in Figure 6.1, the dummy's neck axial forces registered using ID1 are permanently with negative values suffering up to a 200N compression, which indeed does not match the range values of Karwala-Avionaut's impact test's dummy. On the contrary, the dummy's neck axial forces registered using ID2 are far more precise and similar to those obtained experimentally. This includes tension and compression transitions, as well as more similar maximum values of compression, -120N versus -60N, and of tension, 80N versus 65N. Furthermore, during the analysis of recline angle variation, it is also necessary to at least ensure that the neck injury threshold is not surpassed and, for this to be possible, a low level of discrepancy between MADYMO and a real-life impact test must be achieved.

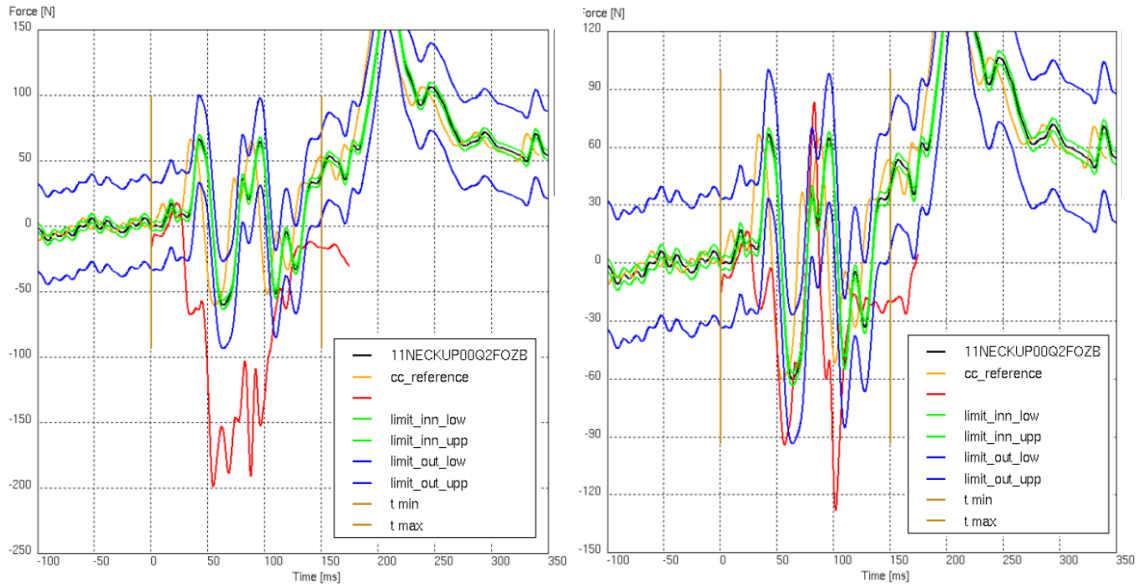

Figure 6.1 - a) Neck axial force CORA comparison for ID1 validation model (r=0.198)
b) Neck axial force CORA comparison for ID2 validation model (r=0.345)

To sum up, the final validation model that was selected after this thorough process is that described in Chapter 5, where all parameters that were considered important or relevant have been explained and carefully described. Although having obtained a final CORA rating of 0.765 in an alternative validation model, the chosen validation model corresponded to a final CORA rating of 0.713, which can be reviewed as a fairly good score [36], especially considering the complexity of this project's model. The CORA ratings for each of the output signals available and their respective weights for the final CORA rating are presented in Table 6.3.

Table 6.3 - CORA ratings for dummy's output signals and weights of final validation MADYMO model

Variable	*Axis*	*Cora Signal Identifier*	*CORA rating weight*	*CORA rating*
Head Acceleration	X	**11HEAD0000Q2ACXA**	0.2	0.790
	Y	11HEAD0000Q2ACYA	0	0.611
	Z	**11HEAD0000Q2ACZA**	0.2	0.587
Neck Force	X	11NECKUP00Q2FOZB	0	0.345
Neck Torque	X	11NECKUP00Q2MOXB	0	0.631
	Y	**11NECKUP00Q2MOYB**	0.2	0.602
	Z	11NECKUP00Q2MOZB	0	0.567
Thorax Acceleration	X	**11THSP0000Q2ACXA**	0.2	0.768
	Y	11THSP0000Q2ACYA	0	0.410
	Z	**11THSP0000Q2ACZA**	0.2	0.817
Chest Displacement	X	11CHST0000Q2DSXB	0	0.406

Followingly, each signal's time-history is presented using CORA's format, as each curve is displayed along with its objective curve, the resulting corridor curves and the maximum correlation phase shift function (Figure 6.2).

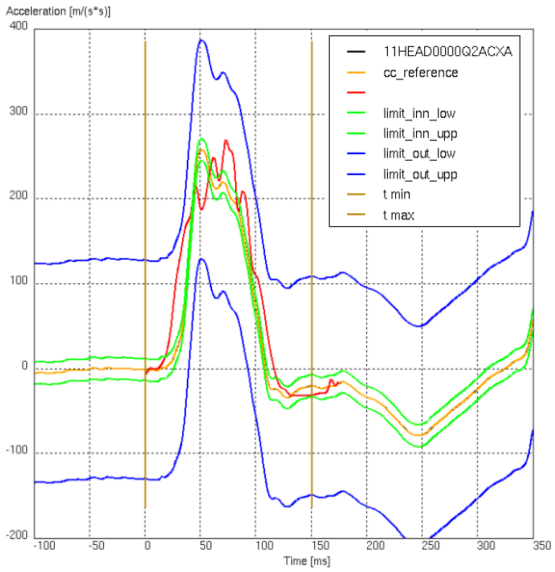
Acceleration [m/(s*s)]
11HEAD0000Q2ACXA
cc_reference
limit_inn_low
limit_inn_upp
limit_out_low
limit_out_upp
t min
t max
Time [ms]

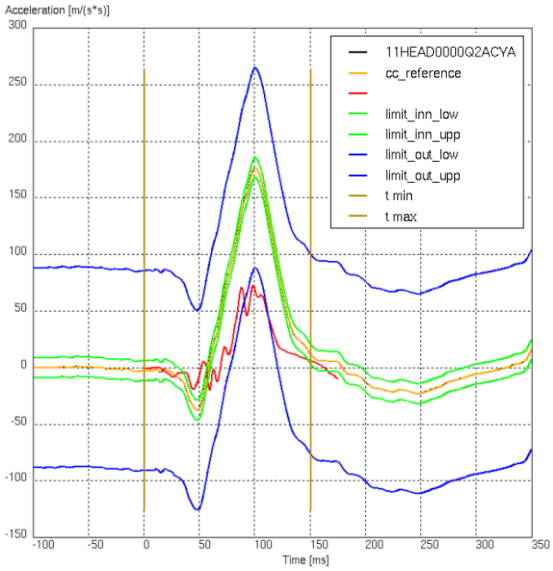
Acceleration [m/(s*s)]
11HEAD0000Q2ACYA
cc_reference
limit_inn_low
limit_inn_upp
limit_out_low
limit_out_upp
t min
t max
Time [ms]

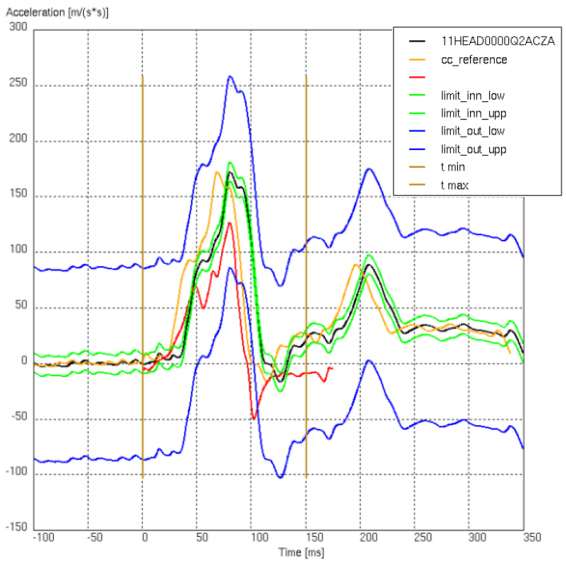
Acceleration [m/(s*s)]
11HEAD0000Q2ACZA
cc_reference
limit_inn_low
limit_inn_upp
limit_out_low
limit_out_upp
t min
t max
Time [ms]

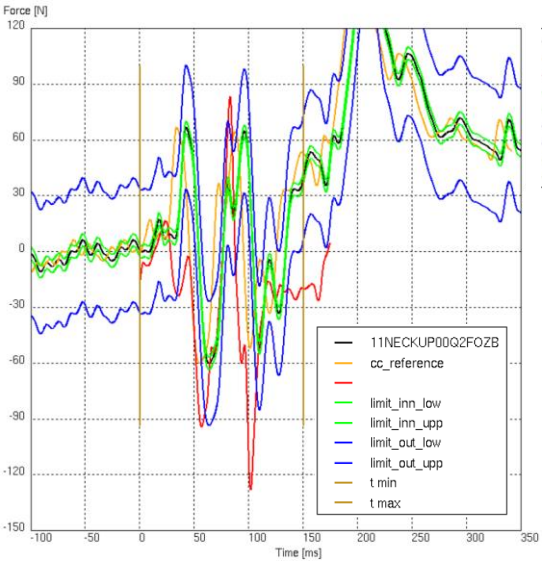
Force [N]
11NECKUP00Q2FOZB
cc_reference
limit_inn_low
limit_inn_upp
limit_out_low
limit_out_upp
t min
t max
Time [ms]

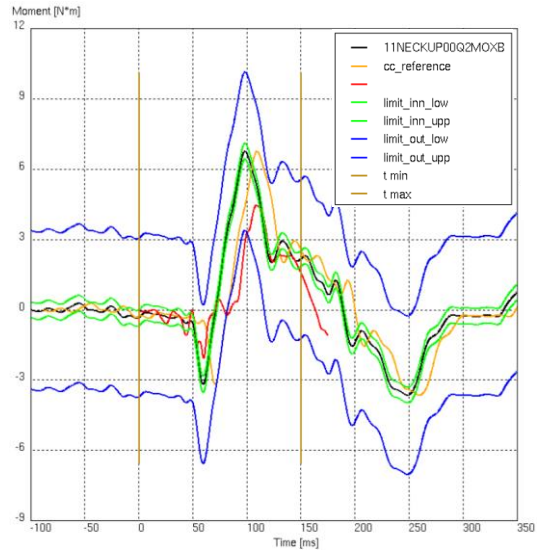
Moment [N*m]
11NECKUP00Q2MOXB
cc_reference
limit_inn_low
limit_inn_upp
limit_out_low
limit_out_upp
t min
t max
Time [ms]

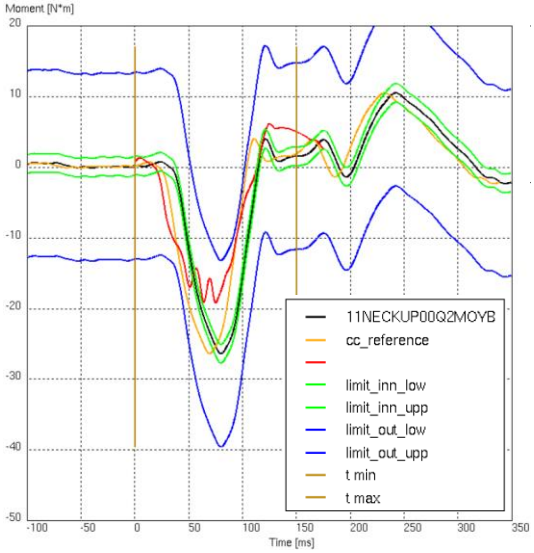
Moment [N*m]
11NECKUP00Q2MOYB
cc_reference
limit_inn_low
limit_inn_upp
limit_out_low
limit_out_upp
t min
t max
Time [ms]

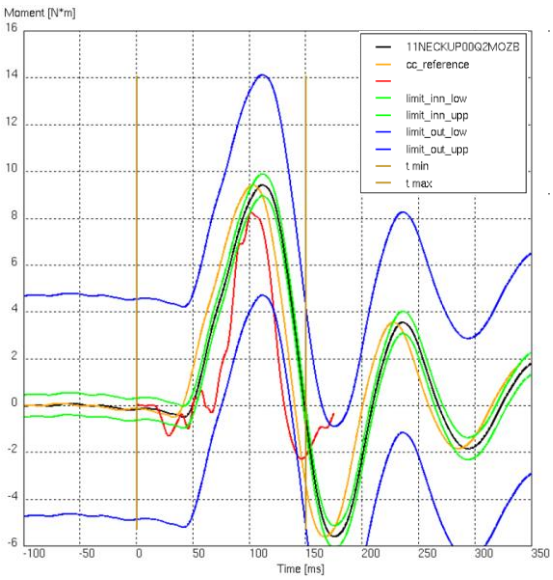
Moment [N*m]
11NECKUP00Q2MOZB
cc_reference
limit_inn_low
limit_inn_upp
limit_out_low
limit_out_upp
t min
t max
Time [ms]

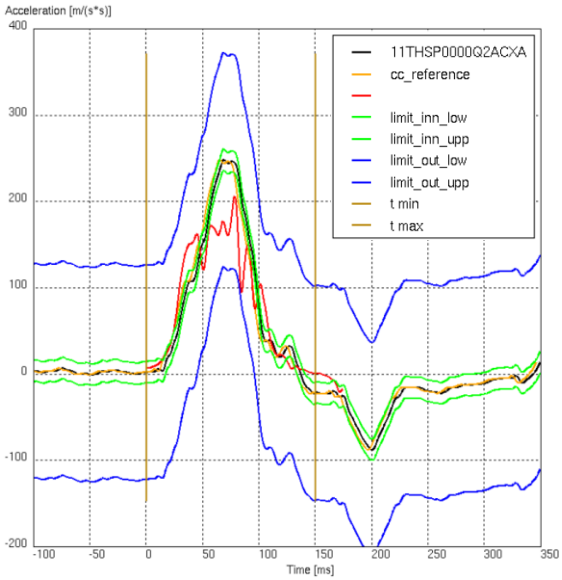
Acceleration [m/(s*s)]
11THSP0000Q2ACXA
cc_reference
limit_inn_low
limit_inn_upp
limit_out_low
limit_out_upp
t min
t max
Time [ms]

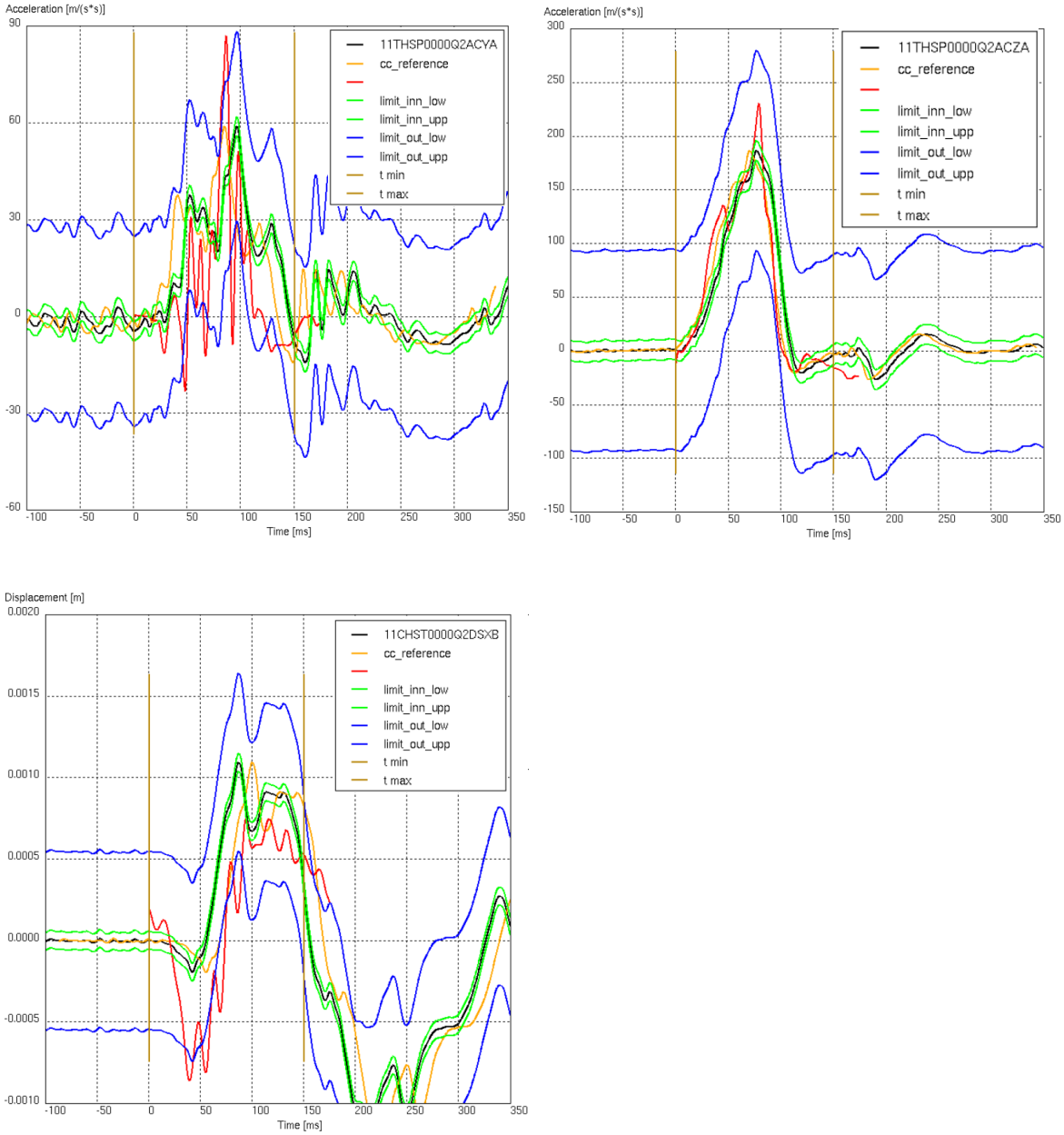

Figure 6.2 - CORA method's curves comparing real-life impact test and MADYMO's final validation model output signals

Lastly, a visual comparison between simulation and real-life frontal impact can be performed using the multimedia file generated by MADYMO and both videos provided by Karwala-Avionaut from an overhead and a lateral view. This analysis performed on the kinematics of the impact test had been performed throughout the whole model validation process, as it

provided useful information on the positioning of all elements in the test, as well as on the interaction experienced between these, especially to that between CRS and seat cushion. One of the most crucial moments to pay attention to when performing the analysis is the instant at which maximum seat penetration is reached. This moment is shown in Figure 6.3 and a notable similarity between the real-life impact test and the final MADYMO validation model can be observed. Both dummies experience similar rotations and displacements and the seat cushion undergoes a similar penetration by the CRS. However, a difference between both tests that can be observed in Figure 6.3 is that the real-life CRS model experiences a slight deformation of its structure, which contrasts with the complete rigidity of the computational model. Nevertheless, changing the rigidity of the CRS model in MADYMO would have increased excessively the model's complexity.

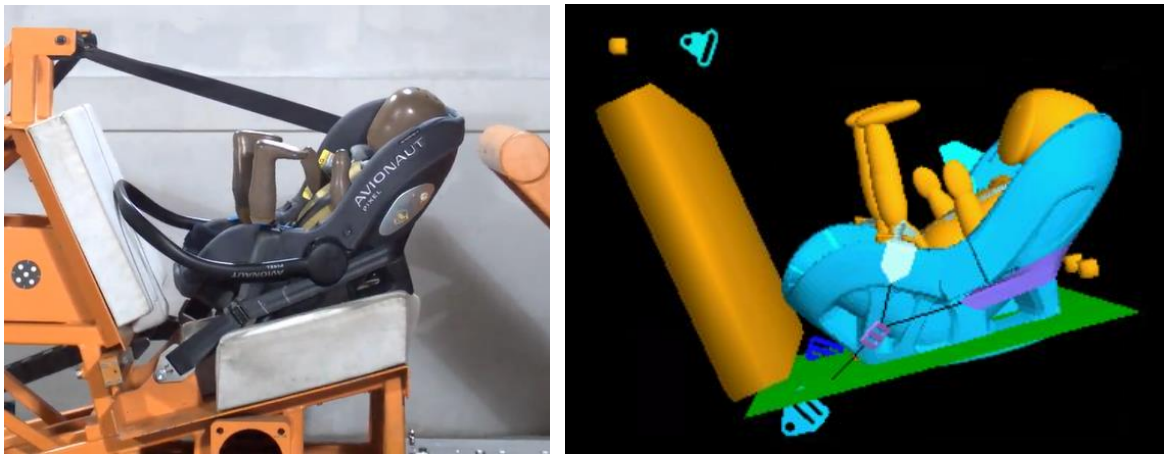

Figure 6.3 - a) CRS maximum seat penetration in real-life frontal impact test (t=89ms)
b) CRS maximum seat penetration in MADYMO simulation (t=90ms)

On the other hand, another relevant instant which can be used to evaluate the level of resemblance between both impact tests is the final one, which, in this case, corresponds to t=175ms. At this point, the dummy's position and the CRS's rotation and position are the key aspects to analyse. This can be observed in Figure 6.4, where both tests have been displayed at t=175ms, which corresponds with the MADYMO simulation's final time, and similar dummy and CRS behaviour can be spotted. The two aspects which most differ between tests are the CRS's rotation and the dummy displacement. In the real-life impact

test, the back of the CRS is slightly more vertical than in the MADYMO simulation. Furthermore, the dummy seems to experience a greater head displacement in the real-life impact test in comparison to that experienced during the MADYMO simulation. However, it is possible to say that the kinematic behaviour of the final validation model and of the real-life model are very similar, thus increasing the reliability of the results obtained with this simulation model in this project.

Figure 6.4 - a) CRS final instant in real-life frontal impact test (t=175ms)
b) CRS final instant in MADYMO frontal impact simulation (t=90ms)

The resulting validation model selected (ID2) offered satisfactory results when it comes to resemblance with the real-life impact test. The final CORA rating obtained with this model was 0.713 and the neck axial force CORA rating obtained was 0.345, which represented the highest correlation score of all simulations. After this validation process, the final model selected would be subjected to the necessary modifications stated in Chapter 5.2 and the final results on recline angle variation may be obtained.

In the Annex II, a sequence of images comparing the MADYMO validation model test and the real-life Karwala-Avionaut homologation test have been included. The frames have been taken every 20ms between t=0ms and t=175ms, including all instants in which data was collected.

6.2 *RECLINE ANGLE VARIATION ANALYSIS*

After all the alternative models with the recline angle varied had been generated, these models were included in the same MADYMO validation model. Once the alternative models were simulated, it is time to analyse the results measured by the dummy's sensors in these simulations. The variables that have been measured are presented in the following section and they are organised depending on the recline angle of the back of the Pixel AV304. To facilitate the manipulation of information, it has been decided to designate each alternative model with the variation of recline angle measured from vertical in comparison to the original model. For this reason, more vertical models are designated with negative values of recline angle variation and more horizontal models with positive values, being -10º the most upright position (34º from vertical) and +10º the most reclined position (54º from vertical).

6.2.1 *ANALYSIS ON INJURY CRITERIA METRICS*

The first variables that are to be analysed are those metrics with the sole purpose of injury criteria creation. These metrics and the values obtained in each simulation model are presented in Table 6.4.

Table 6.4 - Injury criteria metrics obtained for each recline angle

POSITION	RECLINE ANGLE VARIATION	A HEAD 3 MS	A THORAX 3 MS	A PELVIS 3 MS	HIC15	HIC36
Unit	º	m/s²	m/s²	m/s²	-	-
Vertical	-10	282.87	289.04	259.88	59.262	114.56
	-7.5	298.34	290.41	262.67	65.682	116.92
	-5	302.48	317.03	254.65	68.889	121.22
	-2.5	304.57	324.12	312.18	66.306	143.61
Original	0	318.45	308.6	301.96	82.191	140.89
Horizontal	2.5	306.45	311.76	323.01	76.636	127.25
	5	351.9	320.81	310.15	94.546	143.33
	7.5	350.61	316.51	312.99	91.905	143.28
	10	354	316.64	325.95	92.088	144.52
THRESHOLD	-	735.75	539.55	-	600	-

In this case, some very interesting results have been obtained. Firstly, a clear correlation can be observed in A Head 3 MS, as an increase in the recline angle results in higher values of A Head 3 MS. Nevertheless, none of the values obtained surpasses the threshold set at 75g according to the R129, which corresponds to 735.75 m/s^2. This increasing tendency can also be observed in Figure 6.5.

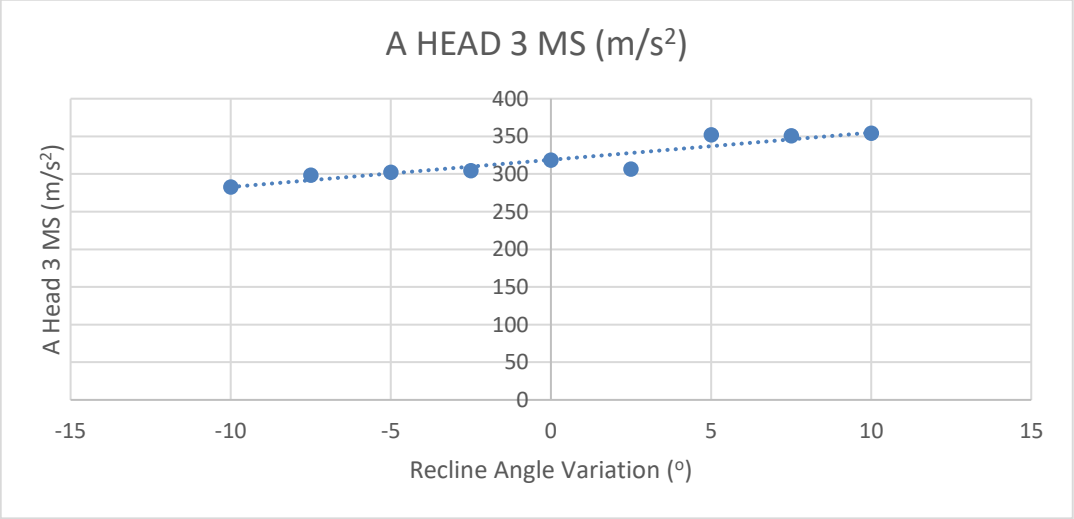

Figure 6.5 - A Head 3 MS vs Recline Angle Variation from original

Secondly, the A Thorax 3 MS metric shows very little correlation to the recline angle with a very small variation of values for this metric. Moreover, none of the values obtained surpasses the threshold set at 55g according to the R129, which corresponds to 539.55 m/s^2. Thirdly, for the A Pelvis 3 MS a greater difference between values can be observed, as values obtained for the three most upright positions are considerably lower than those obtained for the other recline angles. However, the lower area of the dummy could not be validated because Karwala-Avionaut did not provide this information from the real-life frontal impact test, thus these results being less reliable than those obtained for validated body regions. Nonetheless, the correlation given between the A Pelvis 3 MS and the recline angle of the back of the system can be observed in Figure 6.6.

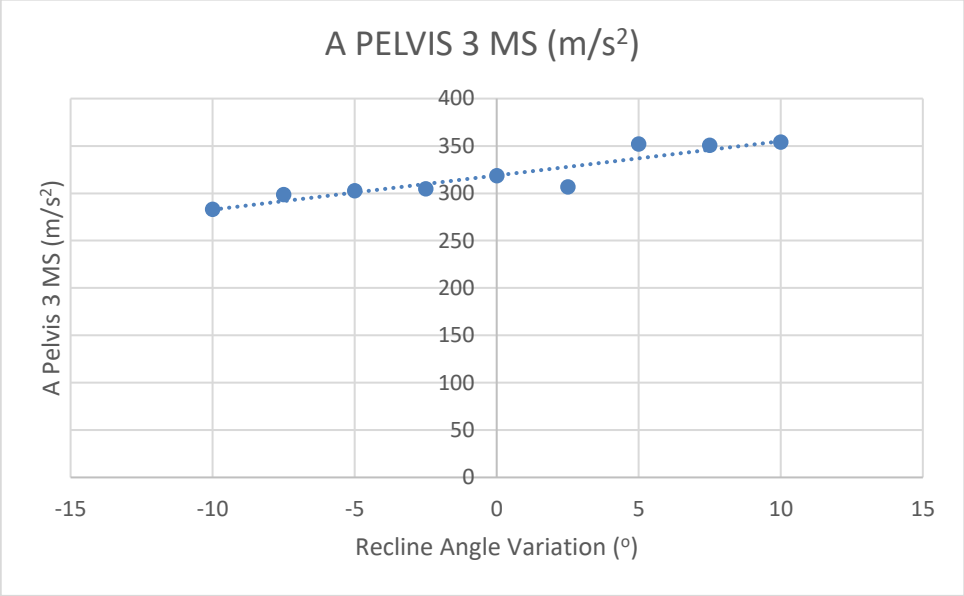

Figure 6.6 - A Pelvis 3 MS vs Recline Angle Variation from original

Lastly, the evolution of the Head Injury Criterion (HIC) can be analysed using the same method as with the other metrics. The Head Injury Criterion is a metric used to evaluate the risk of head injury during a road accident and it is typically calculated for two time windows: 15ms and 36ms. As it has been previously mentioned in Chapter 1.3, the Head Injury Criterion uses the head acceleration output to obtain a number which represents an integral average of these values along the chosen time window (E. 6.1).

$$HIC = max\left[\frac{1}{t_2-t1}\cdot\int_{t_2}^{t_1} a(t)dt\right]^{2.5}\cdot(t_2-t_1) \qquad E.\ 6.1$$

In this case, both values have been calculated as the HIC15 is that with a threshold of 600 for the Q1.5 dummy according to the R129 regulation, and the HIC36 is less sensitive to sudden peaks of acceleration. Analysing the values obtained for these metrics and displayed in Figure and Figure, a clear increase in HIC values can be noted when augmenting the CRS's recline angle. However, the HIC15 values obtained are far from the European regulation's threshold (600), thus fulfilling all alternative models the regulation's limit.

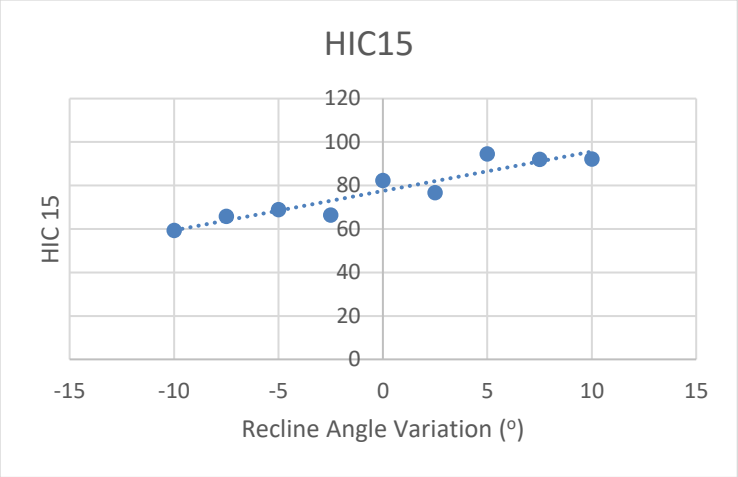

Figure 6.7 - HIC15 vs Recline Angle Variation from original

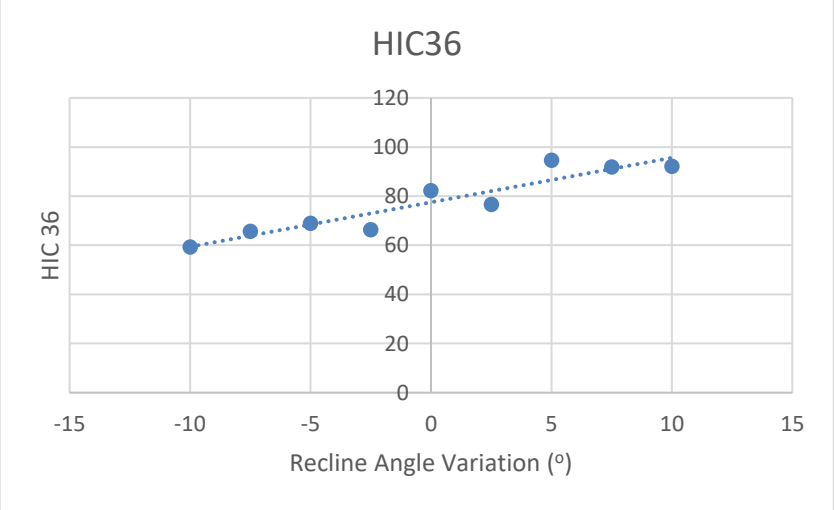

Figure 6.8 - HIC36 vs Recline Angle Variation from original

To sum up, all values obtained for the injury criteria metrics previously mentioned do not surpass maximum thresholds dictated by the R129 regulation. Furthermore, in all values except the A Thorax 3 MS, a notable progression can be observed of higher values measured for more reclined positions. This correlation between recline angle of the back of the Pixel AV304 denotes a less safe configuration for greater recline angles, although values are far from worrying in terms of child safety and non-compliance of the R129 regulation. In Chapter 6.2.2, further analysis on HIC results will be performed, linking these results with peak head acceleration values registered.

6.2.2 ANALYSIS ON ACCELERATIONS

The second variables that are to be analysed are the peak acceleration values obtained in the dummy's head and thorax. These variables' components (X axis and Z axis) have been analysed separately to facilitate drawing conclusions. These peak values registered in each simulation model are presented in Table 6.5. The R129 regulation does not state any thresholds or maximum values allowed for the variables analysed in this section, given that head protection is already supervised using the Head Criterion and A Head 3 MS. Thoracic acceleration is not taken into consideration in the present regulation when it comes to injury criteria.

Table 6.5 - Head and thorax acceleration obtained for each recline angle

POSITION	RECLINE ANGLE VARIATION	HEAD_ACC MAX_X	HEAD_ACC MAX_Z	THORAX_ACC MAX_X	THORAX_ACC MAX_Z
Unit	º	m/s²	m/s²	m/s²	m/s²
Vertical	-10	286.46	62.32	258.98	149.10
	-7.5	305.2	88.68	247.33	171.97
	-5	301.46	81.82	295.77	191.69
	-2.5	296.59	136.88	246.09	231.62
Original	0	307.47	150.48	225.34	238.25
Horizontal	2.5	298.95	149.66	221.12	248.39
	5	298.51	212.04	210.41	275.85
	7.5	288.08	209.37	211.52	274.42
	10	297.92	213.67	211.03	276.27

To start with, it is important to emphasise the convenience of separating both variables into X and Z components. As it has been previously stated multiple times, the collision analysed is a frontal impact, hence accelerations in the Y axis have not been considered relevant to the study. Furthermore, analysing the modulus of the resultant head and thorax acceleration may deprive the observer of notable events. In addition, it is important to remember that the Z axis in head and thorax is located longitudinally to the spine, thus being these magnitudes related to the neck and lumber tension and compression experienced.

Firstly, two different tendencies can be observed in the head acceleration. The values registered for head acceleration in the X axis remain considerably unvaried in all alternative models, with a maximum difference of 6% for peak values, which denotes a lack of correlation between the recline angle and the X component of the head acceleration. On the other hand, a notable correlation between Z component of the head acceleration and the recline angle can easily be identified in Table 6.5, as more reclined back configurations register prominently greater values of head accelerations (Figure 6.9). This can be explained by the reduction of action of the headrest for more reclined angles, thus decreasing the level of restraint to which the head is subjected in the Z-axis. This fact combined with the almost unvaried X component of head acceleration coincides with the results obtained for HIC values and A Head 3 MS (Table 6.4), where more reclined positions lead to a more compromised head protection. Furthermore, an increase in the values of head acceleration in the Z axis forecasts an increase in upper neck tension experienced by the dummy.

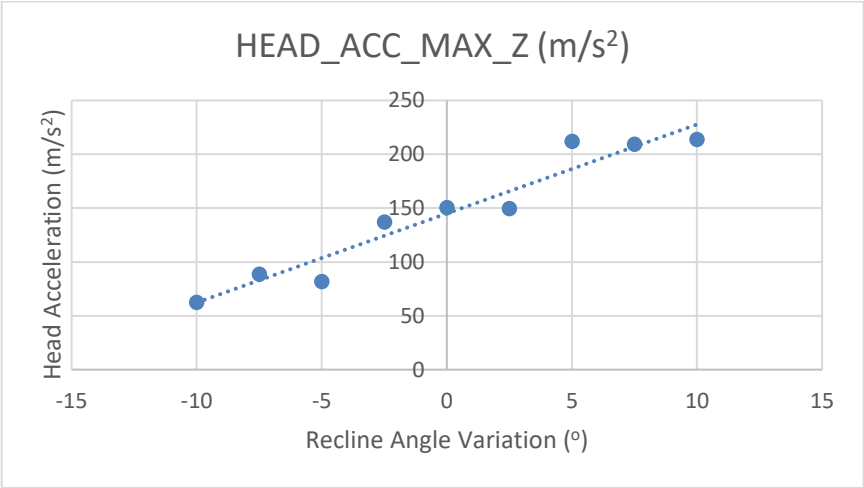

Figure 6.9 – Peak Head Acceleration (Z axis) vs Recline Angle Variation from original

Moreover, this correlation does not only happen for maximum values of head acceleration in the Z axis. In Figure 6.10, all nine head accelerations have been displayed and a similarity between most of them can be observed, except that more reclined models reach higher values of acceleration. The shape of all curves is very similar except for Vert10 and Vert7.5, which have a small valley in value at 45ms, but all curves' shapes follow similar patterns.

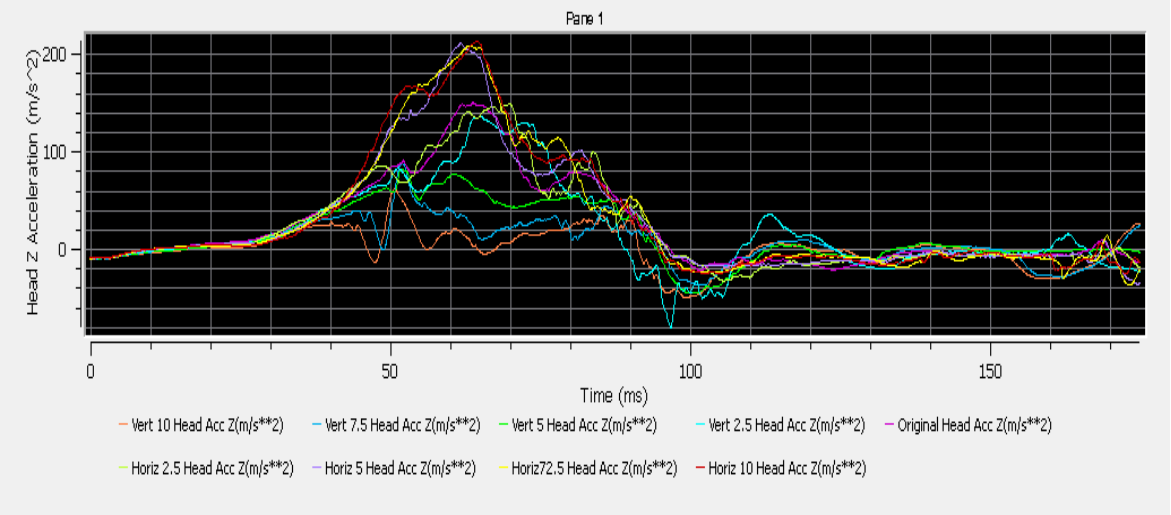

Figure 6.10 - Time-history of Head Acceleration (Z axis) for each recline angle

Secondly, a similar behaviour can be noticed with the acceleration values registered for the thorax, although, in this case, the X components do follow a slight tendency to decrease when increasing the recline angle. This negative-sloped tendency is presented in Figure 6.11 and may be given to smaller contact forces on the thoracic section as the occupant is positioned more horizontal. This way, the more reclined the occupant sits, the less restraint in the X axis it exerts, thus obtaining smaller thorax acceleration in the X axis. On the other hand, a clear positive similar correlation to that of the dummy's head can be observed for Z axis thorax acceleration in Figure 6.12, reflecting a head-thorax dependence in motion.

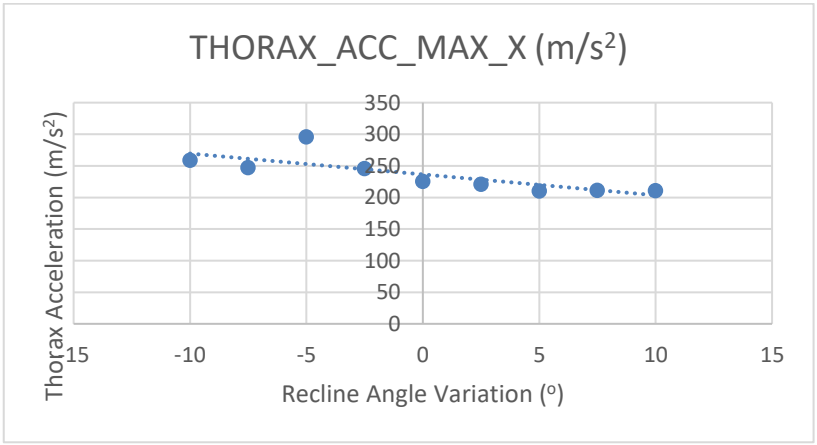

Figure 6.11 - Maximum Thorax Acceleration (X axis) vs Recline Angle Variation from original

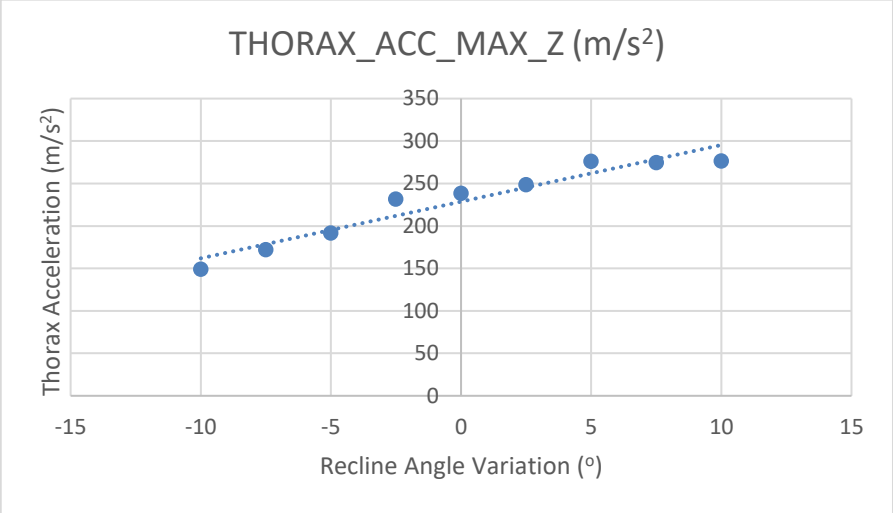

Figure 6.12 - Maximum Thorax Acceleration (Z axis) vs Recline Angle Variation from original

Moreover, this correlation does not only happen for maximum values of thorax acceleration in the Z axis. In Figure 6.13, all nine thorax accelerations have been displayed and a similarity between most of them can be observed, except that more reclined models reach higher values of acceleration. The shape of all curves is very similar except for Vert10, Vert7.5 and Vert5, which have a small valley in value at 45ms, but the curves' shapes follow similar patterns. These curves are particularly similar to those registered for Z axis head acceleration (Figure 6.10), denoting a correct performance of the dummy's superior region.

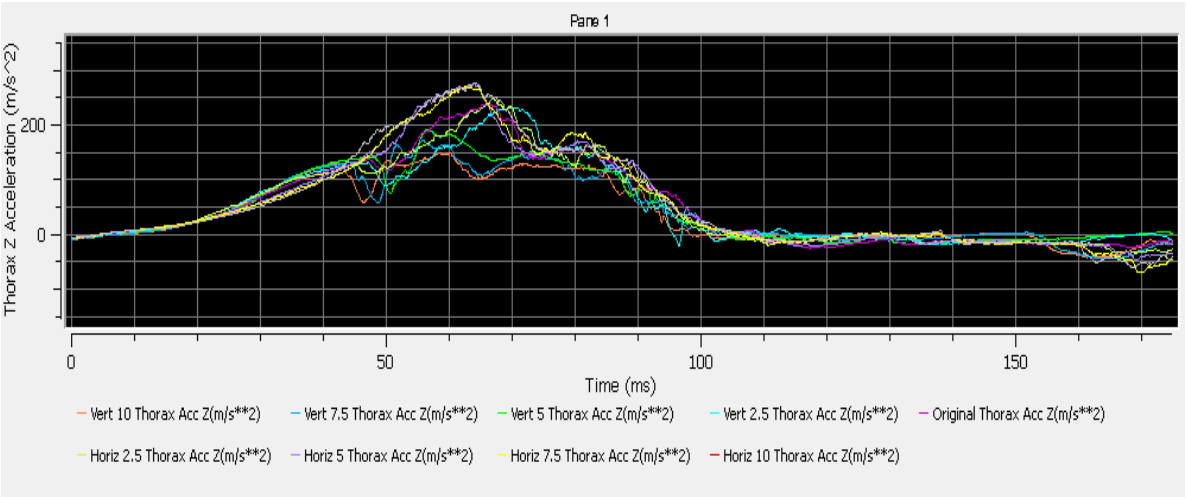

Figure 6.13 - Time-history of Thorax Acceleration (Z axis) for each recline angle

6.2.3 ANALYSIS ON NECK FORCES AND MOMENTS

The third group of variables that is to be analysed are those corresponding to upper neck forces and moments. These metrics and the values obtained in each simulation model are presented in Table 6.6. Similarly to the data presented in Chapter 6.2.1, these results are linked to the neck injury criteria, which allows to perform an evaluation on the convenience of certain configurations. In this case, three different types of values have been analysed: forces, moment and neck injury criteria. The upper neck forces have been divided into the X (transversal) and Z (axial) components and the Z component has been divided into maximum tension and compression, to analyse the maximum values registered of each type of load. On the other hand, the only torque analysed is that obtained in the Y axis, as it is used in the neck injury criterion. Lastly, the N_{ij} criterion has been taken into consideration analysing the tension-extension (NTE) and compression-extension regions (NCE), as flexion in the upper neck is only given during the pre-simulation time (-400ms, 0ms) and in the final instants (150, 175ms).

Table 6.6 - Neck forces and moments obtained for each recline angle

POSITION	RECLINE ANGLE VARIATION	NECKUP FX	NECKUP FZ Compression	NECKUP FZ Tension	NECKUP MY Extension	NTE	NCE
Unit	º	N	N	N	Nm	-	-
Vertical	-10	-356.62	-174.11	66.78	-16.22	0.9687	0.9457
	-7.5	-358.02	-157.66	85.71	-16.68	1.0230	0.9528
	-5	-404.78	-179.84	50.05	-18.46	0.9894	1.1894
	-2.5	-404.72	-249.19	85.19	-20.09	1.2235	1.0205
Original	0	-424.37	-113.34	60.54	-20.78	1.2610	1.1752
Horizontal	2.5	-470.76	-106.91	81.37	-23.11	1.3609	1.1009
	5	-412.06	-106.96	216.88	-20.69	1.3653	1.1486
	7.5	-381.24	-107.42	207.74	-19.65	1.3994	1.0370
	10	-339.74	-103.98	315.04	-17.74	1.1829	0.6837
THRESHOLD	-	-	-960	780	-	1	1

To begin with, it is important to remember that, during the validation process, not only was the upper neck axial force the hardest variable to model, but it also determined the final validation model selected, which was that with the highest CORA rating obtained for this variable. However, the CORA rating obtained was 0.345 and, although values were comprehended in a similar order of magnitude, the precision obtained with the model was not ideal. For this reason, results obtained using upper neck axial force values or anything related must be carefully analysed, as the level of resemblance between reality and the computational model may be scarce.

Furthermore, it is also beneficial to remember that the injury criteria selected for the Q1.5 dummy's upper neck have been copied from those used for the CRABI 12-month-old dummy. This had been done based on the injury criteria proposed by R. Eppinger et al [73] for the CRABI 12-month-old, where upper neck tension and compression thresholds were defined, as well as the N_{ij} intercept values. Moreover, C. P. Sherwood and J. R. Crandall [67] used very similar injury thresholds for the CRABI 12-month-old and the Q1.5 dummies (HIC, upper neck tension, chest displacement and lower neck flexion moment). Given the lack of upper neck injury criteria for the Q1.5 dummy and all that has been mentioned, it was decided to copy the upper neck tension and compression thresholds and the N_{ij} intercept values from the CRABI 12-month-old to the Q1.5 dummy (Table 6.7).

Table 6.7 - Neck injury criteria used for Q1.5 dummy from CRABI 12-month-old

Criterion	*Abbreviation*	*Unit*	*Threshold for Q1.5*
Upper neck peak tension	Tz	N	780
Upper neck peak compression	Cz	N	960
Tension Intercept (N_{ij})	T - N_{ij}	N	1460
Compression Intercept (N_{ij})	C - N_{ij}	N	1460
Flexion Intercept (N_{ij})	E - N_{ij}	Nm	43
Extension Intercept (N_{ij})	F - N_{ij}	Nm	17

Regarding result analysis, firstly, the upper neck force compiled in the X axis follows an interesting pattern showed in Figure 6.14. Initially, an increase in recline angle results in an increase in force value, which may be caused by greater impact with the headrest. However, from 46.5 onwards, the force's value starts decreasing as a result of an increase in the head acceleration in the Z axis, which favours the head's slipping, thus reducing the head's impact with the headrest.

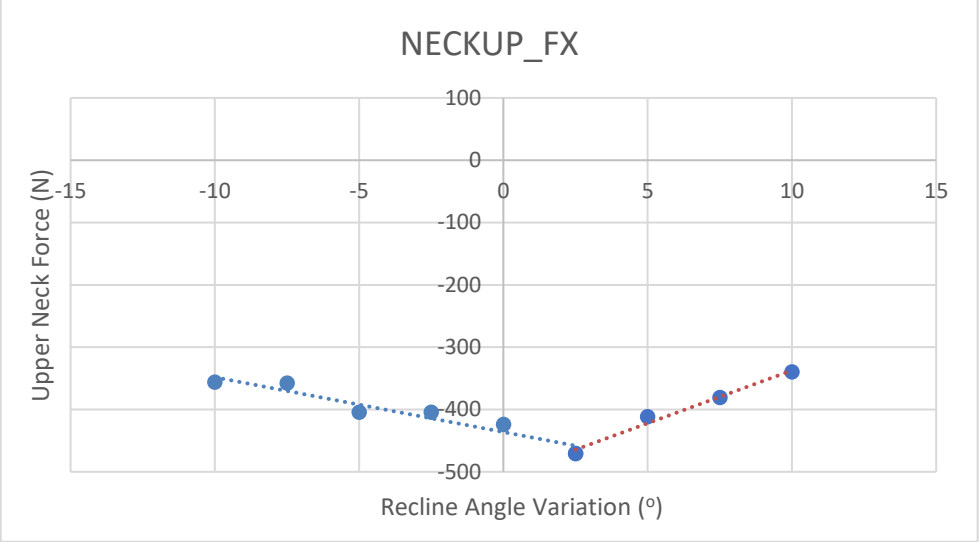

Figure 6.14 - Upper Neck Force (X axis) vs Recline Angle Variation from original

Secondly, the upper neck axial force has been divided into peak compression and tension values to avoid missing on important information. Very interestingly, the peak compression values experience a reduction in value as the recline angle increased (Figure 6.15), except for the Vert2.5 model, in which an excessive head penetration on the top of the CRS was observed that might have caused the upper neck force to go off the identified trend and produced the outlier value shown in red. On the contrary, the peak tension values were recorded for more reclined configurations, especially for recline angles over 46.5º; cases in which the tension measured in the upper neck goes off in up to a 250% increase (Figure 6.16). Nevertheless, both values are found way below the thresholds set for the CRABI 12-month-old dummy, which denotes a safe upper neck axial loading.

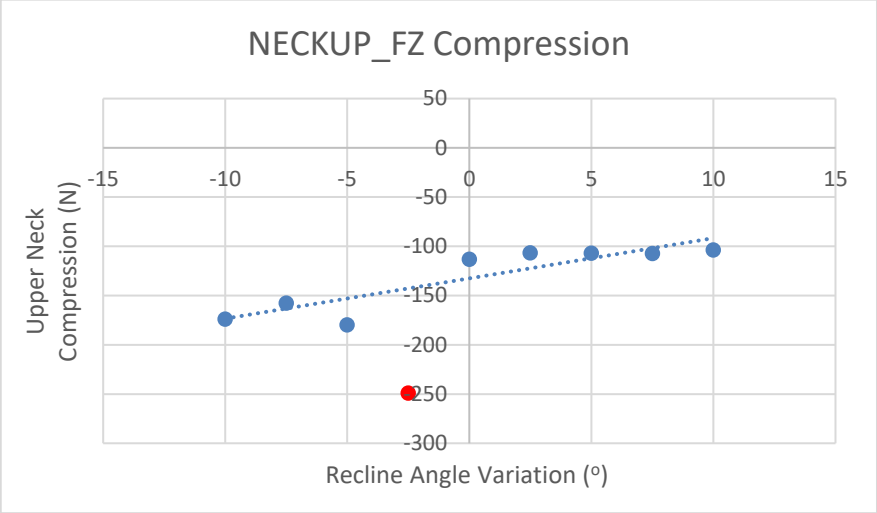

Figure 6.15 - Upper Neck Peak Compression vs Recline Angle Variation from original

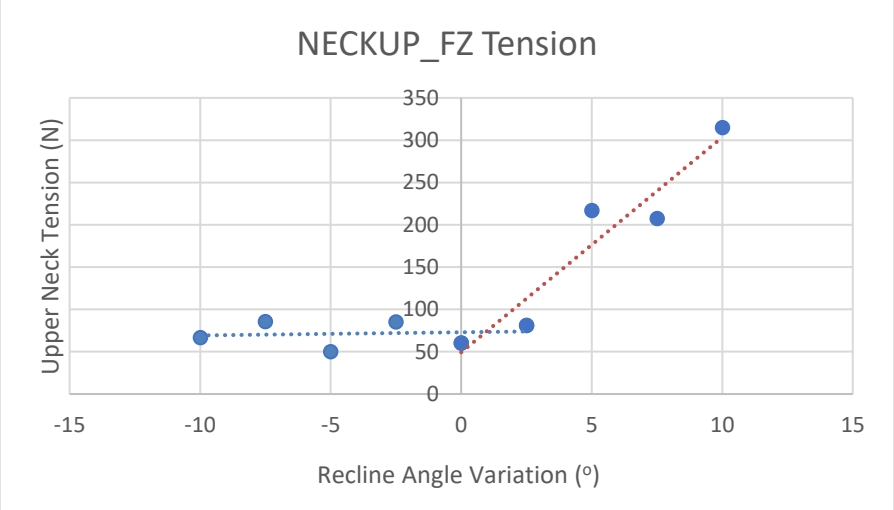

Figure 6.16 - Upper Neck Peak Tension vs Recline Angle Variation from original

Elaborating further on the previous idea, Figure 6.17 shows the time-history registered for each alternative model and several aspects can be pointed out. Firstly, it can be observed that simulation Vert2.5 experienced an unusual event, as its spectrum is completely different from the rest. Furthermore, models with high compression values follow similar patterns and models with high tension values too. The highest tension values obtained for the 3 most reclined configurations are obtained during the time in which the dummy's head is sliding on the CRS's headrest. This demonstrates that high tension values are registered for more

reclined configurations due to the lack of restraint exerted by the CRS on the dummy's head along the Z axis. For this reason, the head's inertia when contacting the reclined headrest stretches the neck's vertebrae, generating a larger tension load due to inappropriate head restraining. On the other hand, compression values do not vary greatly and the instants at which they are reached differ between models.

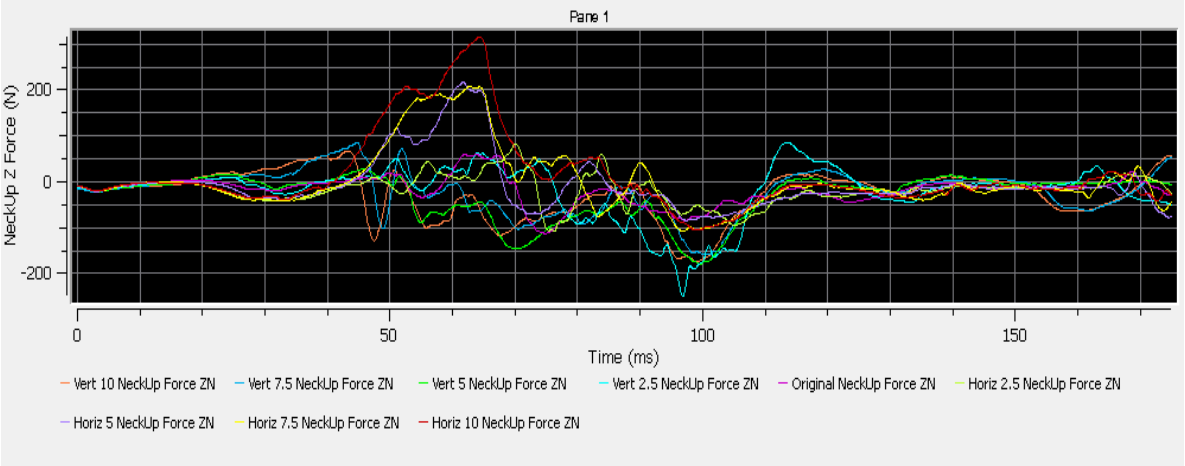

Figure 6.17 - Time-history of Upper Neck Axial Force (Z axis) for each recline angle analysed

Followingly, the moment registered in the Y axis of the upper neck mainly acquires negative values during the simulations except for the last 25ms recorded, thus experiencing the dummy an extension. All simulations record similar shapes of time-history functions, although with different values, with predominant extension and peak value at t=70ms . Values of upper neck moment increase for higher recline angles till 46.5º, where torque values' tendency shifts (Figure 6.18).

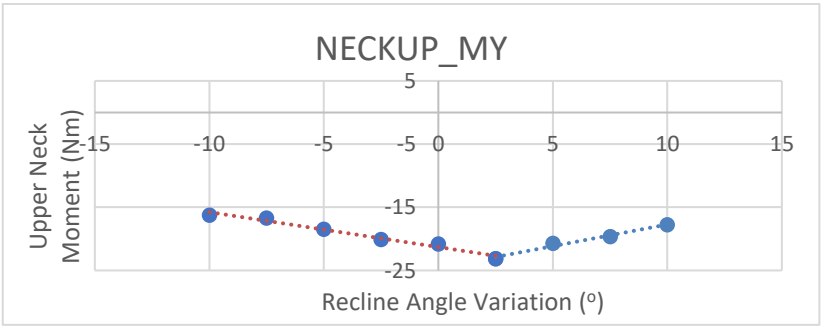

Figure 6.18 – Upper Neck Maximum Moment (Y axis) vs Recline Angle Variation from original

Lastly, results obtained for the N_{ij} upper neck injury criterion must be analysed. It is beneficial to remember that this criterion includes four different loading states depending on the axial force's nature (compression or tension) and the bending moment's nature (flexion or extension). The nomenclature used for each loading state is presented in Figure 6.19, which also includes a colour code that corresponds to that used in Figure 6.20.

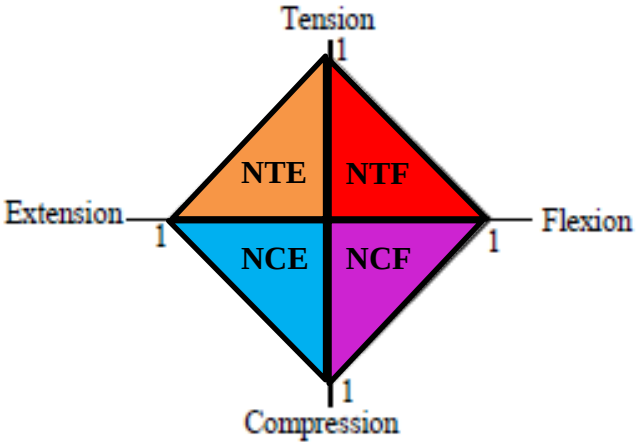

Figure 6.19 - Normalized SNPRM neck injury criteria for all dummy sizes with nomenclature. Adapted from: R. Eppinger et al, 1999

As it has been previously mentioned, a flexion moment is only registered during the pre-simulation period (-400ms, 0ms) and the last instants of simulation (150ms, 175ms), which implies that only loading states with extension ($M_y<0$) are relevant to the study. This can be observed in Figure 6.20, in which the summation of all 4 loading states considered for the N_{ij} criterion are presented. The highest values registered correspond to the NTE and NCE criteria and it is not until t=120ms that a flexion moment is registered. Suffice it to say, each time only one loading state can be given, hence at every instant all values of NTE, NCE, NTF and NCF must be equal to zero except for one, which corresponds to the active loading state.

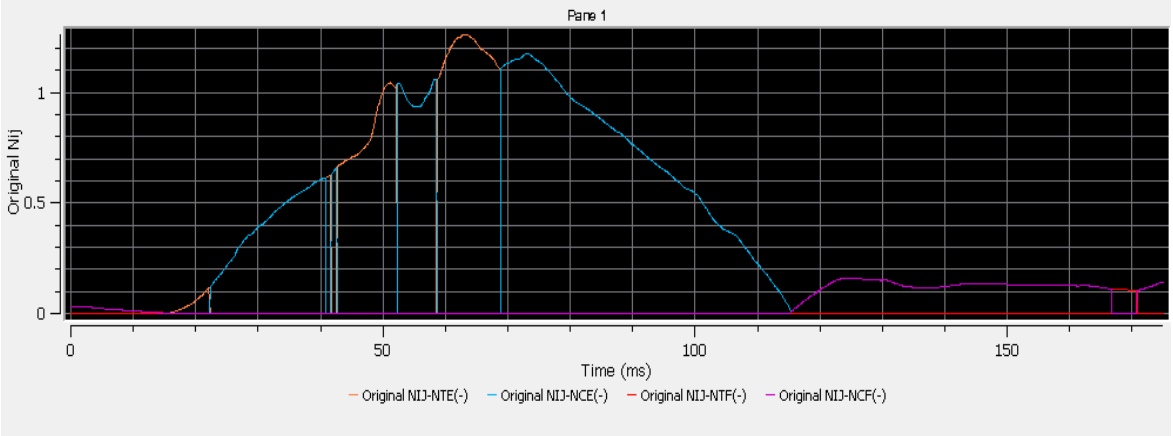

Figure 6.20 - Time-history of N_{ij} criterion regions registered with original Pixel AV304 model

Lastly, the values obtained for NTE and NCE criteria are very near or over the neck injury criterion threshold of 1 (Figure 6.21). However, as it has been previously stated, the intercept values used belong to the CRABI 12-month-old, therefore the estimation made diminishes the reliability of the results. Nevertheless, two aspects can be highlighted. Firstly, the tension-extension loading state is riskier than the compression-extension state, which matches with what had been observed in Figure 6.17. Secondly, the surpassing of the N_{ij} threshold is caused by excessive upper neck moment, which are close to the intercept used from the CRABI 12-month-old dummy. However, Karwala-Avionaut's test also registered moment values superior to the extension's intercept, which makes this event less alarming.

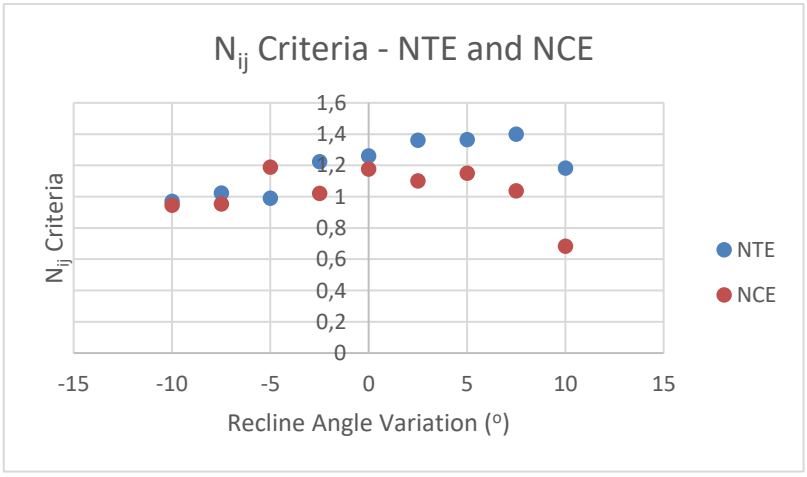

Figure 6.21 – N_{ij} criteria (NTE and NCE) vs Recline Angle Variation from original

6.2.4 ANALYSIS ON LUMBAR FORCES AND MOMENTS

The last group of variables that is to be analysed are those corresponding to lumbar forces and moments. These metrics and the values obtained in each simulation model are presented in Table 6.8. In this case, similarly to what has been done with upper neck forces, the values registered of lumbar forces have been evaluated separately on each axis: X and Z components. The X component corresponds to a transversal force generated by the contact between the lumbar spine and the back of the CRS. The Z component corresponds to the axial force experimented by the lumbar spine during the impact test. On the other hand, the lumbar moment analysed is found in the Y axis, given that the other components can be disregarded in frontal impact tests. Furthermore, at the moment, no injury criteria are linked to lumbar forces and moments, therefore no thresholds are being considered in this section.

Table 6.8 - Lumbar forces and moments obtained for each recline angle

POSITION	RECLINE ANGLE VARIATION	LUMBAR FX	LUMBAR FZ	LUMBAR MY
Unit	º	N	N	NM
Vertical	-10	-787.79	-754.01	40.09
	-7.5	-819.69	-640.14	41.88
	-5	-805.91	-349.02	40.15
	-2.5	-457.21	-222.77	21.73
Original	0	-233.97	-197.76	11.11
Horizontal	2.5	-217.98	-189.24	10.66
	5	-189.80	-298.66	11.38
	7.5	-241.20	-324.01	12.02
	10	-232.34	-400.57	13.27

To start with, prior to the analysis of results obtained on lumbar forces and torques, it is important to emphasise that the validation process performed in the first stage of the project did not include the validation of data registered in the dummy's low region: legs, pelvis and abdomen. For this reason, lumbar forces and moments measured must be rigorously analysed, as this body region, technically speaking, has not been validated with the real-life frontal impact test, and conclusions must be carefully drawn.

As it is presented in Table 6.8, the highest values of lumbar forces and lumbar moment registered during the simulation correspond to smaller values of recline angles. This can occur due to the absorption of impact performed by the lower back for positions in which the back of the CRS is located perpendicular to the direction of motion. In exchange for this excessive lumbar loading, peak values of head and thorax acceleration obtained are lower, as more energy has been absorbed by the occupant's back. Surprisingly, this progression stops for recline angles over 46.5º, moment in which axial loading starts to increase when augmenting the recline angle measured from vertical (Figure 6.22). This can be justified by the increase in tension suffered by the lumbar spine in the same way that happened with the upper neck's tension forces registered, as the spine tends to stretch more when the occupant adopts a more horizontal position.

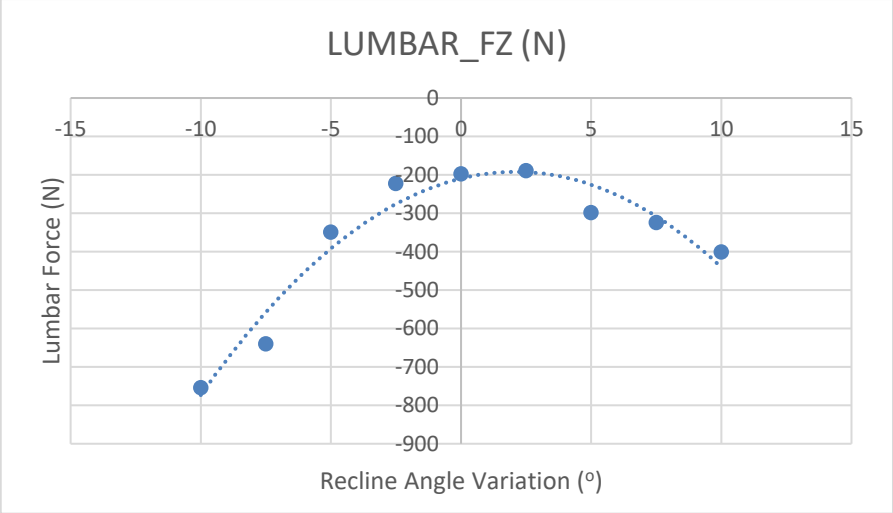

Figure 6.22 – Lumbar Force (Z axis) vs Recline Angle Variation from original

On the other hand, surprisingly values of lumbar force measured in the X axis and lumbar torque in the Y axis experience a very abrupt change in value at approximately 45º from vertical. Both variables acquire similar values for negative variations of angles and similar values for positive variation of angles, but these two values are very different. This can be observed in Figure 6.23 and Figure 6.24 and implies that a certain recline angle variation could lead to a drastic reduction, or increase, in transversal lumbar force and Y axis lumbar moment.

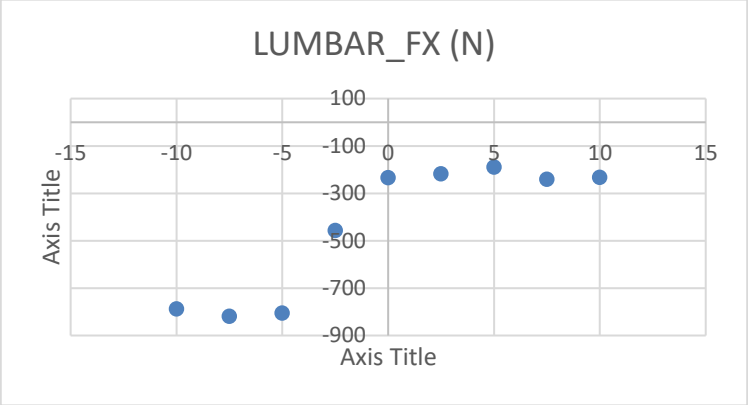

Figure 6.23 - Lumbar Force (X axis) vs Recline Angle Variation from original

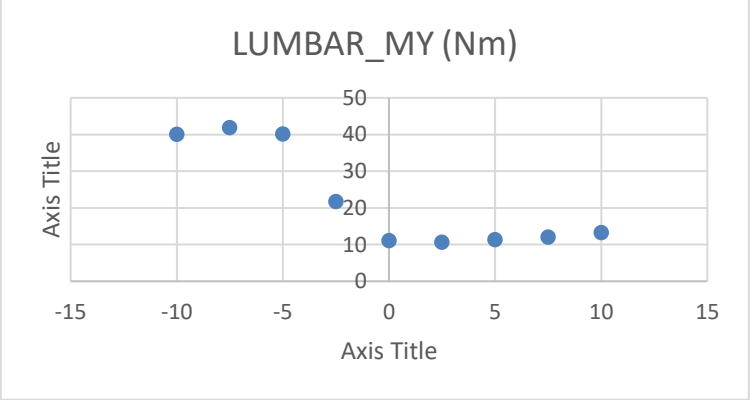

Figure 6.24 - Lumbar Moment (Y axis) vs Recline Angle Variation from original

These mentioned changes in peak lumbar force values are also translated into a change in shape of the X axis lumbar force time-history, as it can be observed in Figure 6.25.

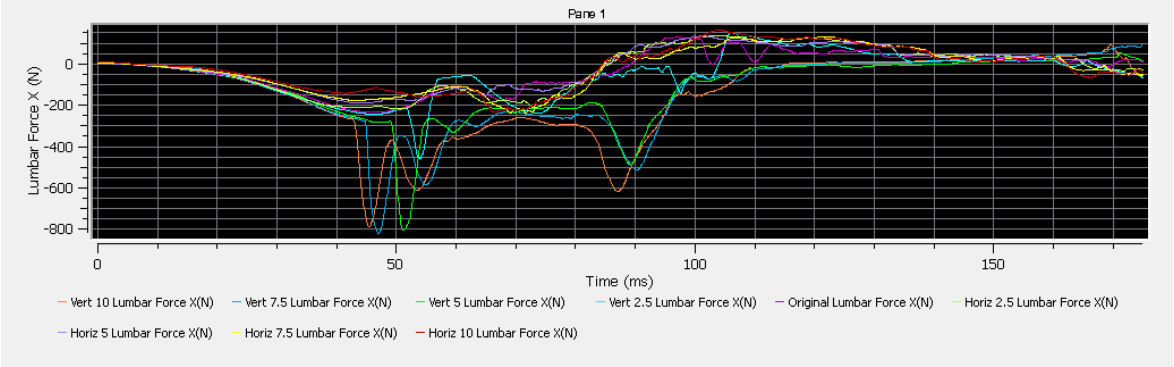

Figure 6.25 - Time-history of Lumbar Force in X axis for each recline angle analsyed

Lastly, the loads experienced in the lumbar region of the Q1.5 dummy represent the greatest drawback of a more upright position. The most vertical configurations are characterised for lower accelerations and lower upper neck forces and moments. However, when it comes to analysing the lumbar forces and moments, it is obvious that the greatest values of lumbar force in X and Z axis, as well as lumbar moment in Y axis, are registered for the most upright configurations. In addition, an evaluation of possible injury due to excessive lumbar loading would provide an objective insight on the convenience of less reclined systems in case babies can withstand the mentioned loads. The closest information that has been found on the matter is a study performed by López Valdés et al [74], in which a T7-T9 fail was registered at 12Nm in the mid-thoracic segment of a 7-year-old cadaver. However, age group and spinal segment do not match, therefore injury risk cannot be analysed.

Nevertheless, it is important to remember that Yoganandan et al [49] stated that an excessively upright position in rear-facing CRSs could lead to the obstruction of the baby's airways. However, this is considered to happen for recline angles below 30º and the most upright position analysed in this project corresponds to a recline angle of 34º from vertical, which would not be considered a dangerous position in terms of airway obstruction.

Chapter 7. CONCLUSIONS AND FUTURE PROJECTS

The conclusions obtained in this study will be first analysed based on the fulfilment of the objectives initially set in Chapter 4.2.

1. ***Generation of a validated simulation model of the CRS under study in a frontal impact test following R129 in MADYMO.*** This objective has been fully accomplished as the following partial objectives have been achieved:

a) ***R129 test bench modelling.*** The R129 test bench was successfully modelled and introduced in the MADYMO simulations. All necessary elements including seat belt buckles and anchor points, lap belt, shoulder belt, back cushion and seat cushion were added. The foam characterisation was successfully performed using LS-DYNA and the behaviour of the contact declared between CRS and seat cushion was classified as satisfactory, using the headform impact test provided by *Universidad de Zaragoza*.

b) ***Pixel AV304 model inclusion and Q1.5 dummy positioning.*** The original Pixel AV304 was successfully included in the MADYMO file. The initial Q1.5 dummy positioning was classified as satisfactory compared to that observed in Karwala-Avionaut's real-life test. Furthermore, three elements were added to the CRS model to improve the item's behaviour and model the CRS's foam in which the occupant is seated, including the declaration of contact characteristics for head and back.

c) ***Final validation model CORA rating over 0.6***. The highest global CORA rating obtained was 0.611, which is higher than the minimum set, and the highest final CORA rating obtained was 0.765, which can be considered as a great result for a frontal impact test. Nevertheless, the final CORA rating obtained for the final validation model was 0.713, which corresponded to a global CORA rating of 0.594. This was the model chosen due to better correlation for upper neck axial force.

2. ***Analysis on effect of recline angle variation of the back of a CRS in occupant's security.*** This objective has been fully accomplished as the following partial objectives have been achieved:

a) ***Generation of alternative CAD models of the Pixel AV304 with different recline angles***. Besides meshing and manipulating the original Pixel AV304 CAD model, 8 alternative models were successfully designed with LS-PrePost to obtain different recline angles of the back of the system. This allowed the obtention of 9 different CRS models with a maximum variation of 10º (from 34º to 54º from the vertical direction) in intervals of 2.5º between models for the recline angle.

b) ***Evaluation of injury criteria of all alternative models.*** All the stated injury criteria were analysed and put to judgement. Out of all the criteria considered for the Q1.5 dummy, only the neck injury criterion (N_{ij}) classified some models as invalid due to excessive extension bending ($M_y<0$). However, it is important to remember that the intercepts considered belong to the CRABI 12-month-old. The resting criteria considered were far from their respective thresholds, thus fulfilling regulations and safety principles for infants.

c) ***Evaluation and analysis of possible correlation between CRS recline angle and occupant protection.*** Some interesting correlations were observed during the analysis of results and they are presented in Chapter 6.2. Firstly, clear increase in head and thorax acceleration in the Z axis were observed for more reclined configurations, which resulted in higher HIC values, whereas X axis accelerations remained very similar. Secondly, regarding upper neck loading, more upright configurations produced higher compression loading, whereas more reclined configurations produced higher tension loading as a result of an increase in the head's acceleration in the Z axis. Lastly, lumbar loading was classified as the greatest drawback for more vertical configurations, as forces and moments registered in this region acquired worrying values and should be taken into consideration.

3. ***Recommendation of an optimal recline angle of the back of the Pixel AV304 child restraint system which maximises the occupant's security and protection.*** Taking into consideration all the information that has been previously stated and the results obtained and analysed, it has not been possible to obtain a clear optimal recline angle of the back of the Pixel AV304 that maximizes security and ergonomics. However, it is possible to make certain recommendations to the matter. The most upright configuration that has been considered corresponds to a recline angle of 34º from vertical. This configuration appears to be the safest for the infant with all the variables considered except for the lumbar forces and moments and the upper neck compression. Nevertheless, the upper neck peak compression registered in this case corresponds to an 18% of the threshold considered. On the other hand, the lumbar region has not been fully validated in this project due to the lack of signals of the lumbar region from the real-life impact test performed by Karwala-Avionaut. Furthermore, no injury criterion has been defined for lumbar forces and moments for dummies of younger occupants. In addition, it has been proved that more upright configurations for rear-facing CRSs can lead to airway obstruction as the child's head hangs forward [49]. This problem cannot be easily measured and may require real-life experiments to be determined if such vertical configurations still present this problem. Lastly, occupant ergonomics cannot be easily evaluated and is intrinsically related to the airway obstruction problem, as more reclined configurations can be translated to greater comfort.

After the fulfilment of objectives has been analysed, it is important to emphasise that the upper neck injury criteria thresholds and intercepts used in this project for the Q1.5 dummy model belong to the CRABI 12-month-old. This entails that the development of real upper neck injury criteria for the Q1.5 dummy would increase the reliability of the results obtained in this study, as well as of the conclusions drawn. This would contribute to the feasibility of obtaining a clear optimal recline angle for the rear-facing CRS analysed, as at present the results obtained for upper neck loading are not fully reliable; especially those obtained for the upper neck injury criterion (N_{ij}).

Further investigation on the effect of recline angle variation on child safety can still be performed. This analysis could be performed using a human body model (HBM) substituting the Q1.5 dummy and evaluating the similarity between both models. Furthermore, in case of official upper neck injury criteria development for Q1.5 dummy, results could be evaluated again taking into considerations these hypothetic modifications. In addition, more reliable results could be obtained in case of including information on lumbar acceleration and forces for the validation model. Lastly, an optimal recline angle could be obtained by elaborating an optimization model with the weights desired for the variables that are considered more relevant.

Chapter 8. BIBLIOGRAPHY

[1] W. H. Organization, *Global Status on Road Safety 2018*. 2018.

[2] J. W. Gardner and J. S. Sanborn, "Years of Potential Life Lost (YPLL) - What Does it Measure?" 1990.

[3] National Highway Traffic Safety Administration, "Traffic Safety Facts - Children," vol. 2018, no. April, pp. 1–12, 2018.

[4] L. Jakobsson, I. Isaksson-Hellman, and B. Lundell, "Safety for the Growing Child - Experiences From Swedish Accident Data," *Proc. 19th Int. Tech. Conf. Enhanc. Saf. Veh.*, 2005.

[5] J. I. Nazif-Munoz, A. Blank-Gommel, and E. Shor, "Effectiveness of child restraints and booster legislation in Israel," *Inj. Prev.*, vol. 24, no. 6, pp. 405–411, 2018, doi: 10.1136/injuryprev-2017-042458.

[6] "Simcenter Madymo - Mathematical Dynamic Models - AdvancedSim Tech." https://advancedsimtech.com/tass-international/simcenter-madymo/ (accessed Jun. 04, 2021).

[7] D. Gao and C. W. Wampler, "On the Use of Head Injury Criterion (HIC) to Assess the Danger of Robot Impacts," *IEEE Robot. Autom. Mag.*, vol. 16, no. 4, pp. 71–74, 2009, doi: 10.1109/MRA.2009.934824.

[8] J. S. Dufek, N. A. Ryan-Wenger, J. D. Eggleston, and K. C. Mefferd, "A Novel Approach to Assessing Head Injury Severity in Pediatric Patient Falls," *J. Pediatr. Heal. Care*, vol. 32, no. 2, pp. e59–e66, 2018, doi: 10.1016/j.pedhc.2017.09.012.

[9] L. Chybowski and W. Przetakiewicz, "Estimation of the Probability of Head Injury at a Given Abbreviated Injury Scale Level by Means of a Fuction of Head Injury Criterion," *Syst. Saf. Hum. - Tech. Facil. - Environ.*, vol. 2, no. 1, pp. 91–99, 2020, doi: 10.2478/czoto-2020-0012.

[10] R. Eppinger *et al.*, "Development of Improved Injury Criteria for the Assessment of Advanced Automotive Restraint Systems - II," *Nthsa*, no. November, 1999.

[11] S. Baker and B. O'Neill, "The Injury Severity Score: A Method for Describing Patients with Multiple Injuries and Evaluating Emergency Care," 1974.

[12] A. G. Rapsang and D. C. Shyam, "Compendio de las escalas de evaluación de riesgo en el

paciente politraumatizado," *Cir. Esp.*, vol. 93, no. 4, pp. 213–221, 2015, doi: 10.1016/j.ciresp.2013.12.021.

[13] M. Seshadri, "CORrelation and Analysis (CORA) in Visual-Environment," pp. 1–2, 2016.

[14] N. Yoganandan, A. Nahum, and J. Melvin, "Chapter 6: Mathematical Models, Computer Aided Design and Occupant Safety," in *Accidental injury. Biomechanics and Prevention. Vol 9*, 2015, pp. 143–182.

[15] J. R. Crandall, B. S. Myers, D. F. Meaney, and S. Z. Schmidtke, "Chapter 7: Pediatric Computational Models," in *Pediatric Injury Biomechanics*, 2013, pp. 287–334.

[16] S. Ag, "Simcenter Madymo Introduction Training - Day 1," 2020.

[17] S. Ag, "Simcenter Madymo Introduction Training - Day 3," 2020.

[18] Siemens Industry Software and Services BV, "Chapter 5: Finite Element Model," in *Simcenter Madymo Theory Manual*, 2020, pp. 65–144.

[19] S. Ag, "Simcenter Madymo Introduction Training - Day 2," 2018.

[20] "2-Point and 3-Point Seat Belts | Child Passenger Safety Malaysia." https://cpsmalaysia.org/2019/06/20/2-point-and-3-point-seat-belts/ (accessed Jun. 12, 2021).

[21] Y. Haland, "The Evolution of the Three Point Seat Belt From Yesterday to Tomorrow," *Ircobi*, no. September, pp. 3–15, 2006.

[22] Siemens Industry Software and Services BV, "Chapter 8: Belt Model," in *Simcenter Madymo Theory Manual*, 2020, pp. 167–182.

[23] Siemens Industry Software and Services BV, "Appendix B: Hysteresis," in *Simcenter Madymo Theory Manual*, 2020, pp. 297–312.

[24] Siemens Industry Software and Services BV, "Chapter 7: Restraint," in *Simcenter Madymo Theory Manual*, 2020, pp. 149–166.

[25] N. Yoganandan, A. Nahum, and J. Melvin, "Chapter 4: Anthropomorphic Test Devices and Injury Risk Assessments," in *Accidental injury. Biomechanics and Prevention. Vol 9*, 2015, pp. 83–108.

[26] Siemens Industry Software and Services BV, "Chapter 1: Introduction," in *Simcenter Madymo Model Manual*, 2020, pp. 9–20.

[27] Siemens Industry Software and Services BV, "Chapter 24: Q1.5 Child Dummy," in *Simcenter Madymo Model Manual*, 2020, pp. 299–308.

[28] M. Hobday and A. Michelle Hobday, "Child Restraint Systems and the transition to standard seatbelts: a review of the literature," no. June, 2018, [Online]. Available: www.c-

marc.curtin.edu.au.

[29] C. Tingvall, "Children in cars. Some aspects of the safety of children as car passengers in road traffic accidents," *Int. J. Heal. Promot. Educ.*, no. 4, p. 36, 1987, doi: 10.1080/14635240.2000.10806170.

[30] "Sistemas de sujeción y asientos de seguridad para niños | Qantas MX." https://www.qantas.com/mx/es/travel-info/children/child-restraints.html (accessed Jun. 17, 2021).

[31] D. Domenech, N. Parera, and G. Maturana, "Comparative protocol study between R44 and I-Size regulations for child restraint systems," *SAE Tech. Pap.*, no. September, p. 2018, 2018, doi: 10.4271/2018-36-0124.

[32] P. Lesire, "Safety benefits of the new ECE regulation for the homologation of CRS – an estimation by the CASPER consortium," pp. 1–35, 2011, [Online]. Available: http://www-nrd.nhtsa.dot.gov/pdf/esv/esv23/23ESV-000431.PDF.

[33] National Highway Traffic Safety Administration, "Federal Motor Vehicle Safety Standards; Child Restraint Systems, Incorporation by Reference," vol. 85, no. 212, 2020.

[34] United Nations, "Uniform provisions concerning the approval of enhanced Child Restraint Systems used on board of motor vehicles (ECRS) Addendum: 128: Regulation: 129," no. August, pp. 1–114, 2013.

[35] "CORA | pdb - Partnership for Dummy Technology and Biomechanics." https://www.pdb-org.com/en/information/18-cora-download.html (accessed Jun. 18, 2021).

[36] S. Eshraghi, D. Hynd, K. Severson, and A. Benjamin Perlman, "Finite element model validation of the hybrid-III rail safety (H3-RS) anthropomorphic test device (ATD)," *ASME Int. Mech. Eng. Congr. Expo. Proc.*, vol. 13, no. November, 2018, doi: 10.1115/IMECE2018-87736.

[37] D. L. Albert, "Variations in User Implementation of the CORA Rating Metric," *Stapp Car Crash J.*, vol. 64, no. November, pp. 1–30, 2020, doi: 10.4271/2020-22-0001.

[38] J. B. Putnam, J. T. Somers, J. A. Wells, C. E. Perry, and C. D. Untaroiu, "Development and evaluation of a finite element model of the THOR for occupant protection of spaceflight crewmembers," *Accid. Anal. Prev.*, vol. 82, no. September, pp. 244–256, 2015, doi: 10.1016/j.aap.2015.05.002.

[39] J. Gilchrist, M. Ballesteros, and E. Parker, "Vital Signs: Unintentional Injury Deaths Among Persons Aged 0–19 Years — United States," *Mortal. Wkly. Rep.*, vol. 61, 2012.

[40] European Road Safety Observatory, "Traffic safety basic facts 2017: Children," p. 25, 2017, [Online]. Available: https://ec.europa.eu/transport/road_safety/sites/roadsafety/files/pdf/statistics/dacota/bfs2017_children.pdf.

[41] G. Lee, C. N. Pope, A. Nwosu, L. B. McKenzie, and M. Zhu, "Child passenger fatality: Child restraint system usage and contributing factors among the youngest passengers from 2011 to 2015," *J. Safety Res.*, vol. 70, pp. 33–38, 2019, doi: 10.1016/j.jsr.2019.04.001.

[42] K. CJ, "An evaluation of child passenger safety: The effectiveness and benefits of safety seats," vol. DOT HS 806, no. February, pp. 1–482, 1986.

[43] B. Henary *et al.*, "Car safety seats for children: Rear facing for best protection," *Inj. Prev.*, vol. 13, no. 6, pp. 398–402, 2007, doi: 10.1136/ip.2006.015115.

[44] "Car Seats and Booster Seats | NHTSA." https://www.nhtsa.gov/equipment/car-seats-and-booster-seats (accessed Jun. 20, 2021).

[45] "Asiento de seguridad para niños de EPP | Knauf Automotive." https://knaufautomotive.com/es/el-asiento-de-seguridad-infantil-mas-ligero-del-mundo-con-epp/ (accessed Jun. 20, 2021).

[46] K. de Jager *et al.*, "Assessing new child dummies and criteria for assessment of child occupant," *19th Int. Tech. Conf. Enhanc. Saf. Veh.*, no. June, 2005.

[47] A. Carlsson *et al.*, "IRC-13-104 IRCOBI Conference 2013," pp. 868–881, 2013.

[48] T. Atkinson, A. Fras, and P. Telehowski, "The influence of occupant anthropometry and seat position on ejection risk in a rollover," *Traffic Inj. Prev.*, vol. 11, no. 4, pp. 417–424, 2010, doi: 10.1080/15389588.2010.485284.

[49] N. Yoganandan, A. Nahum, and J. Melvin, "Chapter 23: Best Practice Recommendations for Protecting Child Occupants," in *Accidental injury. Biomechanics and Prevention. Vol 9*, 2015, pp. 697–715.

[50] K. Arbogast and F. Winston, "Accidental Injury: Biomechanics and Prevention.," *Inj. Prev.*, vol. 9, no. 3, pp. 284–287, 2003, doi: 10.1136/ip.9.3.285-a.

[51] C. D. De Lima-Alvarez, E. Tudella, J. Van Der Kamp, and G. J. P. Savelsbergh, "Early development of head movements between birth and 4 months of age: A longitudinal study," *J. Mot. Behav.*, vol. 46, no. 6, pp. 415–422, 2014, doi: 10.1080/00222895.2014.929562.

[52] G. R. Whitman, A. V Hart, L. Sicher, B. Benda, and L. A. D. Aulerio, "Rear-Facing Child Safety Seat Performance in Frontal NCAP Level Crashes," no. 13, pp. 1–14, 2013.

[53] EEVC, "Q-dummies Report: Advanced Child Dummies and Injury Criteria for Frontal Impact," no. 514, p. 51, 2008.

[54] P. Prasad, H. J. Mertz, D. J. Dalmotas, J. S. Augenstein, and K. Digges, "Evaluation of the Field Relevance of Several Injury Risk Functions," *SAE Tech. Pap.*, vol. 2010-Novem, no. November, 2010, doi: 10.4271/2010-22-0004.

[55] N. Yoganandan, A. Nahum, and J. Melvin, "Chapter 2: Automotive Field Data in Injury Biomechanics," in *Accidental injury. Biomechanics and Prevention.*, vol. 9, no. 5, 2015, pp. 33–47.

[56] National Center for Health Statistics (NCHS), *The international classification of diseases*. 2008.

[57] J. R. Crandall, B. S. Myers, D. F. Meaney, and S. Z. Schmidtke, "Chapter 2: Epidemiology of Child Motor Vehicle Crash Injuries and Fatalities," in *Pediatric Injury Biomechanics*, 2013, pp. 33–86.

[58] K. D. Klinich, K. Boyle, L. Malik, M. Manary, and J. Hu, "Installed Positions of Child Restraint Systems in Vehicle Second Rows," *SAE Tech. Pap.*, vol. 2015-April, no. April, 2015, doi: 10.4271/2015-01-1452.

[59] H. Johannsen, X. Trosseille, P. Lesire, and P. Beillas, "Estimating Q-dummy injury criteria using the CASPER project results and scaling adult reference values," *2012 IRCOBI Conf. Proc. - Int. Res. Counc. Biomech. Inj.*, pp. 580–596, 2012.

[60] A. Palisson, F. Cassan, X. Trosseille, P. Lesire, and F. Alonzo, "Estimating Q3 dummy injury criteria for frontal impacts using the child project results and scaling reference values," *Int. Res. Counc. Biomech. Inj. - 2007 Int. IRCOBI Conf. Biomech. Inj. Proc.*, no. September, pp. 263–276, 2007.

[61] T. Ueda, Y. Tatenoi, and T. Nakanishi, "Applications of Occupant Safety Simulation using MADYMO," vol. 58, no. 165, pp. 1–8, 2012.

[62] R. Menon, Y. Ghati, and P. Jain, "MADYMO simulation study to optimize the seating angles and belt positioning of high back booster seat," pp. 1–12.

[63] J. Wismans and J. H. A. Hermans, "MADYMO 3D Simulations of Hybrid III Dummy Sled Tests," 1988.

[64] Y. Hu, C. E. Neal-Sturgess, A. M. Hassan, and R. Guo, "Modelling the effects of seat belts on occupant kinematics and injury risk in the rollover of a sports utility vehicle (SUV)," *SAE Tech. Pap.*, no. 724, pp. 776–790, 2007, doi: 10.4271/2007-01-1502.

[65] R. G. Kendall, C. P. Sherwood, and J. R. Crandall, "A computational study of rear-facing and forward-facing child restraints," *SAE Tech. Pap.*, vol. 1, no. 1, 2008, doi: 10.4271/2008-01-1233.

[66] L. Gras and K. Brolin, "Active Child Models for Traffic Safety Research," *Interim Rep. -1, Chalmers Univ. Sweden*, no. October, p. 33, 2012.

[67] C. P. Sherwood and J. R. Crandall, "Frontal sled tests comparing rear and forward facing child restraints with 1-3 year old dummies," *Annu. Proc. - Assoc. Adv. Automot. Med.*, pp. 169–180, 2007.

[68] C. P. Sherwood, Y. Abdelilah, J. R. Crandall, S. L. Stevens, J. M. Saggese, and M. R. Eichelberger, "The performance of various rear facing child restraint systems in a frontal crash," *Annu. Proc. - Assoc. Adv. Automot. Med.*, pp. 303–321, 2004.

[69] United Nations, "Sustainable Development Goals and Events," 2015. https://sdgs.un.org/goals (accessed Jul. 12, 2021).

[70] S. Haidar and M. Sekh, "Effects of Production Parameters on Density and Tensile Properties of Aluminium MMC Foam," no. July, 2018.

[71] S. Ag, "Simcenter Madymo Reference Manual," 2020.

[72] Granta Design Limited, "GRANTA EduPack Version 20.1.0 [software]," p. 2020, 2020.

[73] R. Eppinger, E. Sun, S. Kuppa, and R. Saul, "Supplement: Development of improved injury criteria for the assessment of advanced automotive restraint systems - II," *Natl. Highw. Traffic Saf. Adminstration (NHTSA); Natl. Transp. Biomech. Res. Cent.*, no. March, p. SES-1--SR-2, 2000.

[74] F. J. Lopez-Valdes, S. Lau, P. Riley, J. Lamp, and R. Kent, "The biomechanics of the pediatric and adult human thoracic spine," *Ann. Adv. Automot. Med.*, vol. 55, pp. 193–206, 2011.

[75] F. J. Lopez-Valdes, S. H. Lau, P. Riley, and R. W. Kent, "Characterization of the In-vitro dynamic behavior of the human thoracic Spine in flexion," *2014 IRCOBI Conf. Proc. - Int. Res. Counc. Biomech. Inj.*, pp. 145–165, 2014.

ANNEX I – ALIGNMENT OF PROJECT WITH SDGS

This Project is aligned with some of the goals and targets stated by the United Nations in 2015 as the Sustainable Development Goals (SDGs). The primary sustainable development goal which this project fulfils is Objective 3, accomplishing targets 3.2, 3.6 and 3.d.

Goal 3: *"Ensure healthy lives and promote well-being for all at all ages."* [69]

Target 3.2: *"By 2030, end preventable deaths of newborns and children under 5 years of age, with all countries aiming to reduce neonatal mortality to at least as low as 12 per 1,000 live births and under-5 mortality to at east as low as 25 per 1,000 live births."*[69] This project aims to optimize the security and ergonomics of infants under 3 years old during road trips and motor vehicle crashes, thus contributing to a reduction in the mortality rates of newborns and children. Road accidents are the main cause of unintentional death among children and safer child restraint systems can contribute to the improvement of this aspect.

Target 3.6: *"By 2020, halve the number of global deaths and injuries from road traffic accidents."*[69] This project fully focuses on this target, as its only objective is to reduce casualties and injuries during motor vehicle crashes by enhancing the protection and safety experienced by the CRS's users. An optimal recline angle of the back of the CRS, as well as the investigation carried on the effect of recline angle variation, contributes to the reduction of injury risk.

Target 3.d: *"Strengthen the capacity of all countries, in particular developing countries, for early warning, risk reduction and management of national and global health risks."*[69] Infant casualties and injuries during road traffic accidents are classified as a main global health risk, as they represent one of the main unintentional cause of death among children under the age of 9.[39] The improvement of a CRS

reduces the risk of sever injuries and the probabilities of death during a motor vehicle crash, hence fulfilling this project the stated target.

Goal 9: *"Build resilient infrastructure, promote inclusive and sustainable industrialization and foster innovation."*[69] This project is aligned with this SDG as it aims to upgrade the technological capabilities of the road safety sector. This can shed light on the effect of CRS recline angle variation, hence contributing to the improvement of road safety and future child restraint systems.

Goal 11: *"Make cities and human settlements inclusive, safe, resilient and sustainable."*[69] As it has already been stated in the previous goals with which this project is aligned, this study will help improve road safety, more specifically to children. Target 11.2 directly tackles this situation and promotes the improvement of road safety, especially to the most vulnerable groups among which children are found.

Goal 17: *"Strengthen the means of implementation and revitalize the global partnership for sustainable development."*[69] This project has been carried out thanks to the collaboration between Karwala-Avionaut and the *Instituto de Investigación Tecnológica* of the *Universidad Pontificia de Comillas*. Such alliances between different corporations will contribute to the improvement of all sectors building on the experience, offering better services as a result of the combination of expertise provided by each partner.

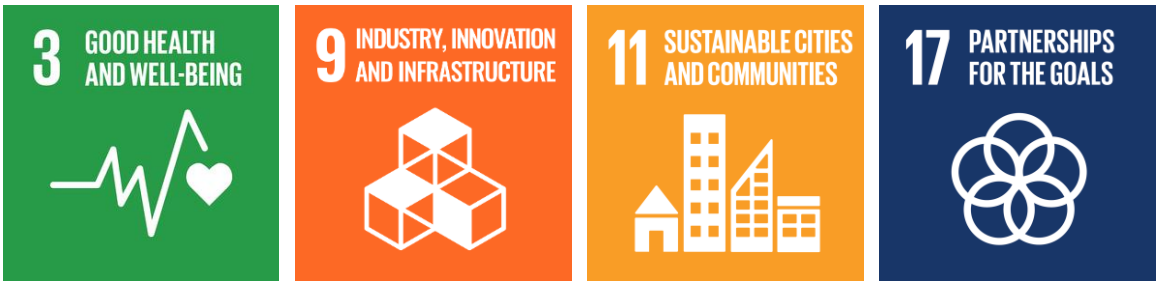

Figure - Sustainable Development Goals 3, 9, 11 and 17. Source: United Nations, 2015

ANNEX II – IMAGE SEQUENCE OF VALIDATION IMPACT TEST

In this section, a comparison between Karwala-Avionaut's homologation test and this project's validation model is presented. With the goal of visualising the resemblance in motion of both tests, a sequence of images has been presented here below to display this.

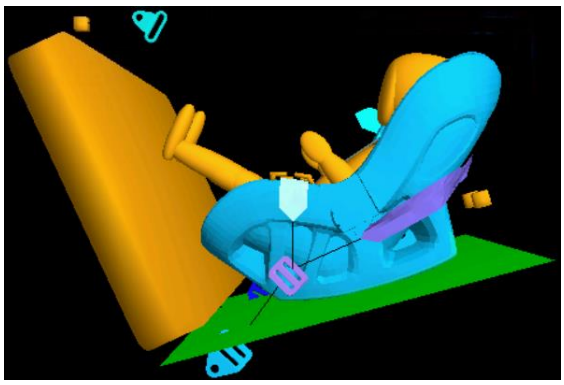

t = 0ms

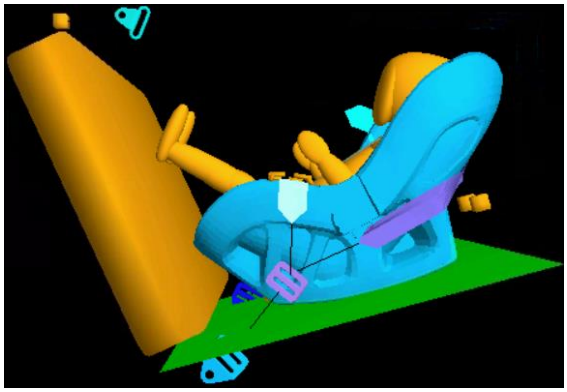

t = 20ms

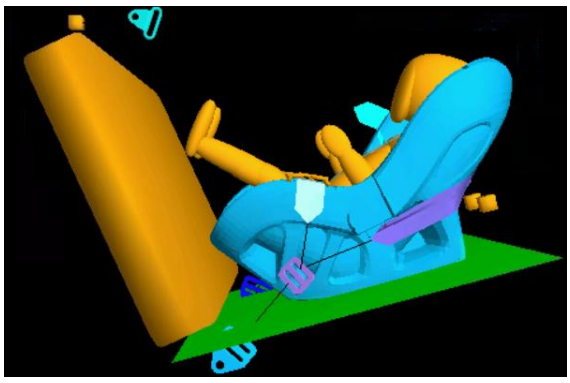

t = 40ms

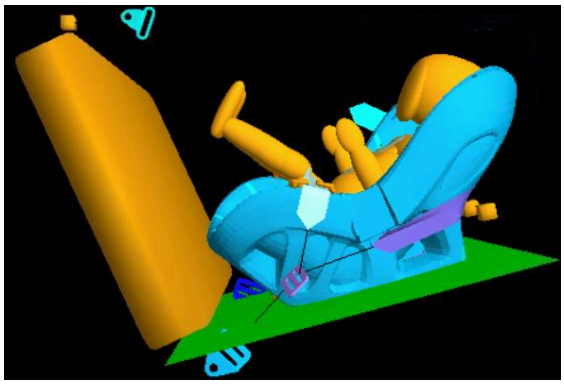

t = 60ms

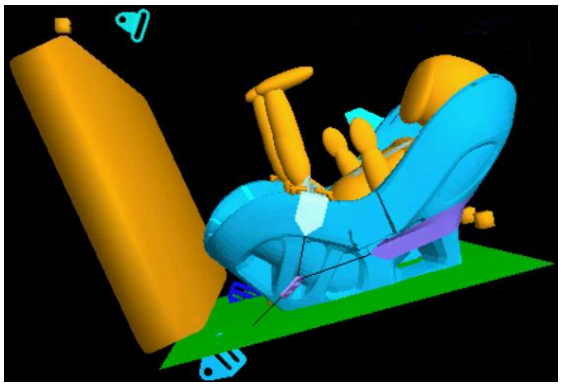

t = 80ms

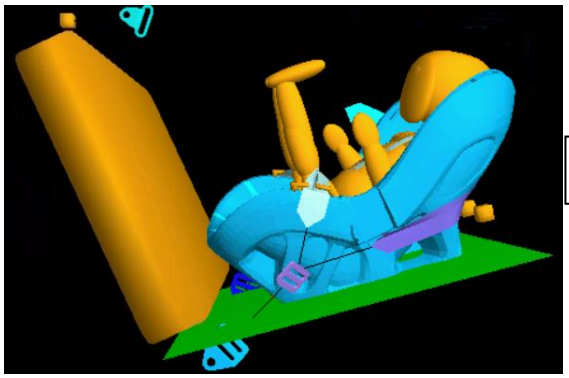

t = 100ms

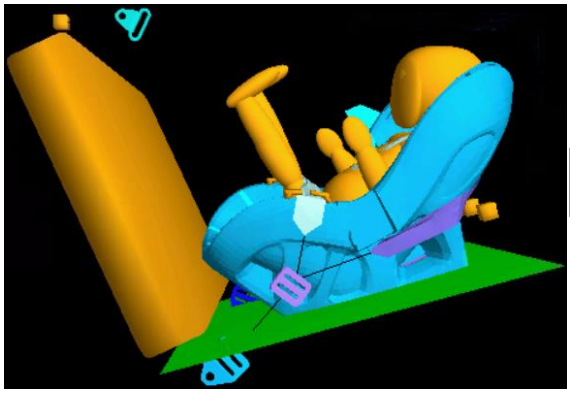

t = 120ms

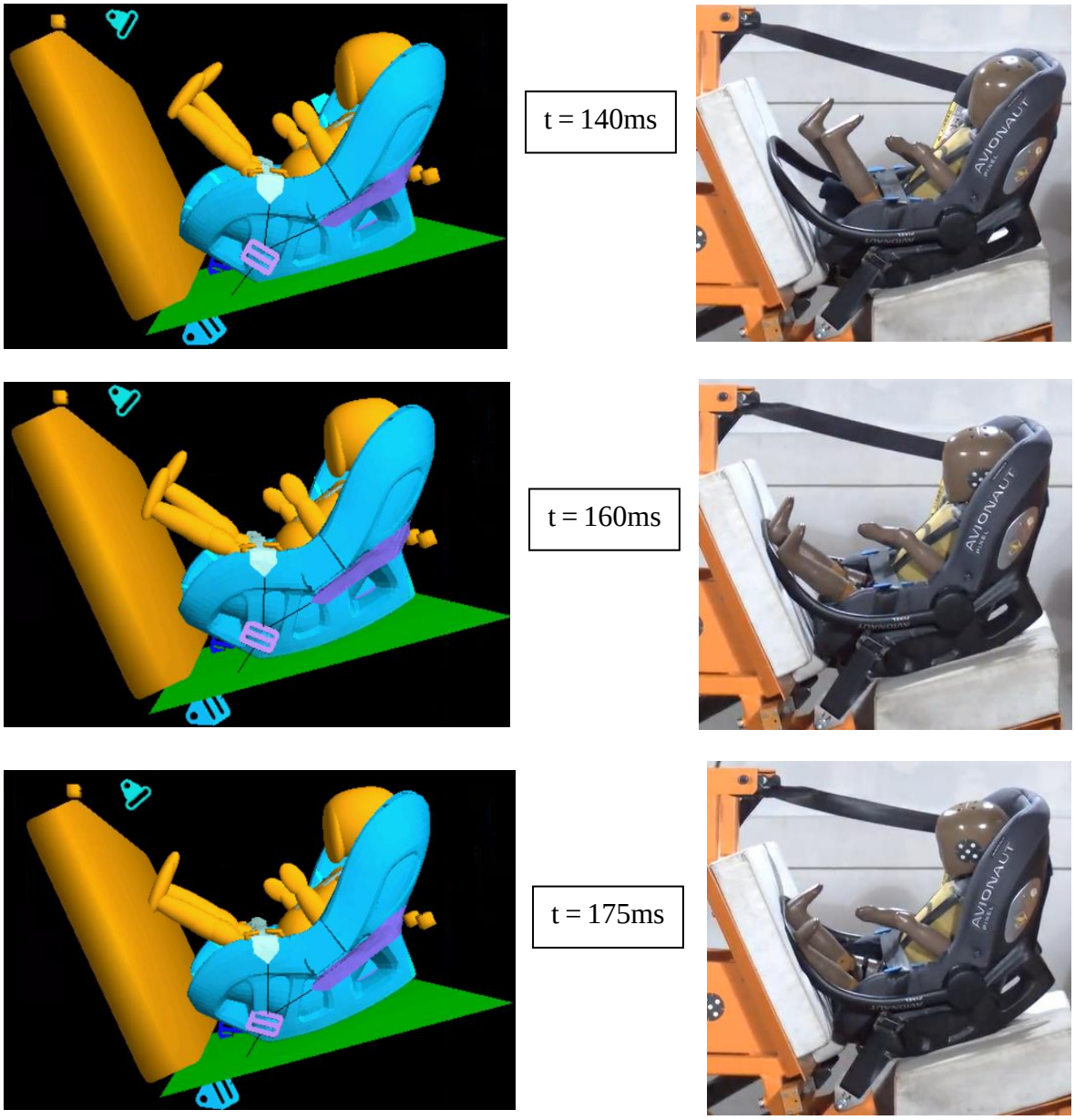

Figure - Sequence of images of validation test model (left) and Karwala-Avionaut homologation test (right). Initial time t=0ms. Final time t=175ms. Time Interval Δt=20ms.